REPORT DOCUMENTATION PAGE

Form Approved
OMB No. 0704-0188

1. REPORT DATE *(DD-MM-YYYY)*	**2. REPORT TYPE**	**3. DATES COVERED** *(From - To)*
	Journal Article	

4. TITLE AND SUBTITLE
Polycyanurate Networks with Enhanced Segmental Flexibility and Outstanding Thermochemical Stability (Pre-Print)

5a. CONTRACT NUMBER

5b. GRANT NUMBER

5c. PROGRAM ELEMENT NUMBER

6. AUTHOR(S)
Andrew J. Guenthner, Matthew C. Davis, Michael D. Ford, Josiah T. Reams, Thomas J. Groshens, Lawrence C. Baldwin, Lisa M. Lubin, Joseph M. Mabry

5d. PROJECT NUMBER

5e. TASK NUMBER

5f. WORK UNIT NUMBER
Q0BG

7. PERFORMING ORGANIZATION NAME(S) AND ADDRESS(ES)

Air Force Research Laboratory (AFMC)
AFRL/RQRP
10 E. Saturn Blvd.
Edwards AFB, CA 93524

8. PERFORMING ORGANIZATION REPORT NO.

9. SPONSORING / MONITORING AGENCY NAME(S) AND ADDRESS(ES)

Air Force Research Laboratory (AFMC)
AFRL/RQR
5 Pollux Drive
Edwards AFB, CA 93524-7048

10. SPONSOR/MONITOR'S ACRONYM(S)

11. SPONSOR/MONITOR'S REPORT NUMBER(S)
AFRL-RQ-ED-JA-2012-446

12. DISTRIBUTION / AVAILABILITY STATEMENT
Approved for public release; distribution unlimited

13. SUPPLEMENTARY NOTES
For publication in Macromolecules
PA Case Number: 13016; Clearance Date: 4 Jan 2013.

14. ABSTRACT
The synthesis and physical properties of cyanurate networks formed from two new tricyanate monomers, 1,3,5-tris[(4-cyanatophenylmethyl]benzene, and 3,5-bis[(4-cyanatophenylmethyl)]phenylcyanate, are reported and compared to those of and 1,1,1-tris[(4-cyanatophenyl)]ethane (also known as ESR-255). All three networks possessed somewhat different aromatic contents and cross-link densities, however the thermochemical stability of these networks, as determined by TGA, was outstanding, with that of 1,3,5-tris[(4-cyanatophenylmethyl)]benzene being among the best known for organic cyanate esters despite its comparatively high segmental flexibility. Moreover, the moisture uptake of cured 1,3,5-tris[(4-cyanatophenylmethyl)]benzene, at 2.2% after 96 hours immersed in 85 °C water, was comparatively low for a cyanate ester network with a glass transition temperature of 320 °C at full cure. When cured for 24 hours at 210 °C, the dry glass transition temperatures of the networks ranged from 245 to 285 °C, while the wet glass transition temperatures ranged from 225 – 240 °C. The similarity in glass transition temperatures resulted from a lower extent of cure in the networks with more rigid segments. In essence, for networks with very high glass transition temperatures at full cure, the process conditions, rather than the rigidity of the network, determined the attainable glass transition temperature. Because networks with a higher extent of cure tend to exhibit slower long-term degradation, in this case, the networks with greater segment flexibility enabled superior performance despite exhibiting a lower glass transition temperature at full cure. These results illustrate that, in contrast to the prevailing heuristics for improving the performance of high-temperature thermosetting polymer networks, a more flexible network with a lower glass transition temperature at full cure can offer an optimal combination of thermomechanical and thermochemical performance.

15. SUBJECT TERMS

16. SECURITY CLASSIFICATION OF:			**17. LIMITATION OF ABSTRACT**	**18. NUMBER OF PAGES**	**19a. NAME OF RESPONSIBLE PERSON**
					Dr. Joseph Mabry
a. REPORT	**b. ABSTRACT**	**c. THIS PAGE**	SAR	116	**19b. TELEPHONE NO** *(include area code)*
Unclassified	**Unclassified**	**Unclassified**			

Standard Form 298 (Rev. 8-98)
Prescribed by ANSI Std. 239.18

Polycyanurate Networks with Enhanced Segmental Flexibility and Outstanding Thermochemical Stability

Andrew J. Guenthner[*1], Matthew C. Davis[2], Michael D. Ford[2], Josiah T. Reams[3], Thomas J. Groshens[2], Lawrence C. Baldwin[2], Lisa M. Lubin[4], and Joseph M. Mabry[1]*

[1]Air Force Research Laboratory, Propulsion Directorate, Edwards AFB, CA 93524
[2]Naval Air Warfare Center, Weapons Division, China Lake, CA 93555
[3]National Research Council / Air Force Research Laboratory, Edwards AFB, CA 93524
[4] ERC Incorporated, Edwards AFB, CA 93524

Author e-mail: andrew.guenthner@edwards.af.mil

Abstract

The synthesis and physical properties of cyanurate networks formed from two new tricyanate monomers, 1,3,5-tris[(4-cyanatophenylmethyl]benzene, and 3,5-bis[(4-cyanatophenylmethyl)]phenylcyanate, are reported and compared to those of and 1,1,1-tris[(4-cyanatophenyl)]ethane (also known as ESR-255). All three networks possessed somewhat different aromatic contents and cross-link densities, however the thermochemical stability of these networks, as determined by TGA, was outstanding, with that of 1,3,5-tris[(4-cyanatophenylmethyl)]benzene being among the best known for organic cyanate esters despite its comparatively high segmental flexibility. Moreover, the moisture uptake of cured 1,3,5-tris[(4-cyanatophenylmethyl)]benzene, at 2.2% after 96 hours immersed in 85 °C water, was comparatively low for a cyanate ester network with a glass transition temperature of 320 °C at

full cure. When cured for 24 hours at 210 °C, the dry glass transition temperatures of the networks ranged from 245 to 285 °C, while the wet glass transition temperatures ranged from 225 – 240 °C. The similarity in glass transition temperatures resulted from a lower extent of cure in the networks with more rigid segments. In essence, for networks with very high glass transition temperatures at full cure, the process conditions, rather than the rigidity of the network, determined the attainable glass transition temperature. Because networks with a higher extent of cure tend to exhibit slower long-term degradation, in this case, the networks with greater segment flexibility enabled superior performance despite exhibiting a lower glass transition temperature at full cure. These results illustrate that, in contrast to the prevailing heuristics for improving the performance of high-temperature thermosetting polymer networks, a more flexible network with a lower glass transition temperature at full cure can offer an optimal combination of thermomechanical and thermochemical performance.

Keywords: thermosetting resin; cyanate ester; cure kinetics

Introduction

Tightly cross-linked macromolecular networks with maximum continuous use temperatures above 175 °C, formed by thermal cure of polyfunctional monomers, represent an extremely important class of polymeric structural and adhesive materials, with a broad range of applications in the electronics, energy storage, and aerospace industries. Among these, cyanate ester resins[1-3] (R-O-C≡N) made from trifunctional monomers have been studied[4,5] as potential materials for applications ranging from aircraft engine turbine brush seals,[6-8] to nano-structured bio-sensors,[9] due to their excellent high-temperature mechanical performance combined with ease of processing. However, cyanate ester monomers also possess unusual characteristics that make them ideally suited to the study of high-performance thermosetting networks, such as the highly selective formation of a single cross-linked network product[10] (a polycyanurate network), no need to balance stoichiometry, effective control of polymerization rate through a wide range of available catalysts, low shrinkage on cure that minimizes residual stresses,[11,12] outstanding short-term thermal stability of the network, and simple verification of the chemical structure of the insoluble cured network (including quantitative information on side product formation) through FT-IR spectroscopy.[13] As a result, studies of the relationships among structure, processing, and properties involving polycyanurate networks can provide significant insights into the properties of thermosetting networks in general.

When developing new high-performance thermosetting monomers, it has generally been assumed that the glass transition temperature (T_g) of the fully cured network (herein referred to as a "fully-cured T_g") should be as high as possible, provided that an acceptable degree of toughness can be maintained. For single-components networks with one well-defined type of chemical cross-link, the fully-cured T_g depends on the density of cross-links and branch points,

along with the rigidity of the network segments, but not on the details of the cure process. As a result, the "fully cured" T_g provides a useful quantitative (though limited) indication of the relative flexibility of network segments. For cyanate esters such as Primaset® PT-30 with fully cured T_g's as high as 400 °C,[14] however, complete conversion of the monomer to cyanurate may require undesirably high temperatures.[15] Therefore, the network properties depend on the "as cured" rather than the fully-cured T_g. In many thermosetting materials, vitrification (the point when network development drives the glass transition temperature above the cure temperature) has been assumed to result in cessation of cure, resulting in an "as cured" T_g that is roughly the same as the maximum cure temperature. As a result of these assumptions, the long-established approach to developing high T_g thermosetting resins has been to 1) make the network segments as rigid, and cross-link densities as high, as constraints imposed by brittleness permit, and 2) utilize the maximum permissible cure temperature. Even though cyanate esters have been known for many years to violate the assumptions relating the T_g and maximum cure temperature,[16] the approach to developing cyanate esters has been the same as the one outlined above for high-temperature thermosetting networks in general.

Recently, however, it has become more widely appreciated that in thermosetting networks, slow conversion of monomer continues to take place in the glassy state,[17] and thus that "as cured" T_g's may significantly exceed maximum cure temperatures. The kinetics of cure for both epoxy and cyanate ester resins near T_g have been studied recently.[18,19] However, many aspects of cure well below T_g remain relatively unexplored. From a performance standpoint, though, the highly desirable combination of good thermomechanical performance (which demands a high T_g) and affordable processing (which requires low cure temperatures) means that a deeper understanding of cure well below T_g will become increasingly important.

Well below T_g, large-scale molecular motion in the developing network is generally absent. As illustrated in Figure 1, the ability for cure to proceed in a system containing reactive groups only at chain ends is likely to depend strongly on the degree of localized motion available to these chain ends. The flexibility of the individual network segments thus plays a key role in either facilitating or hindering the formation of networks with very high levels of conversion. The incorporation of flexible chemical linkages that enable such motions, however, tends to result in a lower fully-cured T_g. Due to the historical considerations outlined earlier, the concept of incorporating more flexible network segments to facilitate cure well below T_g has thus far received little consideration in the development of high-temperature thermosetting polymers. The trade-offs, however, between achieving full cure and maintaining a high T_g are technologically quite important because the long-term hydrolytic stability of cyanate esters, for instance, depends critically on achieving close to 100% conversion,[20] while the toughness of cyanate esters has been shown to more than double when conversion is increased from 95% to near 100%.[21] Despite their importance, these trade-offs have not been explored systematically in many types of thermosetting resins.

We recently compared the performance of the commercial polycyanurate Primaset® PT-30, which forms a highly rigid network, with a more flexible analog, and found that many, though not all, of the expected disadvantages associated with more flexible network segments were mitigated by the relative ease of achieving close to complete conversion in the more flexible network.[22] However, we also found that the thermochemical stability of the more flexible network was significantly reduced. In addition to degrading application-related performance, the reduction in thermal stability prevented a clear determination of the fully cured T_g of the more flexible network. A thermochemically more stable network with enhanced

segment flexibility was thus needed to systematically understand the trade-offs between segment flexibility, "as cured" and fully cured T_g, and performance.

a)

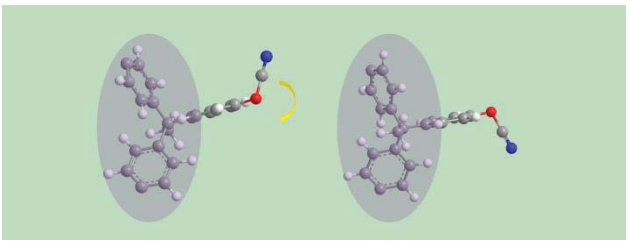

b)

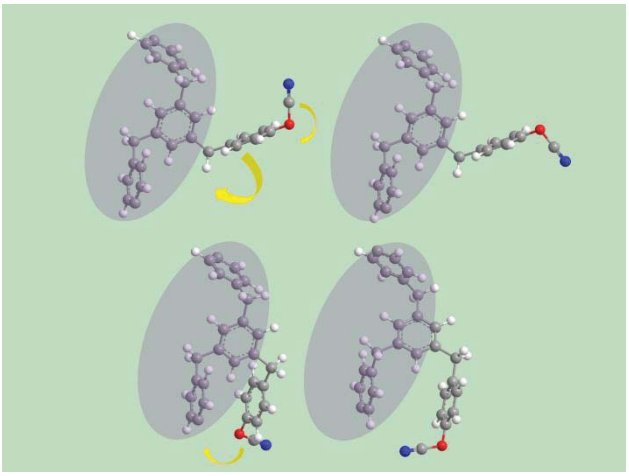

Figure 1. Schematic illustration of the envisioned effect of network segment flexibility on the reactivity of cyanate esters in the glassy state. After vitrification, portions of the network away from the chain ends (indicated by the darker ellipses) exhibit highly restricted motion, and the ability of the reactive groups to move into the correct position and orientation for further cure depends on the local motions of the nearby chain segment, as illustrated by the arrows. a) a portion of the network formed from the rigid monomer ESR-255, having a limited range of motion b) a portion of the network formed from the more flexible monomer **1** (see Scheme 1) that exhibits a greater range of plausible motion due to a larger number of more freely rotating bonds.

As reported in this paper, a newly synthesized cyanate ester monomer (**1**) affords enhanced network segment flexibility with no loss in thermochemical stability compared to more rigid analogs (see Chart 1 for chemical structures). The synthesis of this monomer, along with the synthesis of more rigid single-component analogs, thus enabled a clear comparison of the effect of network segment flexibility on both extent of cure and T_g. The comparisons indicated that the "as cured" T_g (using identical cure conditions) was, though far above the cure temperature itself, still limited to a maximum value determined primarily by the cure conditions rather than by the rigidity of the network segments. In contrast, the fully cured T_g of the networks clearly decreased with increasing segment flexibility. Therefore, under a given set of cure conditions, near complete conversion was only possible in networks having sufficient segment flexibility. Because near complete conversion is often a requirement for acceptable long-term performance, in this case the more flexible network, contrary to expectations based on the prevailing heuristics described previously, may provide the best performance. Therefore, in addition to developing a new cyanate ester monomer with superior performance, new insights have been gained into the role of network segment flexibility and its usefulness in optimizing performance. These insights will greatly aid both process and product development for a wide range of thermosetting polymers used in many high-performance electronics, aerospace, and energy applications.

Chart 1. Chemical structures of new tricyanate esters (**1**) and (**2**), and more rigid analogs ESR-255 and PT-30.

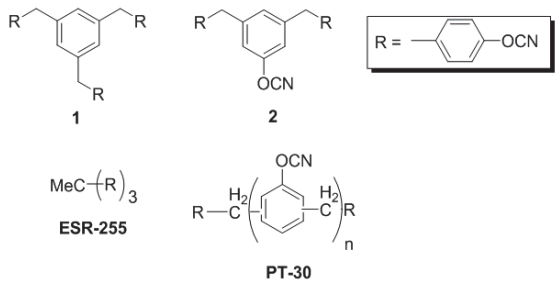

Results and discussion

Synthesis of the new monomers 1 and 2. The synthesis of tricyanate **1** is shown in Scheme 1. The preparation of 1,3,5-triaroylbenzenes such as **5** has been typically accomplished via the enaminoketone generated from acetophenones and expensive dialkyl acetals of dimethylformamide.[23,24] In this case, *para*-methoxyacetophenone was condensed with methyl formate using potassium *tert*-butoxide as base to give the potassium salt **4** in good yield.[25-27] This salt was then cyclotrimerized in hot glacial acetic acid to give **5** in good yield.[28] Reduction of the carbonyls by sodium borohydride gave the diastereomeric mixture of triol **6**. Hydrogenolysis of **6** by catalytic transfer hydrogenation[29-32] gave the unreported symmetrical tribenzylbenzene **7**. Demethylation of **7** by molten pyridine hydrochloride gave the triphenol **8**.[33] Single-crystal X-ray analysis proved the structure of **8** (see Supporting Information Section S1). Finally, **8** was cyanated with cyanogen bromide and triethylamine base to give tricyanate **1** at 30% overall yield in the six steps from *para*-methoxyacetophenone. NMR spectra for monomers **1**, **2**, and ESR-255 are shown in Supporting Information Section S1.

Scheme 1. Chemical synthesis route to tricyanate **1**.

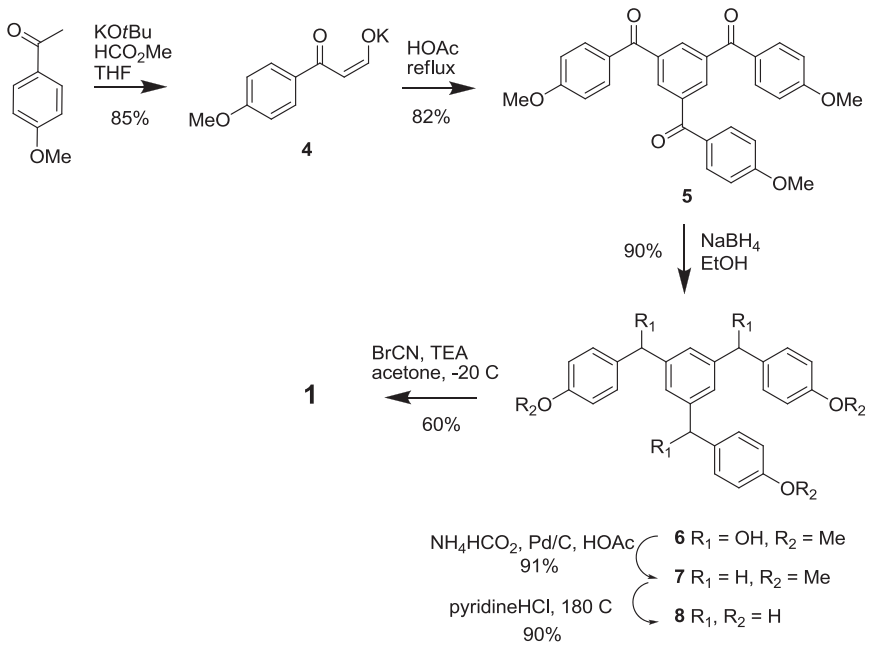

The synthesis of tricyanate **2** is shown in Scheme 2. 5-Hydroxyisophthalic acid was heated with dimethylsulfate and potassium carbonate in acetone to give the trimethyl derivative **9**.[34] Hydrolysis by refluxing in aqueous potassium hydroxide gave the diacid **10**.[35] Reaction with thionyl chloride followed by Friedel-Crafts acylation of anisole gave the unreported diketone **11** in 52% yield over the two steps. Reduction with lithium tetrahydroaluminate in tetrahydrofuran gave the diastereomeric mixture of diol **12**. Hydrogenolysis of the benzylic alcohols in refluxing acetic acid with palladium catalyst gave the dibenzyl compound **13**.[36] Deprotection followed by cyanation in similar fashion to that described above gave tricyanate **2** in 8% yield over the seven steps.

Scheme 2. Chemical synthesis route tricyanate **2**.

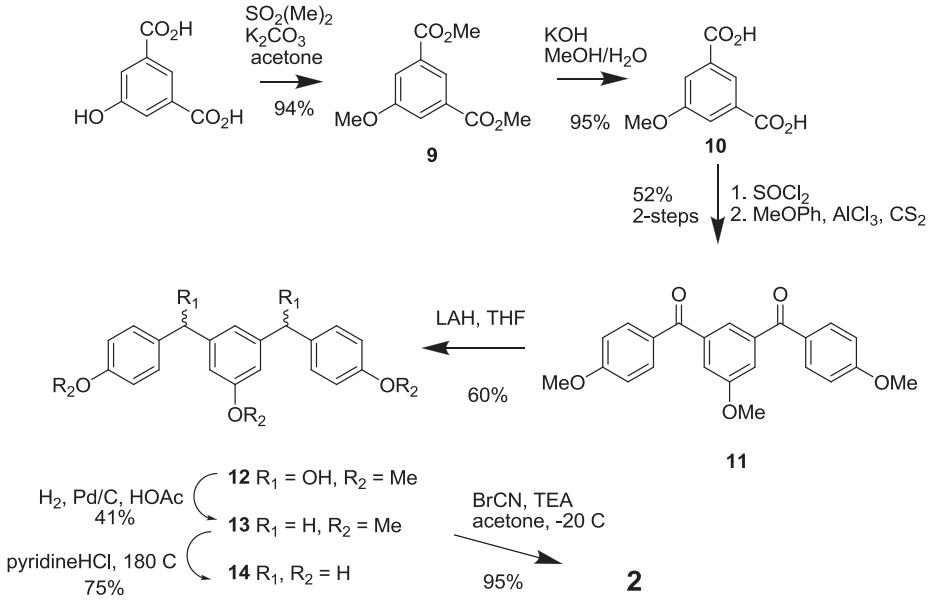

In addition to the new monomers **1** and **2**, the rigid cyanate ester known as ESR-255, originally reported by Shimp *et al.*,[37] was also prepared. These three compounds form a convenient series for comparison purposes: all are composed of three cyanated phenyl rings; ESR-255 has no flexible methylene linkages between rings, **2** has two flexible methylene linkages and is a small-molecule analog of the oligomeric commercial Primaset® PT-30 resin, while **1** has three methylene linkages and thus features the greatest degree of network segment flexibility.

Thermomechanical analyses. By avoiding aliphatic network junctions, themochemical stability comparable to Primaset® PT-30 was maintained in the more flexible network formed from cured **1**, as illustrated by the comparative TGA data in Figure 2. Note that **2** shows similar thermochemical degradation behavior to that previously reported for PT-30,[22,38] as expected. The char yields of over 70% at 600 °C in both nitrogen and air observed in cured **1** are among

the best known for cyanate esters, though many other recent approaches[39-41] may ultimately provide better heat and flame resistance overall, and more detailed long-term testing will be needed to determine the applicability of these results to, for example, the thermo-oxidative stability of composite structures. Despite having the highest aliphatic content and largest molecular weight between network junctions (see Table 1) of all of the materials studied, the network formed by curing **1** was the most chemically stable at elevated temperatures. Comparing the data for cured **1** and cured **2** reveals that the increased phenyl content relative to cyanurate did not improve the char yield.

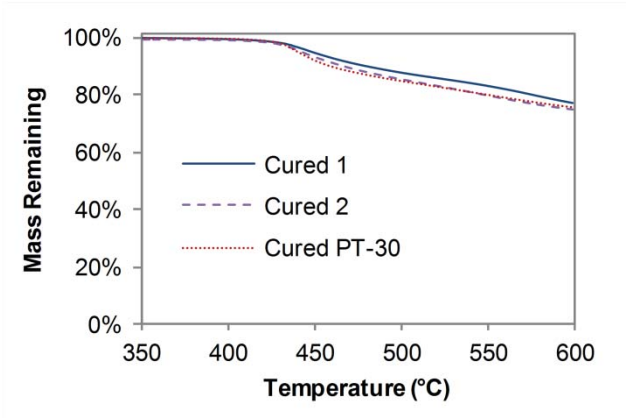

Figure 2a. TGA of cured cyanate ester networks featuring only phenyl rings and methylene bridges, under nitrogen. Note that data for PT-30 has previously been published (reference 22).

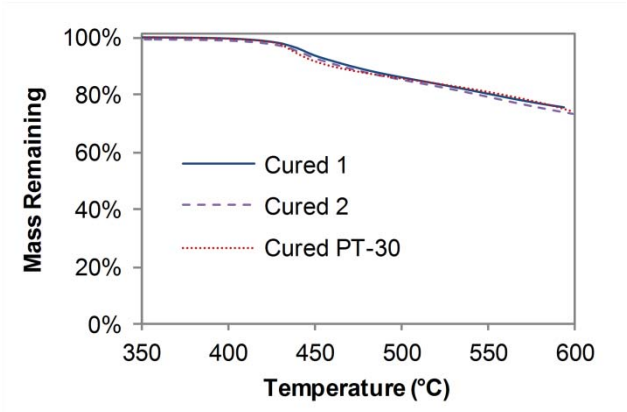

Figure 2b. TGA of cured cyanate ester networks featuring only phenyl rings and methylene bridges, in air.

Table 1

Chemical Characteristics of Cyanurate Networks Relevant to TGA Results

Monomer	Weight Fraction of Pure Cyanurate Network Classified as:			Average Molecular Weight Between Network Junctions (g/mol)[d]	Char Yield in Air at 600 °C (wt%)
	Phenyl[a]	Aliphatic[b]	Cyanurate[c]		
1	0.65	0.09	0.27	157	74
2	0.60	0.08	0.33	127	73
ESR-255	0.60	0.07	0.33	122	59

a. Includes phenyl rings (not cyanurate rings) and their associated hydrogens
b. Includes aliphatic carbons and their associated hydrogens
c. Includes cyanurate rings and their neighboring oxygen bridges
d. Note that branch points in the monomer count as network junctions, and short side-chains (e.g. terminal methyl groups not along a path between junctions) are not included

Figure 3 shows the TGA data for cured ESR-255 compared to **1** and **2**. Despite having as low or lower aliphatic content than either **1** or **2**, the weight loss at high temperatures in ESR-255 was significantly higher than that of both **1** and **2** under both nitrogen and air. As with previously studied flexible tricyanate esters,[22] ESR-255 features an aliphatic network junction comprised of an aliphatic carbon next to a methyl group. Based solely on empirical observation of both these and previously studied cyanate esters without considering mechanistic details, we surmise that while some types of junctions formed by tertiary or quaternary aliphatic carbons may adversely affect thermochemical stability, the presence of methylene bridges between phenyl groups does not significantly detract from the thermochemical stability of highly aromatic cyanate esters. In the specific case of ESR-255, the presence of unreacted cyanate esters groups at high temperatures (as detailed in later sections) may also negatively affect thermochemical stability. The aforementioned conclusions are in general agreement with the results of previous

comparative studies of thermochemical stability in cyanate esters.[1,42] The outstanding thermochemical stability of cured **1** also means that any significant loss in mechanical stiffness below 400 °C in the fully cured network may be attributed definitively to a comparatively low value of the glass transition temperature brought about by more flexible network segments, rather than, as was the case with previously synthesized flexible cyanurate networks,[22] some combination of mechanical and chemical effects.

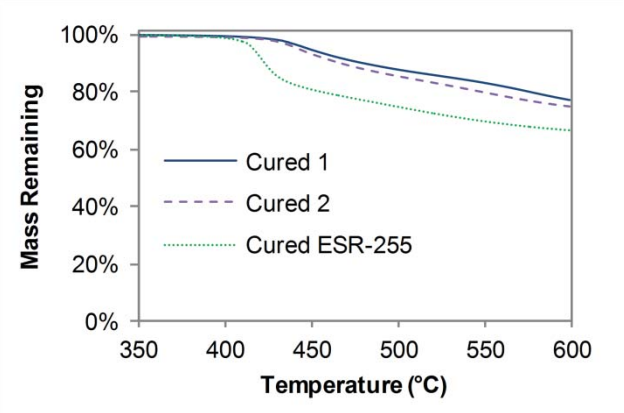

Figure 3a. Comparative TGA of all samples synthesized for this work, under nitrogen.

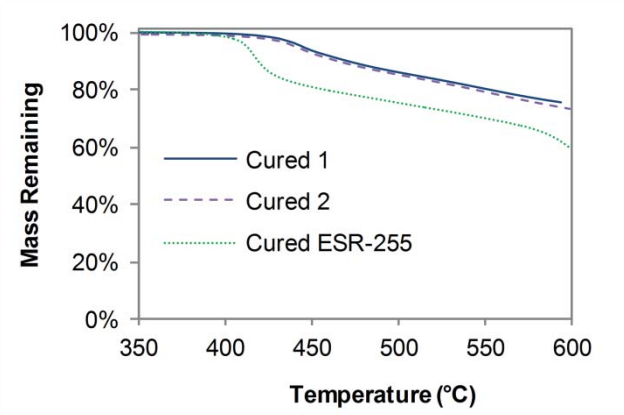

Figure 3b. Comparative TGA of all samples synthesized for this work, in air.

Cure Kinetics and T_g. The impact of selectively incorporating methylene groups on flexibility and the subsequent impact on ease of cure in cyanate esters can be seen by

examination of non-isothermal DSC data. Figure 4 compares the DSC exotherm of monomers **1**, **2**, and ESR-255 calculated using a re-scanned baseline (that is, by subtracting the heat flow seen on the second heating from that seen on the first heating). Whereas **1** exhibited a symmetrical curve with an enthalpy of cyclotrimerization of around 120 kJ/cyanate eq. (slightly higher than expected), **2** exhibited a more asymmetric curve with a close to expected enthalpy of 106 kJ/eq. In contrast, ESR-255 showed a highly asymmetrical curve with an "open" tail. Previous work on cyanate ester resins,[16] as well as our own verification using modulated DSC (see Supporting Information Section S2) indicated that the open-ended nature of the exothermic peak was not due to a baseline shift, but rather resulted from continued slow cure of the sample. Although the apparent enthalpy of cure of ESR-255 based only on the non-isothermal DSC curve was a lower than expected 93 kJ/eq, combined FT-IR and isothermal DSC analysis (see Supporting Information Section S3), determined that the actual enthalpy of cure for ESR-255 was, as expected, 110 ± 7 kJ/eq. Hence ESR-255 attained a conversion of only around 85%, even when heated to 350 °C.

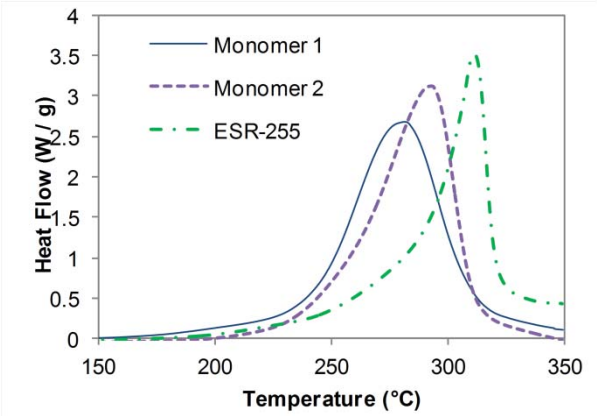

Figure 4. Comparative non-isothermal DSC at 10 °C /min. of tricyanate monomers, showing exothermic region.

Insight into the differing non-isothermal DSC behavior of these three monomers can be gained by considering the evolution of the sample T_g during the DSC scan, as illustrated in Figure 5. The T_g of the sample, which changes due to cure during the DSC scan, is estimated with the aid of the diBenedetto equation from conversion data computed via a running integration of the heat flow. Figures 5a-5c show the sample T_g superimposed on the scan temperature and the heat flow, all as a function of time elapsed from the start of heating at 50 °C. The diBenedetto equation previously has been used quite successfully to predict the T_g of partly cured cyanate esters,[43,44] most likely due to their well-defined cure chemistry. The same well-defined cure chemistry of cyanate esters enables reliable computation of the conversion from the heat flow data.[1] Details of the determination of the diBenedetto equation parameters for monomers **1**, **2**, and ESR-255 are provided in Supporting Information Section S4.

In Figure 5a, it can be seen that the T_g rapidly approaches, but never actually reaches, the scan temperature for monomer **1**. For monomer **2**, as seen in Figure 5b, the T_g surpasses the scan temperature (that is, the sample vitrifies) but then the T_g stabilizes as conversion nears completion, remaining only modestly higher than the scan temperature. For ESR-255, as seen in Figure 5c, even after vitrification, the cure is still far from complete. Additional cure drives the T_g upwards quickly enough that the sample is pushed deeper into the glassy state. The characteristic open-ended "L"-shaped DSC trace thus appears to signify a sample that has vitrified well short of complete conversion. Figures 5b and 5c also show that, as has been well-documented for cyanate esters, cure below T_g can take place at a slow but significant rate. The particular shape of the T_g curve in Figure 5c after vitrification suggests that the "as-cured" T_g should be approximately a linear function of the cure temperature (with a slope greater than one)

for samples that have vitrified but are well short of full conversion, as we recently observed for dicyanate esters.[13]

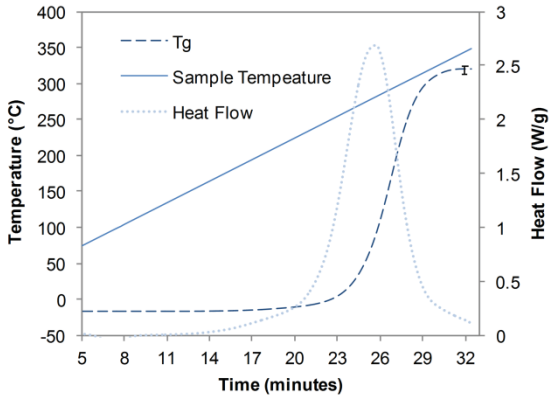

Figure 5a. Comparison of sample temperature and estimate of T_g (with heat flow also plotted for reference) during the DSC scan of **1**.

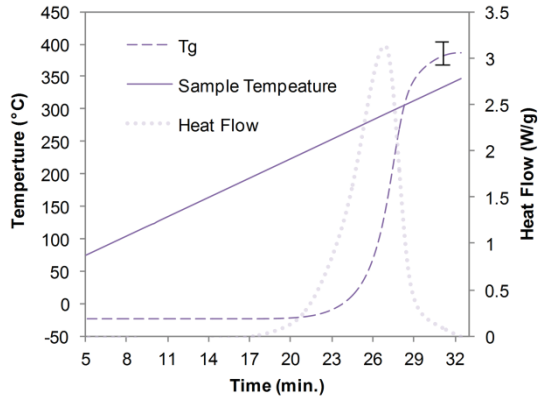

Figure 5b. Comparison of sample temperature and estimate of T_g (with heat flow also plotted for reference) during the DSC scan of **2**. Note that the error in the estimated T_g is comparatively large for **2** due to greater uncertainty in the diBenedetto parameters.

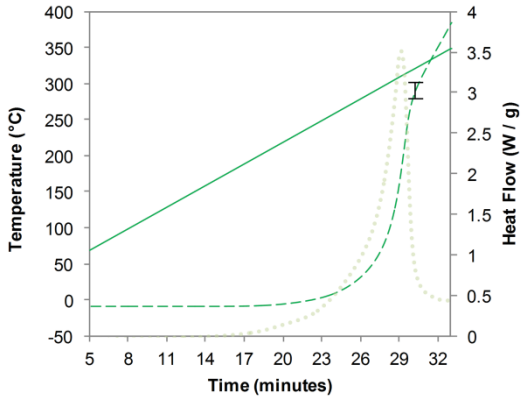

Figure 5c. Comparison of sample temperature and estimate of T_g (with heat flow also plotted for reference) during the DSC scan of ESR-255.

The behavior of ESR-255 seen in Figure 5c has significant implications for the study of high-temperature thermosetting polymers. For one, it suggests that, if following the standard practice of using a "residual heating" to determine the extent of cure by DSC, precautions must be taken to ensure that full cure of the sample is in fact achieved. If not, then a technique such as the combined DSC/FT-IR approach we describe in Supporting Information Section S3 must be utilized if true conversions are to be measured. As the ESR-255 data illustrates, the errors in conversion caused by ignoring incomplete cure may be substantial. The significant amount of cure below T_g implies that *in-situ* cure of vitrified cyanate esters can occur during standard characterization procedures; such *in-situ* cure can lead to incorrect T_g measurements, and may even cause the spurious appearance of two separate T_g's when in fact only one is present.[45] Also, such behavior can cause an "as-cured" T_g values to move outside the range of measurement during a standard DSC scan, leading to the incorrect conclusion that because no glass transition was observed, the "as-cured" T_g must lie outside the scan range. Such phenomena are important to consider when investigating high T_g thermosetting polymers such as cyanate esters.

Due to the possibility of *in-situ* cure, dynamic TMA measurements must be carried out at a very rapid heating rate to determine the "as-cured" T_g for dry samples (shown in Table 2, with plots and more details provided in Supporting Information Section S5). The T_g values were similar after 24 hours of cure at 210 °C under a nitrogen atmosphere with no added catalyst, with the value for the more rigid ESR-255 being slightly lower, perhaps due to its markedly slower cure kinetics. These results contrast with the "fully cured" T_g (determined by re-heating samples previously cured to 350 °C), which, as also seen in Table 2, varied as expected with the rigidity of the network segments and cross-link density. Using the diBenedetto equation to convert the "as cured" T_g values to "as cured" conversions confirms the trend seen in the non-isothermal DSC data, namely, monomer **1** cured the most readily of the three monomers examined, while ESR-255 cured least readily. These results have important technological implications. Specifically, when cyanurate networks are not fully cured, the residual cyanate ester groups are prone to reactions with water at elevated temperature that eventually lead to formation of volatiles, which in turn can lead to blistering and loss of structural integrity.[20,46] Hence, the more rigid ESR-255, although exhibiting a similar "as cured" T_g, provides in some aspects a lower level of performance compared to monomer **1** due to a lower level of conversion (approx. 72% for the former versus about 96% for the latter).

Table 2

Results of Thermomechanical Analysis on Cured Cyanate Esters

Monomer	"As Cured" T_g (°C)[a]	"Fully Cured" T_g (°C)[b]	"As Cured" Conversion[c]
1	280 ± 15	338 ± 10	0.96 ± 0.03
2	286 ± 15	(>340)	0.91 ± 0.03
ESR-255	245 ± 15	(>419)[d]	0.72 ± 0.03

a. After 1 hr at 150 °C followed by 24 hrs at 210 °C, under nitrogen. T_g indicated by peak in loss component of stiffness, corrected for thermal lag and heated at 50 °C / min. to avoid *in-situ* cure.
b. Determined on heating at 10 °C/min., subsequent to initial temperature ramp to 350 °C
c. Based on diBenedetto equation (see Supporting Information Section S4)
d. Heated to decomposition, which takes place either before or simultaneous with mechanical softening

In order to better understand the reasons for the lack of complete cure in ESR-255, a more detailed analysis of the cure kinetics based on the Kamal model[47] analyzed via a modified form of Kenny's graphical method[48] was undertaken using isothermal DSC data for monomers **1**, **2**, and ESR-255, with baselines determined in a manner similar to that reported by Sheng et al.[44] Full details and complete results are provided in Supporting Information Section S6. The activation energy, the graphical determination of which is depicted in Figure 6, was only slightly lower for monomer **1** than for monomer **2** or ESR-255 for the auto-catalytic portion of the cure, suggesting that the rigidity of the ESR-255 monomer was not a major impediment to cure prior to gelation. Interestingly, the initial rates of conversion, as seen in Figure 7 at 290 °C, for example, were always significantly higher in monomers **1** and **2** than for ESR-255. The final conversions achieved were also always much lower in ESR-255, despite ample time to reach complete conversion based on the observed rate of cure at the higher temperatures.

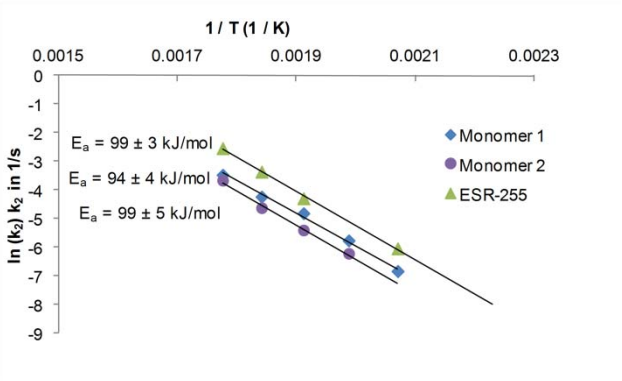

Figure 6. Arrhenius plot of auto-catalytic rate constant k_2 (prior to gelation) for the cyanate ester monomers studied. Note that, because the exponents for each monomer are different, a higher k_2 value does not necessarily translate into a faster reaction rate.

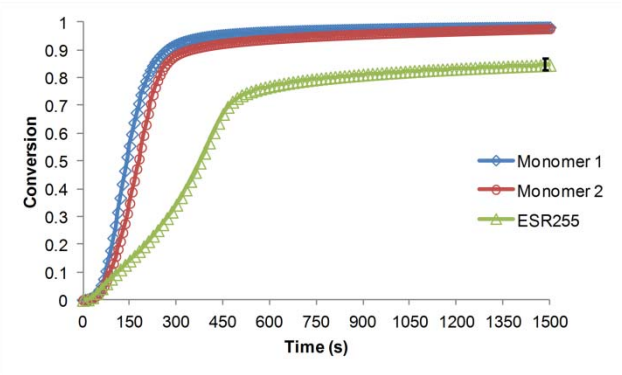

Figure 7. Conversion as a function of time for cyanate esters cured at 290 °C under nitrogen.

To help explain the observed conversion behavior, an estimate of the T_g of the cyanurate networks during the isothermal DSC cure was created (with the same procedure based on the diBenedetto equation used for Figure 5), and is shown in Figure 8. Although the slower cure kinetics of ESR-255 lead to an initially slower increase in T_g, in all cases, the rise in T_g slows dramatically as the T_g reaches the cure temperature (290 °C), causing the sample to vitrify. Since cyanate esters possess the capability to cure slowly in the glassy state, the T_g continues to

rise slowly, even after vitrification. In monomer **1**, vitrification does not take place until conversion is nearly complete, thus further conversion is limited by the low concentration of remaining unreacted groups and further increases in T_g are small. By contrast, in ESR-255, vitrification takes place well short of full conversion, and thus the rate of conversion in the glassy state appears to be somewhat higher. This result, when combined with a higher sensitivity of the T_g to small changes in conversion (as seen in the diBenedetto parameters for ESR-255), leads to a comparatively rapid rise in T_g, at least initially, after vitrification in ESR-255.

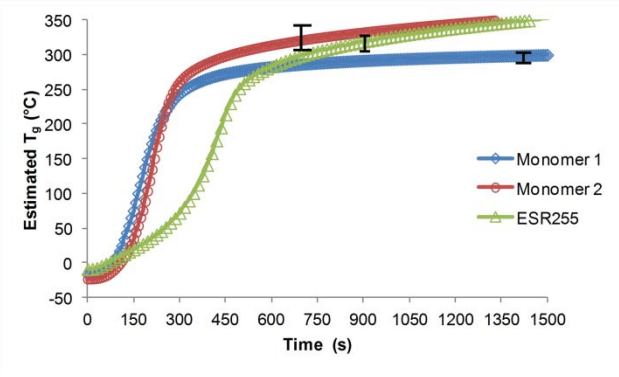

Figure 8. Estimated T_g as a function of time for cyanate esters cured at 290 °C under nitrogen.

Although the data shown in Figure 8 are for relatively short cure times and involve T_g values only modestly higher than the cure temperature, the data in Table 2 confirm that, if given sufficient time, T_g values well in excess of the cure temperature are possible. As with the short-term cure at higher temperatures, however, it would appear that the T_g values tend to converge over time. The faster cure and somewhat higher "as cured" (for 210 °C for 24 hours under nitrogen) T_g values for monomers **1** and **2** than for ESR-255 could be due to differing levels of impurities in the samples. van't Hoff purity determinations (see Supporting Information, Section S7) showed a substantially higher apparent purity for ESR-255. However, a small sample of

monomer **1**, after purification by flash chromatography through silica gel in an ethyl acetate/hexane mixture, showed no differences in either cure kinetics or apparent "as cured" T_g despite a significant increase in the van't Hoff purity estimate (details provided in Supporting Information Section S8).

A more interesting explanation for the data in Table 2 is that, paradoxically, more flexible network segments in cyanate esters allow for higher "as cured" T_g due to their ability to facilitate continued cure after vitrification, as described in the Introduction. In fact, somewhat higher "as cured" T_g values for more flexible networks have been reported in both dicyanates[13] and other tricyanates[15] under similar cure conditions. Because the differences involved are fairly small, more intensive measurements, perhaps in combination with recent developments in the molecular modeling of cyanurate networks,[49,50] will be needed to determine with certainty whether, and under what conditions, a more flexible network can routinely provide a higher T_g. Despite being much higher than the cure temperature, the "as cured" T_g values for these networks are much more similar than the corresponding set of fully-cured T_g values. These results imply that the parameters of cure process, rather than the rigidity of network segments, are the primary determinants of "as cured" T_g in these networks.

Other Physical Properties. The lower cyanurate ring density of monomer **1** would be expected to lead to a lower moisture uptake compared to monomer **2** and ESR-255, based on previous correlations developed for cyanurate networks at high conversion.[51] Indeed, as Table 3 shows, such was the case. In fact, the moisture uptake of cured **1**, at just 2.2% by weight, is among the lowest observed for a cyanurate network with a correspondingly high fully-cured T_g, though similar tricyanates have come fairly close.[52] Although the lower moisture uptake in

combination with the similar dry T_g of cured **1** compared to cured **2** and ESR-255 might be expected to lead to a significantly higher "wet" T_g for cured **1** compared to both cured **2** and ESR-255, previous work on cyanate esters has shown that the drop in T_g on exposure to hot water becomes significantly less pronounced as conversion decreases.[13] Therefore, the lower conversion of cured ESR-255 is expected to compensate somewhat for the higher moisture uptake, resulting in more modest differences in "wet" T_g, as observed (see Table 3).

Table 3

Other Key Physical Properties of Cured Cyanate Esters

Monomer	"As Cured" Density (g/cc)	Theoretical Cyanurate Ring Density at Full Cure (mmol / cc)	Moisture Uptake (wt%)	"Wet" T_g (°C)
1	1.171 ± 0.003	2.48 ± 0.01	2.2 ± 0.2	238 ± 12
2	1.297	3.40	3.3	232
ESR-255	1.270	3.33	3.5	224

Taken together, these results have important implications for the manner in which thermosetting polymers are selected for high-temperature applications. Resins are typically evaluated solely on the basis of a "cured" T_g, with catalyst packages then selected in order to attain sufficient cure for a given set of processing conditions. In such a scenario, a higher fully-cured T_g is most often deemed a superior choice. This prevalent heuristic, however, ignores both the steep dependence of the T_g on the extent of cure, and the effect of different catalyst packages on long-term performance degradation. For cyanurate networks in particular, these two effects are especially pronounced in comparison to other types of thermosetting polymer networks, and thus the prevalent heuristic is less appropriate.

When there is a steep dependence of T_g on the extent of cure, it is most likely, as seen in the data presented herein, that the T_g will reach and eventually exceed the cure temperature, causing the cure process to slow dramatically. As a result, the "as cured" T_g of the network will be limited largely by the cure conditions themselves rather than the fully cured T_g, provided that the fully cured T_g is high enough. As a result, systems with a higher fully cured T_g will exhibit a lower extent of cure, which in many cases is detrimental to long-term performance.[20] The extent of cure (and hence, the attainable T_g) may be increased by substitution of a more active catalyst package, with the trade-off that more active catalyst packages may also accelerate degradation. Under such circumstances, the best performing network may not be the one with the highest fully cured T_g. The optimal network may well be one in which the fully cured T_g equals the maximum attainable T_g for a given set of cure conditions and a catalyst package with acceptable degradation penalties.

As an example, consider the networks formed from the three monomers synthesized in this study. If the cure process were constrained to a temperature of 210 °C and an available time of 24 hours (such constraints may be imposed by, for instance, by the thermal stability of tooling or resin transfer equipment), then, for systems with no added catalyst, the maximum T_g attainable appears to be, on average, roughly 250 - 280 °C. In such cases, a network with a fully cured T_g of just over 280 °C would be ideal, because such a system would exhibit both the highest attainable T_g and full cure. Networks with a higher fully cured T_g, such as ESR-255, will, after cure, attain the same "as cured" T_g (250 - 280 °C), but will, as a result, exhibit significantly less than full conversion, leading to potential long-term degradation. Therefore, for many practical situations, particularly with cyanurate networks, there will exist monomers that form networks that are "too rigid", that is, T_g of the fully-cured network is prohibitively high. The discovery of

monomer **1**, which exhibits a lower T_g in the fully cured state with no loss in thermochemical stability, and with a low water uptake, thus represents a significant step forward, because it will allow for the formation of optimal networks under a wider variety of processing conditions (particularly those involving lower temperatures or milder catalysts) than has previously been possible.

Conclusions

The selective use of methylene spacers in the network segments of highly aromatic thermosetting cyanate ester resins has proven to be an especially valuable technique for providing controlled segmental flexibility while maintaining thermochemical stability and low moisture uptake. In particular, a newly synthesized monomer, 1,3,5-tris[(4-cyanatophenylmethyl)]benzene, exhibits char yields near 75% at 600 °C in air, equivalent to the best known common cyanate ester resins, with a moisture uptake of only 2.2% after 96 hours immersed in 85 °C water. The dry T_g of the fully-cured network produced from this monomer was around 320 °C. Because fully-cured networks prepared from similar monomers with fewer methylene spacers exhibited significantly higher T_g's, the networks did show the expected effects of higher segmental flexibility. However, the T_g of all networks studied was similar after a 24-hour cure at 210 °C, as was the "wet" T_g. Therefore, in practical curing and use situations, the T_g's of these networks are likely to be primarily limited by parameters of the cure process itself, specifically, the dramatic slowing of the cure rate that occurs upon vitrification and the degree of catalysis, regardless of the degree of flexibility. In addition, when T_g's of the fully cured networks are sufficiently high, the more flexible networks will exhibit the highest conversions for a given cure process. Because near complete conversion of cyanate esters typically provides networks with superior physical properties, in this case the most flexible network, with its high

thermochemical stability and low water uptake, may to be the most desirable. These results illustrate that, in contrast to the prevailing heuristics for improving the performance of high-temperature thermosetting polymer networks, a more flexible network with a lower fully-cured T_g can offer an optimal combination of thermomechanical and thermochemical performance. Both the newly synthesized materials, as well as the new insights into structure-process-property relationships that they illustrate, are expected to help advance the state of the art in high-performance polymeric materials for the electronics, aerospace, and energy storage industries.

Acknowledgements

The support of the Office of Naval Research, the Air Force Office of Scientific Research, the Air Force Research Laboratory, and the National Research Council Research Associateship Program (JTR) are gratefully acknowledged. The authors thank Dr. Suresh Suri of AFRL for helpful advice on the flash chromatography of monomer **1**.

Supporting Information Available

X-ray crystal structure and NMR data (Section S1); modulated DSC data (Section S2); determination of enthalpy of cure by DSC/IR technique (Section S3); diBenedetto equation parameters (Section S4); TMA plots and detailed description (Section S5); detailed cure kinetics analysis (Section S6); van't Hoff analysis of monomers (Section S7); properties of highly purified **1** (Section S8). This information is available free of charge via the Internet at http://pubs.acs.org/.

Experimental Section:

Synthesis of the monomers 1,2 and ESR-255

General consideration and instrumentation. The melting points were collected on a Mel-Temp II from Laboratory Devices (Holliston, MA) and are not corrected. All NMR data were collected on a Bruker Avance II 300 MHz spectrometer (^{1}H at 300 MHz, ^{13}C at 75 MHz). Nuclear magnetic resonance data (free-induction decays) were processed using NUTS software from Acorn NMR (Livermore, CA). All spectra are referenced to solvent or tetramethylsilane. The 1,1,1-tris(4-hydroxphenyl)ethane was purchased from TCI America (Portland) and all other reagents were purchased from Sigma-Aldrich (Milwaukee). Elemental analyses were performed by Atlantic Microlab, Inc. (Norcross, GA).

Synthesis of monomer 1

4-Methoxybenzoylacetaldehyde potassium salt hydrate (**4**)

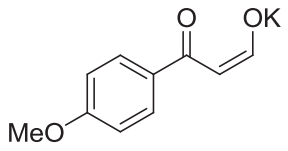

4

A round-bottomed flask (500 mL) equipped with magnetic stirring bar, addition funnel and N_2 bubbler was charged with KO*t*Bu (9.3 g, 83 mmol, 1 equiv) and anhydrous THF (100 mL). After complete dissolution, 4-methoxyacetophenone (12.45 g, 83 mmol) was added and after 20 min, methyl formate (4.98 g, 5.1 mL, 83 mmol, 1 equiv) was added dropwise. The mixture was stirred at rt for 2 h and then diluted with hexanes (200 mL). The mixture was filtered through a medium porosity glass frit. The product was dried to a constant weight in a vacuum oven (10 torr, 50 °C) overnight. The yield was 15.3 g (85 %). Mp > 240 °C. ^{1}H NMR (300 MHz,

DMSO; δ, ppm): 9.34 (d, J = 9.6 Hz, 1H), 7.68 (d, J = 8.5 Hz, 2H), 6.85 (d, J = 8.7 Hz, 2H), 5.37 (d, J = 9.5 Hz, 1H), 3.75 (s, 3H). Elemental analysis calcd for $C_{10}H_9KO_3 \cdot 0.4\ H_2O$: C, 53.74; H, 4.42; found: C, 53.36; H, 4.07%.

1,3,5-Tri(4-methoxybenzoyl)benzene (**5**)

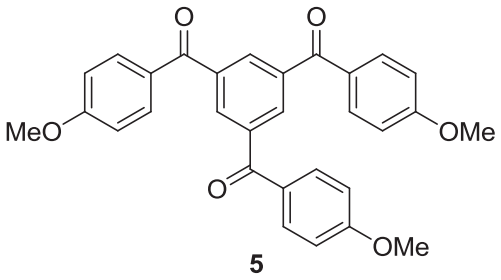

5

A round-bottomed flask (250 mL) equipped with magnetic stirring bar and reflux condenser was charged with **4** (15.1 g, 68 mmol) and glacial HOAc (50 mL). The mixture was refluxed for 30 min. After cooling to rt, the precipitate was filtered on a coarse porosity glass frit. Recrystallization from MeCN gave the title compound as clear, pale yellow rhombs. The yield was 9.2 g (82 %). Mp 179-181 °C [lit.[23] 177 °C]. ^{1}H NMR (300 MHz, $CDCl_3$; δ, ppm): 8.29 (s, 3H), 7.86 (d, J = 8.9 Hz, 6H), 6.98 (d, J = 8.9 Hz, 6H), 3.89 (s, 9H). ^{13}C NMR (75 MHz, $CDCl_3$; δ, ppm): 193.98, 163.93, 138.85, 133.34, 132.79, 129.33, 114.08, 55.73. Elemental analysis calcd for $C_{30}H_{24}O_6$: C, 74.99; H, 5.03; found: C, 74.87; H, 5.01%.

Racemic 1,3,5-Tris[(4-methoxyphenyl)hydroxymethyl]benzene (**6**)

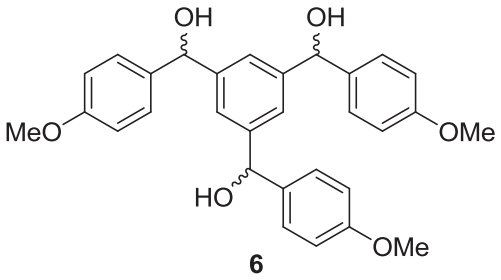

6

A round-bottomed flask (2 L) equipped with magnetic stirring bar, reflux condenser and N_2 bubbler was charged with **5** (20 g, 41 mmol) and EtOH (1 L). The mixture was refluxed and

pulverized $NaBH_4$ (4.7 g, 125 mmol, 3 equiv) was added in portions over 2 h. Reflux was continued 8 h resulting in a deep red solution. The mixture was cooled to rt and quenched with HOAc. The mixture was poured into H_2O (2 L) and the white precipitate was collected on a medium porosity glass frit. Recrystallization from MeCN gave the title compound as a white, microcrystalline powder. The yield was 18 g (90 %). Mp 181-183 °C. ^{1}H NMR (300 MHz, DMSO; δ, ppm): 7.27-7.13 (m, 9H), 6.83 (d, J = 9.4 Hz, 6H), 5.67 (d, J = 3.7 Hz, 3H), 5.55 (d, J = 3.7 Hz, 3H), 3.70 (s, 9H). ^{13}C NMR (75 MHz, DMSO; δ, ppm): 158.00, 145.32, 137.82, 122.39, 113.32, 74.01, 54.98. Elemental analysis calcd for $C_{30}H_{30}O_6$: C, 74.06; H, 6.21; found: C, 74.04; H, 6.26%.

1,3,5-Tris[(4-methoxyphenyl)methyl]benzene (**7**)

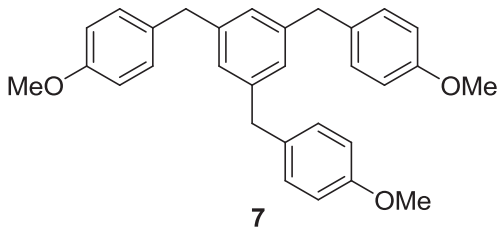

7

A round-bottomed flask (500 mL) equipped with magnetic stirring bar, reflux condenser and N_2 bubbler was charged with **6** (12 g, 25 mmol), 5 % Pd/C catalyst (2 g), ammonium formate (8.8 g, 140 mmol, 6 equiv) and glacial HOAc (250 mL). The mixture was refluxed for 5 h. After cooling to rt, the mixture was filtered through diatomaceous earth to remove the catalyst. The filtrate was partitioned between H_2O (500 mL) and Et_2O (500 mL). The organic layer was separated and washed with H_2O (500 mL) and then brine (500 mL). Rotary evaporation of the

volatiles gave a colorless oil that gradually solidified into a white, waxy solid. The yield was 9.87 g (91 %). Mp 55-57 °C. ^{1}H NMR (300 MHz, DMSO; δ, ppm): 7.07 (d, J = 8.6 Hz, 6H), 6.85 (s, 3H), 6.81 (d, J = 8.6 Hz, 6H), 3.76 (s, 6H), 3.69 (s, 9H). ^{13}C NMR (75 MHz, DMSO; δ, ppm): 157.48, 141.71, 133.09, 129.49, 126.58, 113.72, 54.90, 54.81, 40.16. Elemental analysis calcd for $C_{30}H_{30}O_3$: C, 82.16; H, 6.89; found: C, 82.08; H, 6.88%.

1,3,5-Tris[(4-hydroxyphenyl)methyl]benzene (**8**)

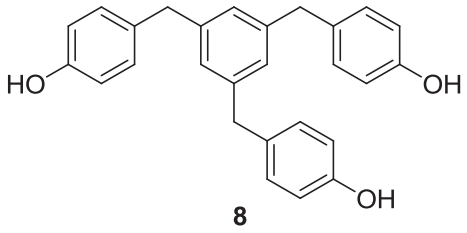

8

A round-bottomed flask (500 mL) equipped with magnetic stirring bar and reflux condenser was charged with **7** (9.87 g, 22 mmol) and pyridine hydrochloride (50 g, 434 mmol, 19 equiv). The mixture was refluxed for 4 h. The mixture was carefully diluted with H_2O (300 mL) whereby a white precipitate formed. The precipitate was collected on a medium porosity glass frit. The precipitate was dissolved in EtOAc (100 mL) and washed with H_2O (100 mL) followed by brine (100 mL). After drying over anhydrous $MgSO_4$, the solvent was rotary evaporated leaving a white solid. Recrystallization from MeOH/H_2O gave the title compound colorless plates. The yield was 8 g (90 %). Mp 205-207 °C. ^{1}H NMR (300 MHz, DSMO; δ, ppm): 9.32 (s, 3OH), 6.93 (d, J = 8.6 Hz, 6H), 6.81 (s, 3H), 6.62 (d, J = 8.4 Hz, 6H), 3.69 (s, 6H). ^{13}C NMR (75 MHz, DMSO; δ, ppm): 155.61, 142.24, 131.86, 129.82, 126.78, 115.46, 40.58. Elemental analysis calcd for $C_{27}H_{24}O_3$: C, 81.79; H, 6.10; found: C, 81.48; H, 6.16%.

1,3,5-Tris[(4-cyanatophenyl)methyl]benzene (**1**)

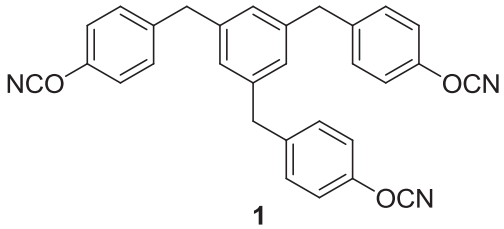

1

A round-bottomed flask (250 mL) equipped with magnetic stirring bar, N_2 bubbler and addition funnel was charged with **8** (3 g, 7 mmol), BrCN (2.81 g, 26 mmol, 3.5 equiv) and acetone (100 mL). The mixture was cooled in a -20 °C bath before TEA (2.1 g, 21 mmol, 3 equiv) was added dropwise in 20 min. Copious solids (TEA·HBr) precipitated during the addition. After 2h, the mixture was poured into cold H_2O (250 mL) and extracted with Et_2O (2X 100 mL). The extracts were collected and washed with H_2O (200 mL) followed by saturated aqueous $NaHCO_3$ (100 mL) and finally brine (100 mL). After drying over anhydrous $MgSO_4$, rotary evaporation left an off-white solid. Recrystallization from EtOH gave the title compound as white needles. The yield was 1.97 g (60 %) Mp 97-99 °C. ^{1}H NMR (300 MHz, $CDCl_3$; δ, ppm): 7.21 (s, 12H), 6.81 (s, 3H), 3.91 (s, 6H). ^{13}C NMR (75 MHz, $CDCl_3$; δ, ppm): 151.53, 141.19, 139.99, 130.85, 127.75, 115.54, 109.05, 40.99. Elemental analysis calcd for $C_{30}H_{21}N_3O_3$: C, 76.42; H, 4.49; N, 8.91; found: C, 76.19; H, 4.37; N, 8.89%.

Synthesis of Monomer 2

Dimethyl 5-methoxyisophthalate (**9**)

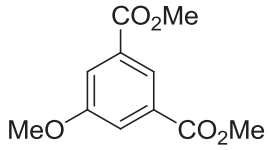

9

A round-bottomed flask (1 L) equipped with magnetic stirring bar and reflux condenser was charged with 5-hydroxyisophthalic acid (18.2 g, 100 mmol), acetone (300 mL), freshly pulverized anhydrous K_2CO_3 (40 g, 289 mmol, 2.8 equiv) and dimethyl sulfate (50 mL, 66.5 g,

520 mmol, 5.2 equiv). After refluxing overnight, the mixture was cooled and poured into H_2O (1 L). The resulting precipitate was collected on a medium porosity glass frit and air-dried several hours. Recrystallization from cyclohexane gave the title compound as a white microcrystalline powder. The yield was 21.1 g (94 %). Mp 110-112 °C [lit.[53] 110-111 °C]. Elemental analysis calcd for $C_{11}H_{12}O_5$: C, 58.93; H, 5.39; found: C, 58.66; H, 5.31%.

5-Methoxyisophthalic acid monohydrate (**10**)

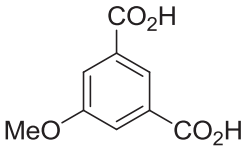

10

A round-bottomed flask (500 mL) equipped with magnetic stirring bar was charged with **9** (21.1 g, 94 mmol), MeOH (200 mL) and a solution of KOH (16 g, 285 mmol, 3 equiv) in H_2O (50 mL). The mixture was refluxed for 6 h. After cooling to rt, the mixture was poured into H_2O (500 mL) and acidified to pH 3 by dropwise addition of conc. HCl. The precipitate was collected on a medium porosity glass frit. Recrystallization from glacial HOAc gave the title compound as a colorless needles. The yield was 19.1 g (95 %). Mp 270-272 °C [lit.[54] 267-268 °C]. ^{1}H NMR (300 MHz, DMSO; δ, ppm): 13.20 (bs, 2 CO_2H), 8.09 (s, 1H), 7.61 (s, 2H), 3.83 (s, 3H). ^{13}C NMR (75 MHz, DMSO; δ, ppm): 167.11, 159.37, 133.74, 122.56, 118.28, 55.65. Elemental analysis calcd for $C_9H_8O_5 \cdot H_2O$: C, 50.47; H, 4.71; found: C, 50.92; H, 4.63%.

3,5-Bis(4-methoxybenzoyl)anisole (**11**)

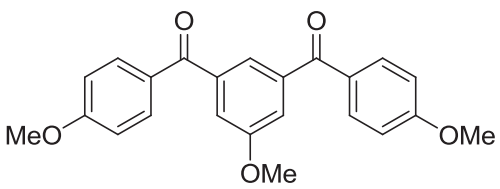

11

A round-bottomed flask (200 mL) equipped with magnetic stirring bar and reflux condenser was charged with **10** (18.2 g, 85 mmol) and $SOCl_2$ (25 mL). An N_2 bubbler piped to a caustic wash bottle was attached and the mixture was gently refluxed for 5 h. The excess $SOCl_2$ was distilled under reduced pressure (10 torr) leaving an off-white solid of 5-methoxyisophthaloyl dichloride. The latter was transferred to a 500 mL round-bottomed flask equipped with magnetic stirring bar and addition funnel with carbon disulfide (50 mL). The mixture was cooled in an ice bath before $AlCl_3$ (17.69 g, 134 mmol, 2 equiv) was added in one portion. The addition funnel was charged with anisole (29 g, 270 mmol, 4 equiv) which was added over dropwise over 30 min. The cooling bath was removed and the mixture was stirred at rt for 3 h. The mixture was carefully poured onto cracked ice (500 g). The mixture was extracted with EtOAc (3X 100 mL). The extracts were collected and washed with H_2O (500 mL) followed by brine (500 mL). After drying over anhydrous $MgSO_4$, the solvent was rotary evaporated leaving a pale yellow oil that eventually solidified under vacuum. Recrystallization of the crude product from EtOH gave the title compound as small colorless needles. The yield was 16.61 g (52 %). Mp 115-117 °C. ^{1}H NMR (300 MHz, $CDCl_3$; δ, ppm): 7.84 (d, J = 8.6 Hz, 4H), 7.62 (t, J = 1.4 Hz, 1H), 7.49 (d, J = 1.2 Hz, 2H), 6.96 (d, J = 9.0 Hz, 4H), 3.91 (s, 3H), 3.88 (s, 6H). ^{13}C NMR (75 MHz, $CDCl_3$; δ, ppm): 194.57, 163.69, 159.71, 139.76, 132.72, 129.78, 123.36, 118.27, 113.88, 55.94, 55.66. Elemental analysis: calcd for $C_{23}H_{20}O_5$: C, 73.39; H, 5.36; found: C, 73.65; H, 5.23%.

Racemic 3,5-Bis[(4-methoxyphenyl)hydroxymethyl)]anisole (**12**)

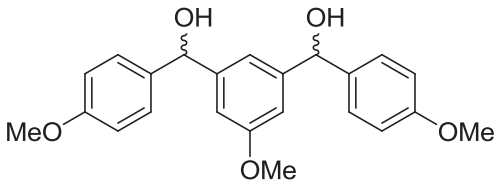

12

A round-bottomed flask (1 L) equipped with magnetic stirring bar was charged with LAH (3.3 g, 87 mmol, 1.9 equiv) and anhydrous THF (500 mL). An N_2 bubbler, addition funnel and reflux condenser were equipped. The mixture was stirred in an ice bath and a solution of **11** (16.61 g, 44 mmol) in THF (50 mL) was charged to the funnel. The addition was made as a gentle stream over 1 h. After stirring at rt for 3 h the reduction was complete. The mixture was carefully quenched by addition of H_2O (3.3 mL) followed by 15 % NaOH (3.3 mL) and finally H_2O (9.9 mL). After stirring overnight, the mixture was filtered through a medium porosity glass frit. The filtrate was rotary evaporated leaving a crude solid. Recrystallization from toluene gave the title compound as a white powder. The yield was 10.1 g (60 %). ^{1}H NMR (300 MHz, $CDCl_3$/DMSO; δ, ppm): 7.27-7.20 (m, 4H), 7.02-6.93 (m, 1H), 6.82-6.74 (m, 6H), 5.63 (s, 2H), 4.22 (bs, 2 OH), 3.73 (s, 6H), 3.69 (s, 3H). ^{13}C NMR (75 MHz, $CDCl_3$/DMSO; δ, ppm): 159.43, 159.35, 158.41, 158.40, 146.43, 146.37, 136.87, 136.85, 127.63, 127.59, 117.09, 116.99, 113.31, 110.43, 110.31, 74.83, 74.81, 54.97, 54.93. Elemental analysis calcd for $C_{23}H_{24}O_5$: C, 72.61; H, 6.36; found: C, 72.88; H, 6.42%.

3,5-Bis[(4-methoxyphenyl)methyl)]anisole (**13**)

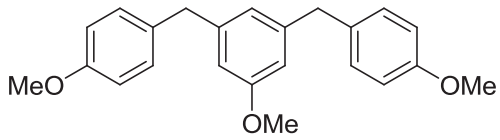

13

A round-bottomed flask (500 mL) equipped with magnetic stirring bar and reflux condenser was charged with a mixture of **12** (10.1 g, 26 mmol), glacial HOAc (300 mL) and 5 % Pd/C (2 g). The mixture was vigorously stirred and heated near boiling under an H_2 atmosphere (1 torr). After 18 h, the mixture was cooled to rt and the catalyst was filtered. Rotary evaporation left an oil which was chromatographed on silica gel eluting with 20 % EtOAc in hexanes. Rotary

evaporation of the fractions gave a colorless oil. Reduced pressure (0.1 torr) distillation gave the title compound in analytically pure form. The yield was 3.87 g (41 %). ^{1}H NMR (300 MHz, $CDCl_3$; δ, ppm): 7.08 (d, J = 8.6 Hz, 4H), 6.81 (d, J = 8.8 Hz, 4H), 6.62 (t, J = 1.4 Hz, 1H), 6.53 (d, J = 1.4 Hz, 2H), 3.84 (s, 4H), 3.77 (s, 6H), 3.69 (s, 3H). ^{13}C NMR (75 MHz, $CDCl_3$; δ, ppm): 160.10, 158.21, 143.28, 133.33, 130.04, 122.21, 114.09, 112.35, 55.46, 55.31, 41.26. Elemental analysis calcd for $C_{23}H_{24}O_3$: C, 79.28; H, 6.94; found: C, 79.31; H, 6.94%.

3,5-Bis[(4-hydroxyphenyl)methyl)]phenol (**14**)

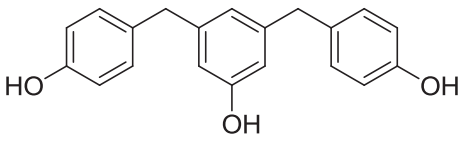

14

A round-bottomed flask (250 mL) equipped with magnetic stirring bar and reflux condenser was charged with **13** (3.87 g, 11 mmol) and pyridine hydrochloride (26 g, 222 mmol, 20 equiv). The mixture was heated by heating mantle to 180 °C for 5 h. After cooling to rt, the mixture was diluted with H_2O (250 mL) whereupon a tan precipitate eventually formed. Filtration followed by recrystallization of the solid from toluene/MeOH gave the title compound as a white, microcrystalline powder. The yield was 2.5 g (75 %). Mp 183-186 °C. ^{1}H NMR (300 MHz, $CDCl_3$; δ, ppm): 9.17 (2, 2OH), 9.11 (s, 1OH), 6.97 (d, J = 8.3 Hz, 4H), 6.67 (d, J = 8.0 Hz, 4H), 6.50 (s, 1H), 6.35 (s, 2H), 3.67 (s, 4H). ^{13}C NMR (75 MHz, $CDCl_3$; δ, ppm): 157.33, 155.48, 143.13, 131.35, 129.59, 119.72, 115.11, 113.06, 40.32. Elemental analysis calcd for $C_{20}H_{18}O_3$: C, 78.41; H, 5.92; found: C, 78.31; H, 5.78%.

3,5-Bis[(4-cyanatophenyl)methyl)]phenylcyanate (**2**)

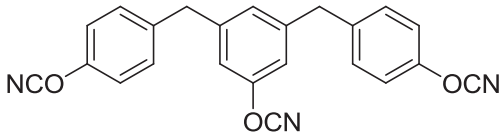

2

A round-bottomed flask (250 mL) equipped with magnetic stirring bar was charged with **14** (1 g, 3.3 mmol), BrCN (1.38 g, 13 mmol, 3.9 equiv) and acetone (50 mL). The mixture was stirred in a -20 °C cooling bath while TEA (1.07 g, 10.6 mmol, 3.2 equiv) was added dropwise. Copious solids (TEA·HBr) precipitated during the addition. After stirring 2 h, the mixture was poured into H_2O (100 mL). The mixture was extracted with EtOAc (2X 50mL). The extracts were combined and washed with H_2O (100 mL) followed by brine (100 mL). After drying over anhydrous $MgSO_4$, the solvent was rotary evaporated leaving the crude product. The title compound was obtained as colorless needles by recrystallization from *i*-PrOH. The yield was 1.2 g (95 %). Mp 119-121 °C. ^{1}H NMR (300 MHz, $CDCl_3$; δ, ppm): 7.24 (m, 8H), 6.94 (s, 2H), 6.92 (s, 1H), 3.99 (2, 4H). ^{13}C NMR (75 MHz, $CDCl_3$; δ, ppm): 153.47, 151.86, 143.97, 138.55, 130.97, 127.92, 115.89, 113.95, 108.89, 108.71, 40.82. Elemental analysis calcd for $C_{23}H_{15}N_3O_3$: C, 72.43; H, 3.96; N, 11.02; found: C, 72.43; H, 3.91; N, 10.98%.

Synthesis of ESR-255

1,1,1-Tris(4-cyanatophenyl)ethane (ESR-255)

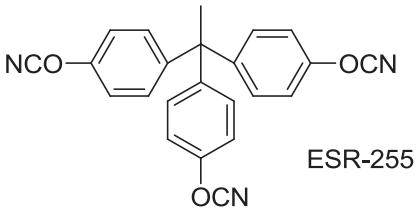

ESR-255

A round-bottomed flask (250 mL) equipped with magnetic stirring bar and addition funnel was charged with 1,1,1-tris(4-hydroxyphenyl)ethane (10.0 g, 32 mmol), BrCN (13.78 g, 130 mmol, 4 equiv) and anhydrous acetone (100 mL). The mixture was cooled in a -20 °C bath before TEA

(11.55 g, 114 mmol, 3.5 equiv) was added dropwise. During the addition, copious solids (TEA·HBr) precipitated. Afterwards, the mixture was stirred in an ice bath for 30 min before pouring into crushed ice and H_2O (500 mL). The mixture was extracted with Et_2O (3X 100 mL). The extracts were collected and washed with H_2O (100 mL) followed by brine (100 mL). After drying over anhydrous $MgSO_4$, the solvent was rotary evaporated leaving an off-white solid (12.59 g). The crude product was recrystallized from EtOH to give the title compound as a white powder. The yield was 6.5 g (52 %). Mp 113-115 °C [lit.[55] 104 °C]. ^{1}H NMR (300 MHz, $CDCl_3$; δ, ppm): 7.28 (d, J = 9.1 Hz, 6H), 7.17 (d, J = 9.0 Hz, 6H), 2.22 (s, 3H). ^{13}C NMR (75 MHz, $CDCl_3$; δ, ppm): 151.48, 146.58, 130.57, 115.34, 108.65, 51.69, 30.92. Elemental analysis calcd for $C_{23}H_{15}N_3O_3$: C, 72.43; H, 3.96; N, 11.02; found: C, 72.35; H, 3.88; N, 11.06%.

Cured network preparation and characterization. Cured resin samples were prepared by melting the monomer powder at 115 - 130 °C at a reduced pressure of 300 mm Hg for 30 minutes, then pouring into either a silicone casting mold (13 mm diameter x 3 mm discs) for multi-step cure, or into a 6 mm diameter x 1 mm high aluminum pan for single-step cure. Multi-step cure involved heating in an oven under nitrogen to 150 °C for 1 hour, followed by 210 °C for 24 hours, with subsequent cooling to below 150 °C prior to de-molding. Heating ramps for multi-step cures were 5 °C / min. Additional details such as the mold fabrication procedures have been published elsewhere.[56]

Thermomechanical analysis of cured samples was performed using a TA Instruments Q400 thermomechanical analyzer (TMA) in dynamic (oscillatory compression) TMA mode. The oscillatory compression mode provides qualitative information on the storage and loss components of the sample stiffness, in addition to sample displacement as a function of temperature. Heating and cooling rates of 50 °C / min were used for “as cured” dry samples,

with 10 °C used for "fully cured" samples, and 20 °C / min used for "wet" samples. These rates are considered optimal for each given situation, and represent a balance between minimizing *in-situ* cure, thermal lag, and (for wet samples) *in-situ* drying. A standard thermal cycling procedure, using limits of 0 °C and 200 °C, was used to determine and correct for the thermal lag. The procedure was employed prior to heating to 350 °C for dry samples, and after heating to 350 °C for wet samples. The mean compressive load on the samples was 0.1 N, with an oscillatory force applied at an amplitude of 0.1 N and a frequency of 0.05 Hz. Complete details, examples, and the rationale for the cycling procedures have been explained at length elsewhere.[56] Thermogravimetric analysis (TGA) was carried out using a TA Instrument Q5000 under 60 mL / min. of either nitrogen or air. For TGA analysis, ~ 2 mg of uncured powder was heated at 10 °C / min. to 600 °C. The density of cured samples was determined via neutral buoyancy of 13 mm x 3 mm discs in $CaCl_2$ / deionized water mixtures, as described elsewhere.[57] Some multi-step cured and post-cured samples were placed in 250 mL of deionized water at 85 °C for 96 hours as a means of testing the effects of exposure to hot water.

References

(1) Hamerton, I., *Chemistry and Technology of Cyanate Ester Resins*. Chapman & Hall: London, 1994.
(2) Nair, C. P. R.; Mathew, D.; Ninan, K. N. Cyanate ester resins, recent developments. In *New Polymerization Techniques and Synthetic Methodologies*, 2001; Vol. 155, pp 1-99.
(3) Fang, T.; Shimp, D. A. Polycyanate Esters -- Science and Applications. *Prog. Polym. Sci.* **1995,** *20*, 61-118.
(4) Yameen, B.; Duran, H.; Best, A.; Jonas, U.; Steinhart, M.; Knoll, W. *Macromol. Chem. Phys.* **2008,** *209*, 1673-1685.
(5) Ganguli, S.; Dean, D.; Jordan, K.; Price, G.; Vaia, R. *Polymer* **2003,** *44* (22), 6901-6911.
(6) Shivakumar, K. N.; Chen, H.; Holloway, G. *J. Reinf. Plast. Compos.* **2009,** *28*, 675-689.
(7) Chen, H.; Shivakumar, K. *Proc. 22nd Am. Soc. Compos., Tech. Conf.* **2007**, 93/1-93/18.
(8) Chen, H. C. *CMC-Comput. Mat. Contin.* **2008,** *8*, 33-42.
(9) Gitsas, A.; Yameen, B.; Lazzara, T. D.; Steinhart, M.; Duran, H.; Knoll, W. *Nano Lett.* **2010,** *10*, 2173-2177.
(10) Fyfe, C. A.; Niu, J.; Rettig, S. J.; Burlinson, N. E.; Reidsema, C. M.; Wang, D. W.; Poliks, M. *Macromolecules* **1992,** *25*, 6289-6301.

(11) Snow, A. W.; Armistead, J. P. *Naval Research Laboratory Memorandum Report 6848*; Naval Research Laboratory: Washington, DC, 1991.
(12) Shimp, D. A.; Craig, W. M., New Liquid Dicyanate Monomer for Rapid Impregnation of Reinforcing Fibers. In *34th International SAMPE Symposium*, SAMPE International: 1989; pp 1336-1346.
(13) Reams, J. T.; Guenthner, A. J.; Lamison, K. R.; Vij, V.; Lubin, L. M.; Mabry, J. M. *ACS Appl. Mat. Interfaces* **2012,** *4*, 527-535.
(14) Marella, V. V. An Investigation on the Hydrolysis of Polyphenolic Cyanate Esters using Near-IR Spectroscopy. M. S. Thesis, Drexel University, Philadelphia, PA, 2008.
(15) Guenthner, A. J.; Lamison, K. R.; Davis, M. C.; Cambrea, L. R.; Yandek, G. R.; Mabry, J. M. In *Cure Characteristics of Tricyanate Ester High-Temperature Composite Resins*, 2011 SAMPE Spring Technical Conference and Exhibition - State of the Industry: Advanced Materials, Applications, and Processing Technology, Long Beach, CA, SAMPE International Business Office: Long Beach, CA, 2011;paper 56-1681.
(16) Mondragon, I.; Solar, L.; Recalde, I. B.; Gómez, C. M. *Thermochim. Acta* **2004,** *417*, 19-26.
(17) Teil, H.; Page, S. A.; Michaud, V.; Månson, J. A. E. *J. Appl. Polym. Sci.* **2004,** *93*, 1774-1787.
(18) Zhao, L.; Hu, X. A. *Polymer* **2010,** *51*, 3814-3820.
(19) Corezzi, S.; Fioretto, D.; Santucci, G.; Kenny, J. M. *Polymer* **2010,** *51*, 5833-5845.
(20) Kasehagen, L. J.; Haury, I.; Macosko, C. W.; Shimp, D. A. *J. Appl. Polym. Sci.* **1997,** *64*, 107-113.
(21) Georjon, O.; Galy, J. *Polymer* **1998,** *39*, 339-345.
(22) Guenthner, A. J.; Davis, M. C.; Lamison, K. R.; Yandek, G. R.; Cambrea, L. R.; Groshens, T. J.; Baldwin, L. C.; Mabry, J. M. *Polymer* **2011,** *52*, 3933-3942.
(23) Al-Saleh, B.; Abdelkhalik, M. M.; Eltoukhy, A. M.; Elnagdi, M. H. *J. Heterocycl. Chem.* **2002,** *39*, 1035-1038.
(24) Elghamry, I. *Synthesis-Stuttgart* **2003**, 2301-2303.
(25) Benary, E.; Meyer, H.; Charisius, K. *Ber. Dtsch. Chem. Ges. A/B* **1926,** *59*, 108-112.
(26) Kelber, C.; Schwarz, A. *Ber. Dtsch. Chem. Ges. A/B* **1912,** *45*, 2484-2489.
(27) Petrov, A. A.; Esakov, S. M.; Ershov, B. A., *J. Org. Chem. USSR (Eng. Trans.)* **1980,** *16*, 1335-1340.
(28) Kaushal, R.; Sovani, S.; Deshpande, S. S., *J. Indian Chem. Soc.* **1942,** *19*, 107-116.
(29) Hanson, R. W. *J. Chem. Educ.* **1997,** *74*, 430-431.
(30) Liu, X.; Lu, G.; Guo, Y.; Guo, Y.; Wang, Y.; Wang, X. *J. Mol. Catal. A: Chem.* **2006,** *252*, 176-180.
(31) Keiboom, A. P. G.; De Kreuk, J. F.; van Bekkum, H. J., *J. Catal.* **1971,** *20*, 58-66.
(32) Ram, S.; Ehrenkaufer, R. E. *Synthesis-Stuttgart* **1988**, 91-95.
(33) Kawada, M.; Kashiwagi, M.; Koito, K. Positively-working photoresist using phenolic resin and quinonediazide. Japanese Patent 04301849, 26 October 1992.
(34) Tanaka, A.; Arai, Y.; Kim, S. N.; Ham, J.; Usuki, T. *J. Asian Nat. Prod. Res.* **2011,** *13*, 290-296.
(35) Morikawa, A.; Kakimoto, M.; Imai, Y. *Macromolecules* **1993,** *26*, 6324-6329.
(36) Horning, E. C.; Parker, J. A. *J. Am. Chem. Soc.* **1952,** *74*, 3870-3872.
(37) Shimp, D. A.; Ising, S. J.; Christenson, J. R., Cyanate Esters -- A New Family of High Temperature Thermosetting Resins. In *High Temperature Polymers and Their Uses*, Society of Plastics Engineers: Cleveland, OH, 1989; pp 127-140.

(38) Jankovic, B. *Thermochim. Acta* **2011,** *519*, 114-124.
(39) Yu, H.; Shen, C. J.; Tian, M. Z.; Qu, J.; Wang, Z. G. *Macromolecules* **2012,** *45*, 5140-5150.
(40) Hamerton, I.; Glynn, S.; Hay, J. N.; Pullinger, M. A.; Shaw, S. J. *Polym. Degrad. Stab.* **2012,** *97*, 679-689.
(41) Ryu, B. Y.; Emrick, T. *Macromolecules* **2011,** *44*, 5693-5700.
(42) Ramirez, M. L.; Walters, R. N.; Savitski, E. P.; Lyon, R. E. *Thermal Decomposition of Cyanate Ester Resins*; DOT/FAA/AR-01/32; Federal Aviation Administration: Atlantic City, NJ, 2001.
(43) Simon, S. L.; Gillham, J. K. *J. Appl. Polym. Sci.* **1993,** *47*, 461-485.
(44) Sheng, X.; Akinc, M.; Kessler, M. R. *J. Therm. Anal. Calorim*. **2008,** 93, 77-85.
(45) Guenthner, A. J.; Lamison, K. R.; Yandek, G. R.; Masurat, K. C.; Reams, J. T.; Cambrea, L. R.; Mabry, J. M., Role of concurrent chemical and physical processes in determining the maximum use temperatures of thermosetting polymers for aerospace applications. In *Abstr. Pap. Am. Chem. Soc.* **2011,** (243rd ACS National Meeting & Exposition, Denver, CO, 2011), *POLY-262*.
(46) Shimp, D. A.; Ising, S. J. *Am. Chem. Soc.: Polym. Mat. Sci. Eng. Preprints* **1992**, *66*, 504.
(47) Kamal, M. R.; Sourour, S. *Polym. Eng. Sci.* **1973,** *13*, 59-64.
(48) Kenny, J. M. *J. Appl. Polym. Sci.* **1994,** *51*, 761-764.
(49) Crawford, A. O.; Hamerton, I.; Cavalli, G.; Howlin, B. J. *PLoS ONE* **2012,** *7*, ee44487.
(50) Crawford, A. O.; Howlin, B. J.; Cavalli, G.; Hamerton, I. *React. Funct. Polym.* **2012,** *72*, 596-605.
(51) Guenthner, A. J.; Lamison, K. R.; Vij, V.; Reams, J. T.; Yandek, G. R.; Mabry, J. M. *Macromolecules* **2012,** *45*, 211-220.
(52) Cambrea, L. R.; Davis, M. C.; Groshens, T. J.; Guenthner, A. J.; Lamison, K. R.; Mabry, J. M. *J. Polym. Sci. Part A: Polym. Chem.* **2010,** *48*, 4547-4554.
(53) Dorfman, L.; Furlenmeier, A.; Huebner, C. F.; Lucas, R.; MacPhillamy, H. B.; Mueller, J. M.; Schlittler, E.; Schwyzer, R.; St. André, A. F. *Helv. Chem. Acta* **1954**, *37*, 59-75.
(54) Calandra, J. C.; Svarz, J. J. *J. Am. Chem. Soc.* **1950**, *72*, 1027-1028.
(55) Shimp, D. A. Blend of tris(cyanatophenyl)alkane and bis(cyanatophenyl)alkane. U.S. Patent 4,709,008, 24 November 1987.
(56) Guenthner, A. J.; Yandek, G. R.; Mabry, J., M; Lamison, K. R.; Vij, V.; Davis, M. C.; Cambrea, L. R., Insights into moisture uptake and processability from new cyanate ester monomer and blend studies. In *SAMPE International Technical Conference*, SAMPE International Business Office: Salt Lake City, UT, 2010; Vol. 55, pp 42ISTC-119.
(57) Lamison, K. R.; Guenthner, A. J.; Vij, V.; Mabry, J. M. *Am. Chem. Soc.: Polym. Mat. Sci. Eng. Preprints* **2011**, *104*, 299-300.

For Table of Contents Use Only

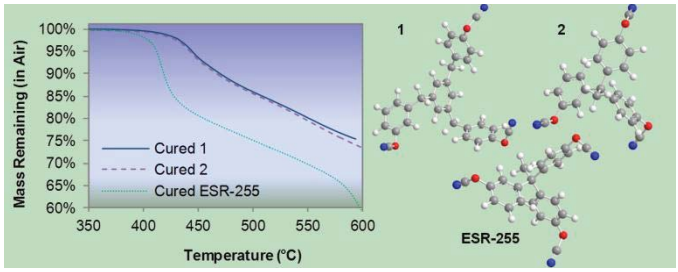

Supporting Information

"Polycyanurate Networks with Enhanced Segmental Flexibility and Outstanding Thermochemical Stability"

Andrew J. Guenthner*[1], Matthew C. Davis[2], Michael D. Ford[2], Josiah T. Reams[3], Thomas J. Groshens[2], Lawrence C. Baldwin[2], and Joseph M. Mabry[1]

[1]Air Force Research Laboratory, Propulsion Directorate, Edwards AFB, CA 93524
[2]Naval Air Warfare Center, Weapons Division, China Lake, CA 93555
[3]National Research Council / Air Force Research Laboratory, Edwards AFB, CA 93524

S1. X-ray Crystal Structure and NMR Data

Figure S1-1 shows the X-ray crystal structure of 1,3,5-tris(4-hydroxyphenylmethyl)benzene, compound **8** in the main manuscript, and the precursor that was cyanated to produce monomer **1** . CCDC 821411 contains the supplementary crystallographic data for compound **8**. This data can be obtained free of charge from The Cambridge Crystallographic Data Centre via www.ccdc.cam.ac.uk/data_request/cif, by e-mailing data_request@ccdc.cam.ac.uk, or by contacting CCDC 12 Union Road, Cambridge CB2 1EZ, UK; fax: +44 1223 336033. Figures S1-2 through S1-4 show the ^{1}H (300 MHz, $CDCl_3$) and ^{13}C (75 MHz, $CDCl_3$) NMR spectra of monomers **1**, **2**, and ESR-255, respectively.

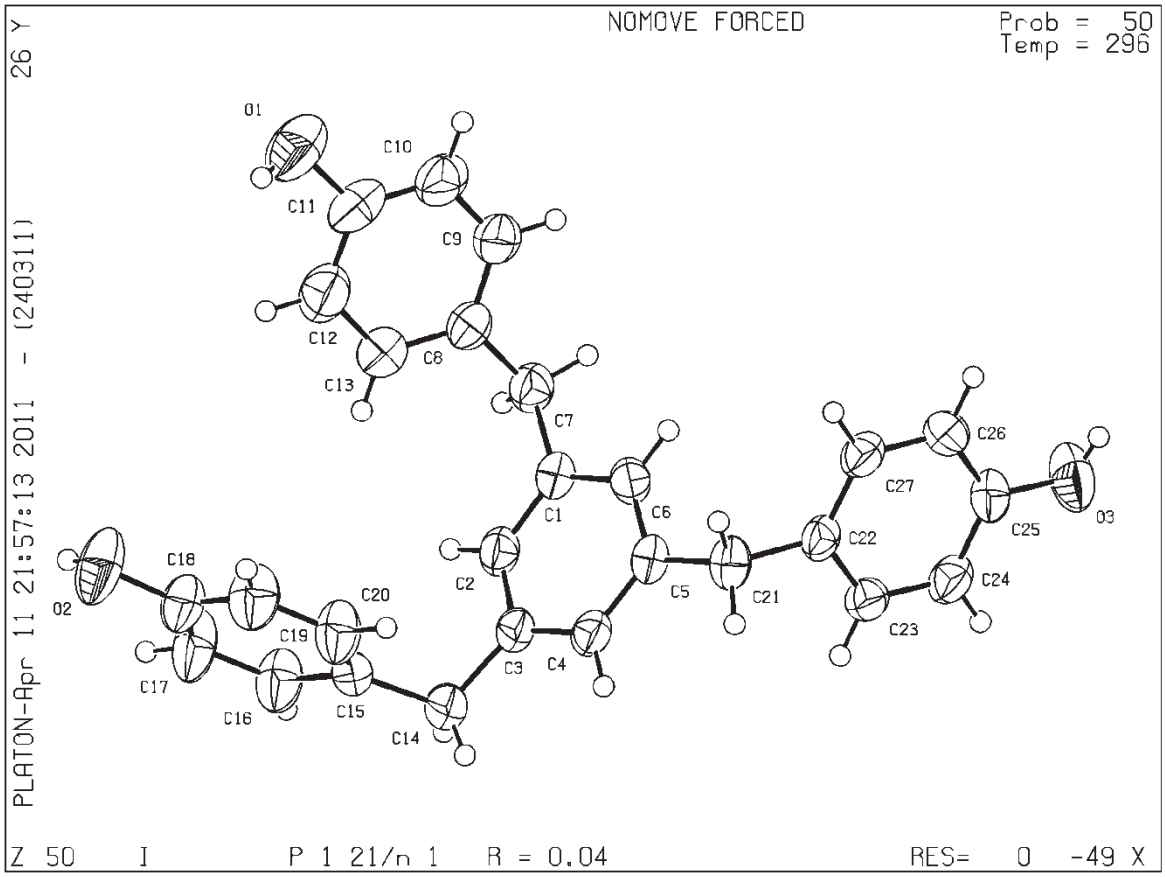

Figure S1-1. Thermal ellipsoid plot of 1,3,5-tris(4-hydroxyphenylmethyl)benzene, compound **8**.

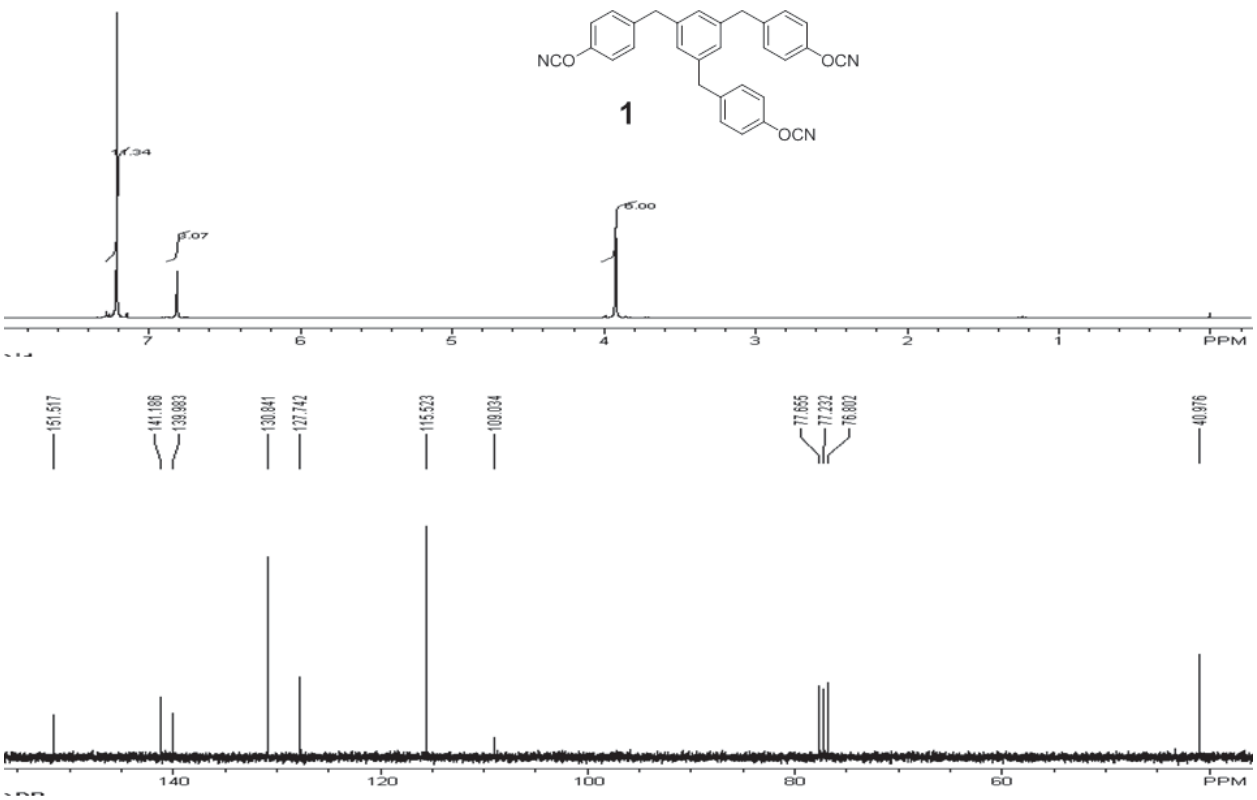

Figure S1-2. ^{1}H (upper) and ^{13}C (lower) NMR spectra of 1,3,5-tris(4-cyanatophenylmethyl)benzene, compound **1**.

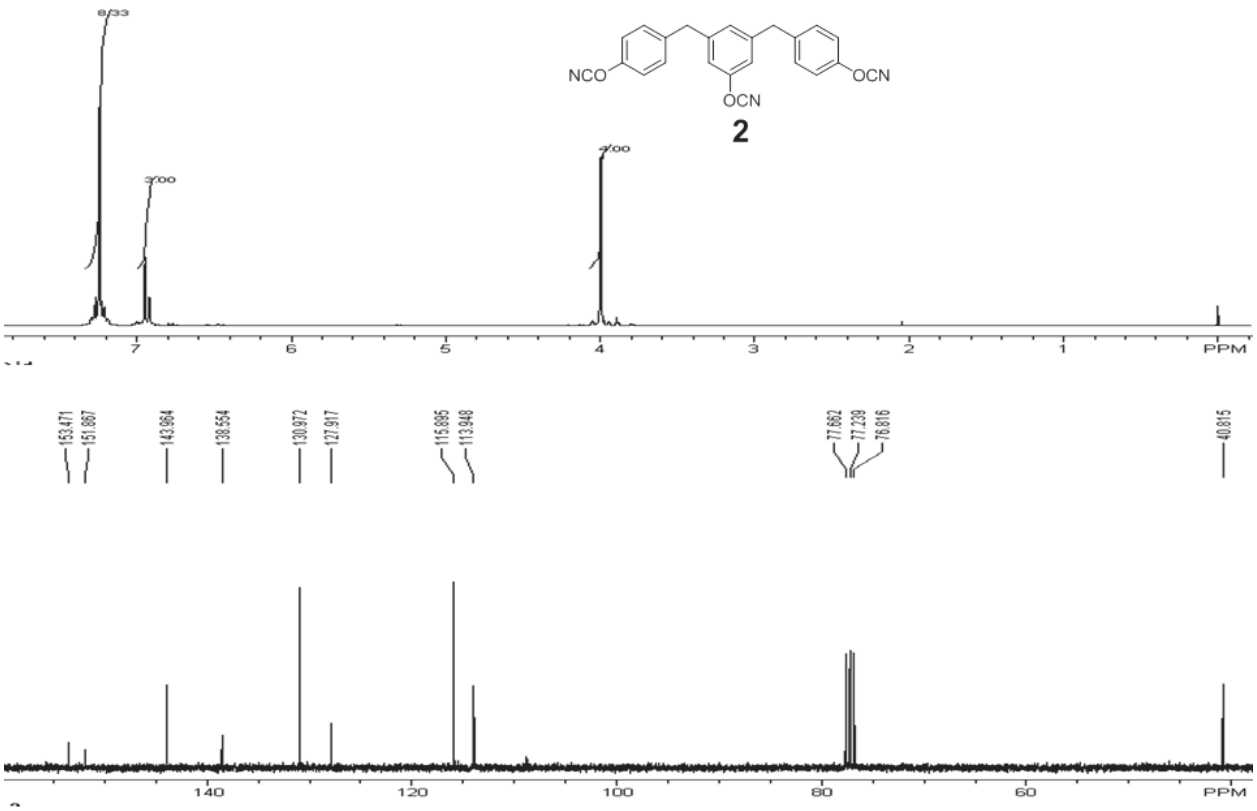

Figure S1-3. ^{1}H (upper) and ^{13}C (lower) NMR spectra of 3,5-Bis[(4-cyanatophenyl)methyl)]phenylcyanate, compound **2**.

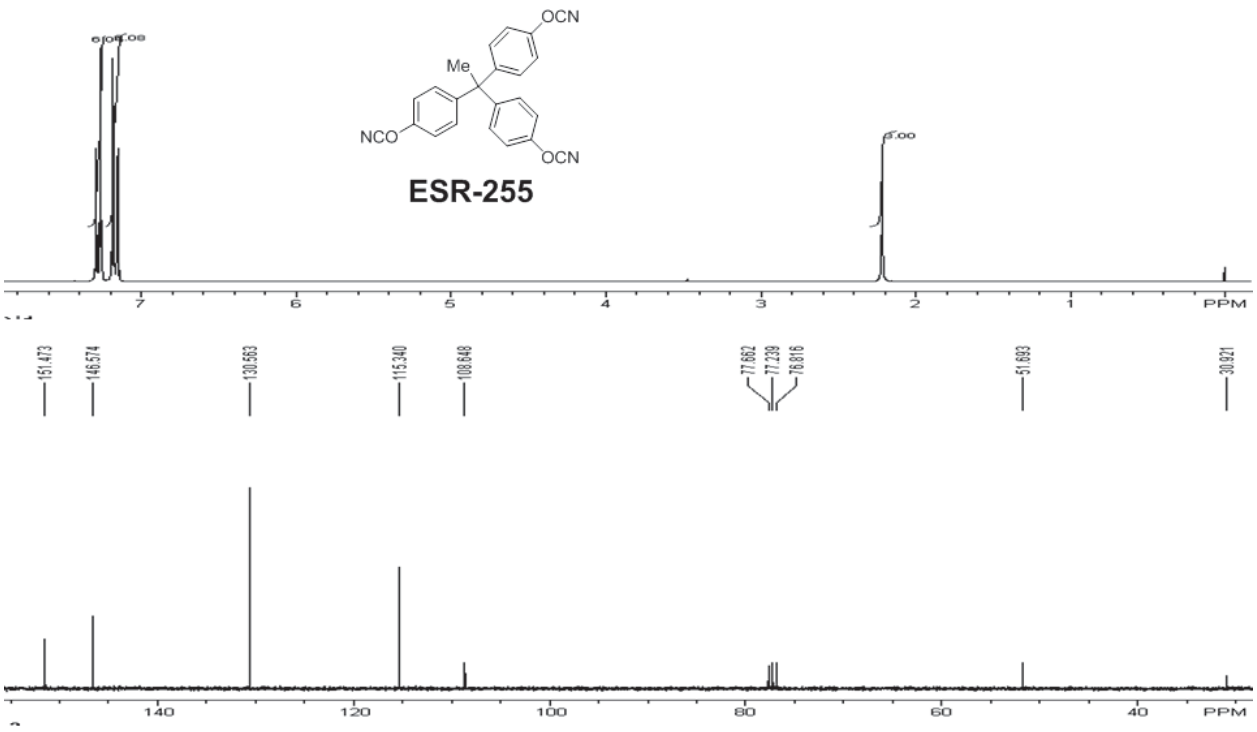

Figure S1-4. ^{1}H (upper) and ^{13}C (lower) NMR spectra of 1,1,1-Tris(4-cyanatophenyl)ethane, ESR-255.

S2. Modulated DSC Data

S2.1 Introduction. The DSC traces for ESR-255 (seen in Figure 5c of the main manuscript, for instance) show an apparently "open-ended" exotherm associated with cure of the cyanate ester groups. Based only on conventional DSC scans, however, it is not possible to differentiate between a truly open-ended exotherm in which cure continues even in the "flat" portion of the curve and a simple shift of the baseline. Using modulated DSC, however, it is possible to distinguish among these alternative possibilities. Continuing cure of the cyanate ester groups would affect only the non-reversing portion of the modulated DSC curve, while a baseline shift would affect the reversing portion (and possibly the non-reversing portion, depending on the cause).

S2.2 Experimental Method. Samples of ESR-255 (~3 mg) were heated at varying rates in a TA Instruments Q200 Differential Scanning Calorimeter in modulated DSC mode under 50 mL/min flowing N_2. A modulation amplitude of 1 °C and a modulation period of 60 s were used over a temperature range of 50 °C to 350 °C. Since quantitative heat flow information was not required, the data shown have not been corrected using a re-scanned baseline.

S2.3 Results and Discussion. Figure S2-1 shows the modulated DSC of ESR-255 heated at a mean rate of 3 °C / min (this sample was melted just prior to starting the DSC run). Though there is a small shift in the reversible component of the heat flow due to vitrification (a kind of "glass transition in reverse" that causes a step decrease in heat capacity), the "open-ended" heat flow curve is clearly due to a continuing non-reversible heat flow. In other words, cure of the cyanate ester definitely continues even in the "flat" portion of the curve. Since degradation of the network begins to have a significant effect on DSC scans above 350 °C (an upturn in the non-reversible heat flow due to this effect is just visible at the end of the scan), there is no practical way to measure the total heat of cyclotrimerization of uncatalyzed ESR-255 (or any other similarly rigid thermosetting polymer requiring high cure temperatures) using

traditional DSC techniques alone. Thus, a method such as the combined DSC/IR technique presented in Section S3 is required. Since the heating rate used in Figure 5 in the main manuscript was somewhat different than the mean heating rate used for modulated DSC (which requires much slower heating in general), the effect of heating rate changes was checked. Figure S2-2 shows a modulated DSC scan of ESR-255 that is identical to the one used to produce Figure S2-1, except that the mean heating rate was increased to 5 °C/min, and in the case pre-melting was not carried out. The mean heating rate used is high for modulated DSC, and hence the reversible heating curve shows some noise at the vitrification point, however, it is clear that the "open-ended" curve is still due to continuing non-reversible heat flow. Hence, the necessary difference in heating rates did not significantly affect the key result, which is that continuing cure, rather than a baseline shift, is responsible for the "open-ended" L-shaped exotherm seen in ESR-255.

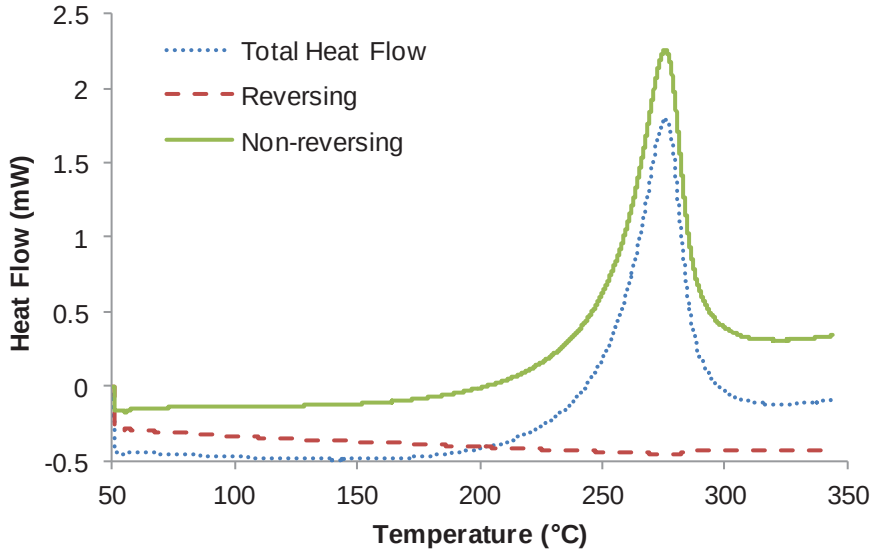

Figure S2-1. Modulated DSC of previously melted ESR-255 at a mean heating rate of 3 °C / min. Note that the shift in heat flow after the exothermic peak is due to mainly to the non-reversing component.

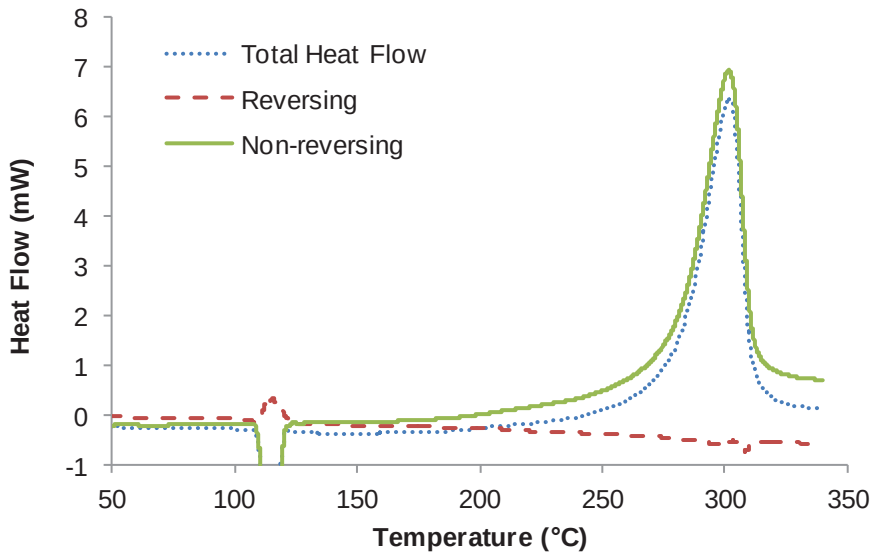

Figure S2-2. Modulated DSC of ESR-255 at a mean heating rate of 5 °C / min.

S3. Combined FT-IR/DSC Method for the Quantitative Determination of Absolute Conversions in Cyanate Esters

S3.1. Introduction. In most thermosetting systems, the absolute conversion (α) may be determined most simply through the use of DSC by making use of the formula

$$\alpha = (\Delta H_0 - \Delta H_r) / \Delta H_0 \qquad \text{(S3-1)}$$

in which ΔH_0 represents the heat of reaction of the monomer, determined by integrating the exothermic reaction peak seen in a first-heating DSC scan, and ΔH_r is the residual heat of reaction of a partially cured sample determined by integrating the exothermic reaction peak using the same heating program and baseline determination technique applied in the calculation in ΔH_0. The key assumptions underlying the method include direct proportionality between the heat released and the extent of conversion and the attainment of complete conversion without significant side reactions. For cyanate esters, the former assumption is almost always valid, since cyanate esters tend to exhibit a characteristic enthalpy of -110 kJ/mol eq. on conversion of a cyanate ester group.[S1] For cyanate esters with a glass transition temperature significantly in excess of 300 °C or with significant steric hindrance to cyanurate formation, however, the latter assumption may be problematic, since significant thermal degradation of cyanurate networks is often detected by DSC at or above about 350 °C. In such cases, a DSC heating scan of the monomer terminated at 350 °C or lower will not lead to full conversion of the monomer, while one terminated above 350 °C will detect heat from both conversion and thermal degradation. A good indicator that the assumption of full cure with no side reactions has been violated is the presence of an "open ended" DSC trace in which the heat flow signal does not return to its baseline vvalue prior to termination of the heating. Note that many DSC traces of this type exhibit an "L-shaped" heating curve that resembles a full peak with a shifted baseline, thus care must be taken to establish the actual baseline (usually by re-heating the sample at the same rate immediately afterword without moving or

handling the sample) when using DSC to assess the heat of reaction for high-temperature thermosetting monomers.

In addition to DSC, infrared spectroscopy (FT-IR or ATR-FTIR) has often been utilized to assess the conversion of cyanate ester to cyanurate. Infrared spectroscopy has the key advantage that residual cyanate ester groups are always visible, due to the presence of strong characteristic absorption bands in the otherwise sparsely occupied region of the infrared spectrum between 2200 and 2300 cm^{-1}. However, infrared spectroscopy is often not considered a quantitative technique unless calibrated by DSC or other measurements, because the absorption intensity for cyanate ester peaks does not decrease linearly with conversion.[S1] The reason for the nonlinearity, however, is usually a change in the physical state of the sample from crystalline solid or small molecular liquid to oligomeric or polymeric gel to rubbery or glassy network sol and finally to glassy or rubbery network with residual cyanate esters as dangling chain ends. Thus, over limited ranges of conversion in which the material remains in the same general state, such as near the end of conversion in which the system consists of a glassy network with cyanate esters as unreacted chain ends, there does exist a linear relationship between the integrated intensity of the cyanate ester peaks and their concentration. For most thermosetting polymers for which DSC provides an absolute measure of conversion, DSC data points are simply used to calibrate the infrared absorption curve.

For high-temperature cyanate esters that cannot be fully cured without thermal degradation in a DSC scan, though, it is still possible to use DSC data points to calibrate an infrared absorption curve, by the method outlined in Section S3.2. This method relies on the existence of a region of conversion in which the infrared absorption is a linear function of cyanate ester concentration (with the linearity extending to 100% conversion) and that can be obtained by heating in a DSC scan under conditions that permit quantitative determination of the heat of reaction. The heat of reaction may not be determined

with quantitative precision if either the heating rate of the DSC scan is too slow, or if the isothermal portion of a DSC scan continues for so long that the conversion rate becomes too low to measure reliably. The essence of the method is that the linearity of both infrared and DSC signals allows for the determination of the differential of the heat of reaction with respect to infrared absorption, enabling the conversion of the residual infrared absorption (which is known absolutely) to an absolute residual heat of reaction (ΔH_r). When added to the known value of the evolved heat of reaction for a given sample, the value of ΔH_0 may be determined, and, in conjunction with the ΔH_r value and Eq. S3-1, the absolute conversion of the sample may be computed. The procedure is outlined in Section S3-2, while validation examples (using cyanates that can be cured completely in the DSC and for which ΔH_0 is known) are presented in Section S3-3. In Section S3-4, the method is used to determine the ΔH_0 value for ESR-255, which cannot be determined by DSC alone as noted in Section S2.

S3.2 Method. Three or four samples cured under different conditions in an oven so as to span a range of conversions from not far beyond the vitrification point to near full conversion were prepared. An ATR-FTIR spectrum of a small piece of each sample was collected using a Thermo Corporation Nicolet 6700 FT-IR Spectrometer in attenuated total reflectance mode from 400 – 4000 cm^{-1} with a resolution of 4 cm^{-1}. Spectra were determined by averaging 32 scans. After being scanned, a small bit of each piece (~ 5 mg) was sealed in a DSC pan and heated to 350 °C at 10 °C/min, followed by cooling at 10 °C/min. to 100 °C and re-heating to 350 °C at 10 °C/min in a TA Instruments 200 DSC under 50 mL/min. of flowing nitrogen. The DSC heat flow was determined at each temperature using the second heating scan as a baseline, and then integrated to determine a residual enthalpy of cure (ΔH_r). In order to estimate the error in ΔH_r, a baseline was selected manually based on the shape of the first heating curve only and used to perform a separate integration. The difference between the two integrated values for the same curve was then recorded as a rough error estimate.

A linear baseline connecting the points at 2000 cm^{-1} and 2500 cm^{-1} was chosen for each FT-IR spectra. The absorbance values were then normalized such that the peak absorbance near 1500 cm^{-1} (representing phenyl group vibrations and thus insensitive to extent of cure), after subtracting the baseline, was set to an arbitrary value of 1. The normalized absorbance values in each spectra (with the baseline subtracted) were then integrated (using a dx of 1.9285 cm^{-1} = an arbitrary value of 1 for convenience based on the format of instrument output) between the apparent edges of the cyanate ester peak (generally 2100 cm^{-1} to 2400 cm^{-1}, but for the re-analysis of older data for BADCy and LECy a range of 2100 cm^{-1} to 2300 cm^{-1} was used to avoid a noisy region in the spectrum). In order to estimate an error for this integrated value, alternative baseline points of 1800 cm^{-1} and 2400 cm^{-1} were chosen. These points represent a sort of "least reasonable" baseline; in contrast to the "most reasonable" baseline points of 2000 cm^{-1} and 2500 cm^{-1}, these points represent what we believe were the furthest limits away from the peak that one could choose as endpoints for a baseline without being completely "unreasonable". The cyanate ester was then re-integrated (without re-normalizing the spectra) using the alternate baseline, and the difference between the results, which represents a measure of the sensitivity of the integration to the choice of baseline, was used as a rough estimate of the error in the measurement. It should be pointed out that the potential baseline error was judged to be by far the largest source of error in the FT-IR measurements.

Once a complete set of FT-IR peak areas and ΔH_r values, with the respective error estimates, was obtained, the FT-IR peak area was plotted as a function of ΔH_r. A linear regression of the data was then performed to determine the x-intercept of the best fit line. In some cases, the errors were many times larger for a single data point than for the others; in such cases, the data point with the large estimated error was simply excluded from the regression (we did not believe a weighted regression was justified because the error values were only rough estimates of variance). The error in the x-intercept was then estimated in two ways: 1) based on the standard error of the regression extrapolated to the x-

intercept, and 2) based on a sensitivity analysis to the estimated variations in each data point, choosing a worst-case scenario in which the variations in each x- and y- value all affected the x-intercept in a similar manner (i.e. assuming, for instance, all values were one estimated y-error lower and one estimated x-error higher than measured, so that all variations increased the x-intercept value). The linearity of the plots in general was also noted. If the assumptions explained in Sections S3.1 are correct (namely, FT-IR and DSC signals that are linearly proportional to cyanate ester concentration over the conversion range from post-vitrification to full cure), then the data points on the plot as constructed should fall on a straight line.

The x-intercept value was interpreted as follows: a positive intercept indicates that some residual heating would be observed even if all cyanate ester groups were consumed, hence it would indicate that the DSC is detecting chemistry other than cure (network thermal degradation, for instance). A negative x-intercept would indicate that even in a sample with no residual cure detected in the DSC, cyanate ester peaks would remain in the FT-IR scan, and hence, that the residual heating scan to 350 °C in the DSC was not sufficient to achieve full conversion. The value of the x-intercept would then represent either the enthalpy of side reactions (for positive values) to be subtracted from the DSC integration to obtain the true residual enthalpy of cure, or (for negative values), the enthalpy to be added to the DSC integration to obtain the true enthalpy of cure of all remaining cyanate ester groups (if in fact they could, hypothetically, be cured completely without side reactions). In equation form,

$$\Delta H_r = \Delta H_{r,DSC} - \Delta H_{xi} \qquad \text{(S3.2)}$$

Where $\Delta H_{r,DSC}$ is the apparent residual enthalpy measured by DSC and ΔH_{xi} is the x-intercept obtained by linear regression of a plot of cyanate ester FT-IR peak intensity (y) vs. apparent DSC residual enthalpy (x) for a series of calibration samples. It should be noted that under most circumstances, ΔH_{xi} would be expected to show no significant differences from zero. Note that this formula also applies to the

determination of ΔH_0 by DSC, which may be considered a special case of the determination of ΔH_r using a monomeric sample. The value of ΔH_{xi} is thus usefully compared to the estimated error in the measurement of ΔH_0 by DSC.

S3.3 Method Validation. For validation of this method, we utilized previously published data on the commercial monomers BADCy and LECy as-supplied from Lonza and cured at various temperatures for 12 hours in order to produce a range of conversions.[S2] The systems were catalyzed with 2 phr nonylphenol and 160 ppm Cu (present as copper(II) acetylacetonate). In this validation case, the DSC residual heating produced a closed curve, hence the absolute conversions were available from the DSC data alone. Thus, the combined DSC/IR technique should result in an adjustment to the residual heat of cure that is not statistically significant.

In Figure S3-1, the residual heat measured by DSC (values published in Reference S2) is plotted against the FT-IR peak intensity integrated from 2100 – 2300 cm^{-1}. For reference, the IR spectra are shown in Figure S3-2 (these data were discussed in Reference S2 but peak integration as described in Section S3.2 had not been performed). A close look at the spectra in Figure S3-2 shows that, particularly at a final cure temperature of 150 °C, the slope of the baseline is somewhat uncertain. As a result, the characteristic uncertainty estimate depicted in Figure S3-1 is comparatively large. It is also easy to see why such estimates of uncertainty are important, because even a small change in the assumed baseline makes a large difference in the integrated intensity. A linear regression of the points in Figure S3-1 yields an x-intercept of -35 J/g, both with and without the 150 °C cure point included. Based on the range of uncertainties reported and the small number of data points, one would expect the true error in the x-intercept estimate to be at least 35 J/g, so that the result is not significantly different than zero. Figures S3-3 and S3-4 present the analogous data for catalyzed LECy. As with the BADCy, the baseline

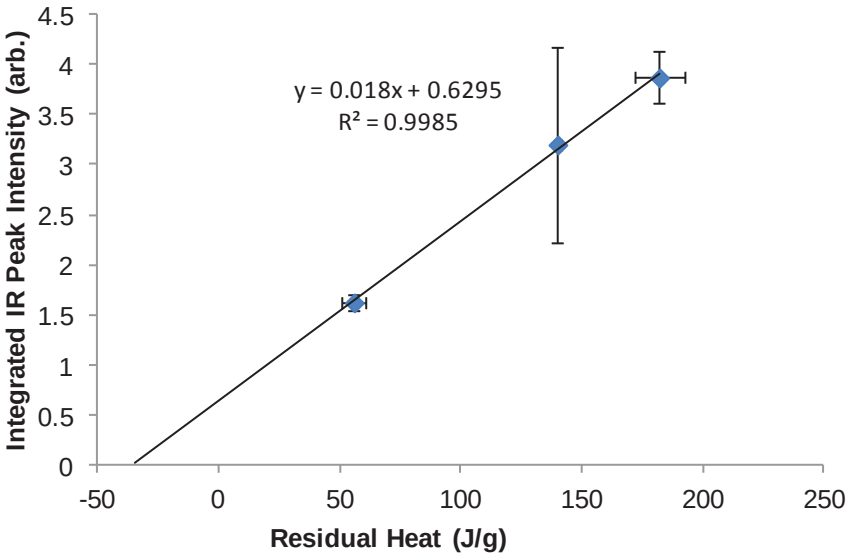

Figure S3-1. DSC-IR linear regression of catalyzed BADCy, showing the relationship between residual heat seen in the DSC scan and integrated FT-IR peak intensity. The expected x-intercept is zero.

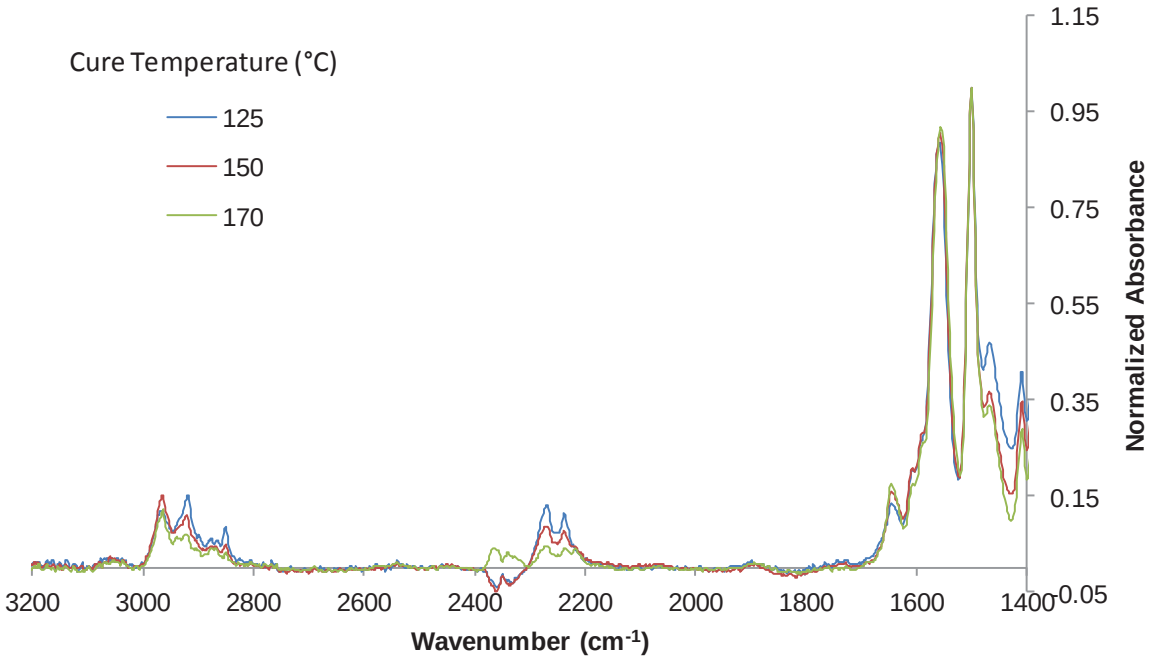

Figure S3-2. Comparative FT-IR spectra of catalyzed BADCy as a function of final cure temperature.

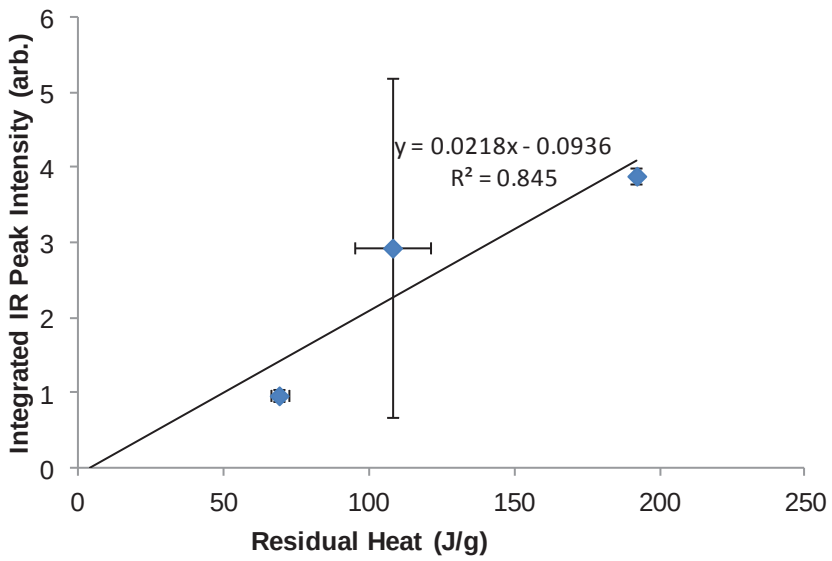

Figure S3-3. DSC-IR linear regression of catalyzed LECy, showing the relationship between residual heat seen in the DSC scan and integrated FT-IR peak intensity. The expected x-intercept is zero.

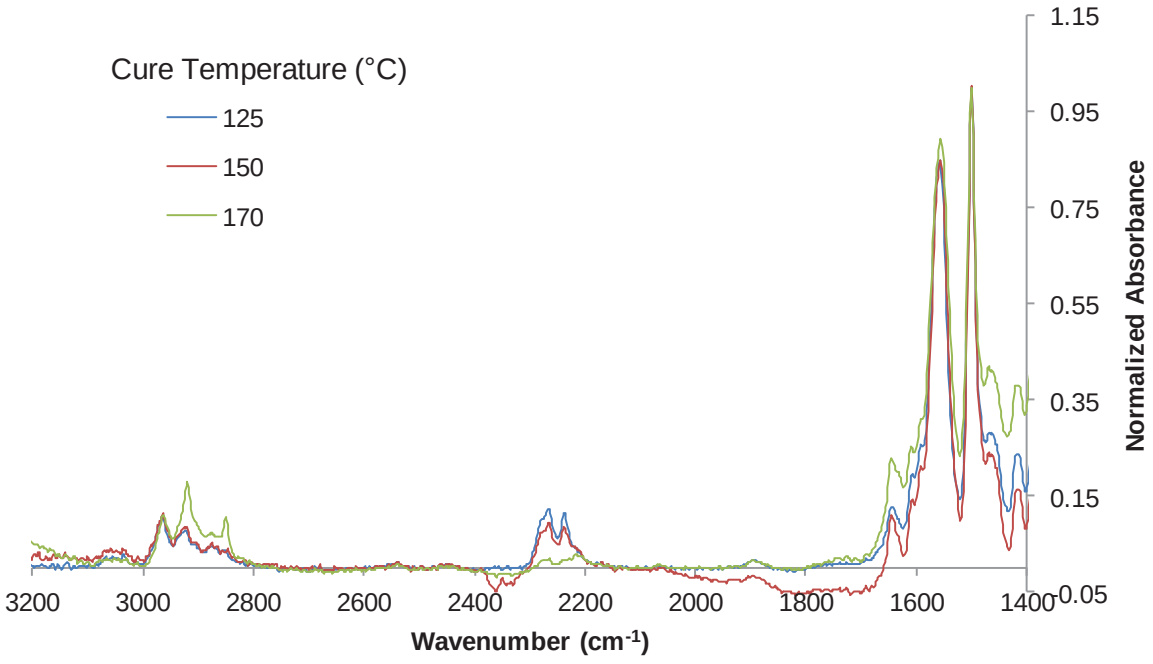

Figure S3-4. Comparative FT-IR spectra of catalyzed LECy as a function of final cure temperature.

of the 150 °C cured sample showed considerable uncertainty. The x-intercept of the DSC/IR comparison plot is an insignificant 5 J/g with the 150 °C data included and 29 J/g without it. Again, given the uncertainties and the small amount of data collected, the x-intercept does not appear significantly different than zero.

Taken together, the validation cases show that, in general, the expected relationship between DSC and FT-IR data does exist. However, these data clearly show the importance of having a precisely determined baseline. They also indicate that in order to obtain a more reliable linear fit of the data, four or five data points will be preferable to only three, since a substantial fraction of the data may suffer from significant uncertainties associated with the assumed baselines. Having four or five data points would allow for meaningful weighted regressions (having only three data points means that in many cases, weighted regressions will effectively include just two data points).

S3.4 Results for ESR-255. Having shown with closed-curved DSC data that (with a margin of error of a few per cent) the DSC/IR technique enables the determination of absolute conversion, the technique was applied to ESR-255. Figure S3-5 shows the DSC/IR correlation plot while the individual FT-IR spectra are shown in Figure S3-6. In this case, the samples analyzed were all uncatalyzed ESR-255 cured for 30, 60, 120, and 240 minutes at 250 °C in an oven. As a further check on the method, we carried out an isothermal cure at 250 °C for 240 minutes in the DSC on a small sample of uncatalyzed ESR-255 powder, and then subjected this *in-situ* DSC cured sample to a residual heating. While the residual heating after 240 minutes is computed as normal, the residual heats at 30, 60, and 120 minutes were computed by adding the peak integral from the residual heating scan to the integrated heat flow between the time of interest (e.g. 30 minutes) and the end of isothermal cure at 240 minutes. These two methods (oven and DSC) should give equal residual heating values. We performed this particular experiment simply as a check on this newly developed method; we would not anticipate performing such a check routinely.

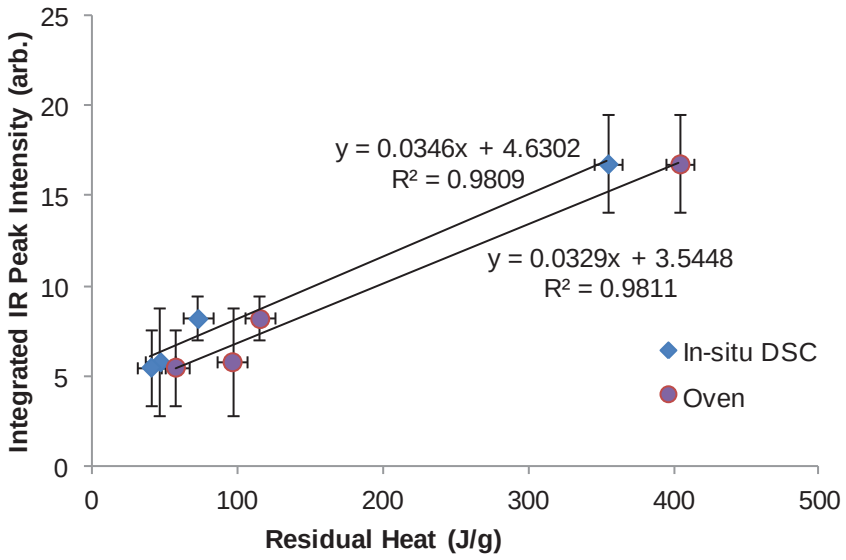

Figure S3-5. DSC/IR correlation plot for uncatalyzed ESR-255 using conventional oven cured samples as well as a sample cured *in-situ* in the DSC as a special check of the method.

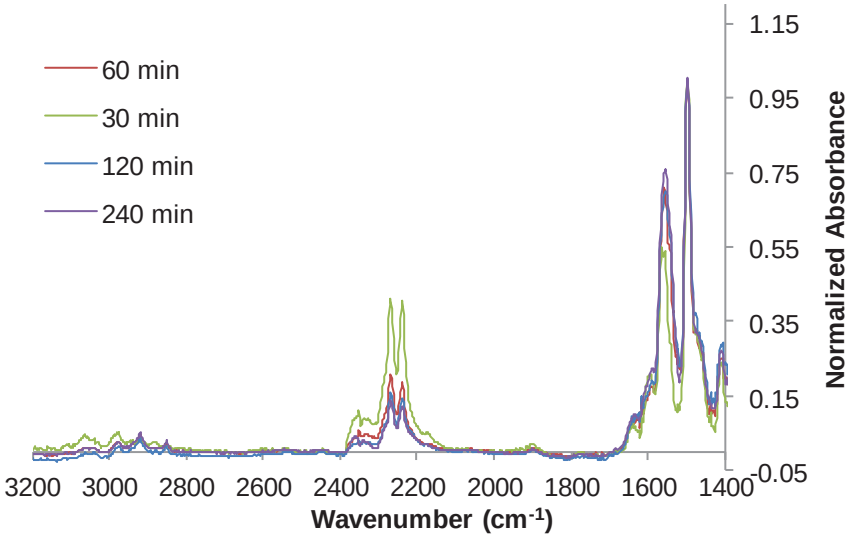

Figure S3-6. Individual FT-IR spectra of uncatalyzed ESR-255 cured in an oven at 250 °C for the times indicated.

As seen in Fig S3-5, the oven cured samples tended to show slightly lower residual heats than comparable samples cured in the DSC. This could be due to a larger expected temperature overshoot in the oven as compared to the precisely controlled DSC. The x-intercept values were -129 ± 28 J/g for *in-situ* DSC cured samples and 102 ± 30 J/g for oven-cured samples. Note that the error estimates are from the equally weighted linear regressions and do not take into account the error in the individual measurements, which is of a similar magnitude. Hence, the total uncertainty in the x-intercept is likely around 50 J/g. The difference between the methods is not significant, however, the intercept itself does appear to be significantly different from zero at about 90% confidence. To obtain the correct ΔH_0, we thus subtracted the x-intercept value of the oven-cured samples (since those samples were used for FT-IR), or -100 J/g from the value obtained by DSC (730 J/g) to yield a ΔH_0 or 830 J/g or (keeping only two significant figures, 110 kJ/mol), with an uncertainty of about 7 kJ/mol. It is worth noting that 110 kJ/mol is in fact the expected value for cyanate esters, and matches the range reported by us using DSC only for uncatalyzed BADCy and LECy.

S4. Determination of diBenedetto Equation Parameters

S4.1 Introduction. For thermosetting polymers with a well-defined network structure for a given conversion, such as cyanate esters, the diBenedetto equation provides a key link among physical properties by relating the glass transition temperature (T_g) of the network to the conversion (α).[S1] The equation takes the form:

$$\frac{(T_g - T_{g0})}{(T_{g\infty} - T_{g0})} = \frac{\lambda\alpha}{1-(1-\lambda)\alpha} \qquad \text{S4-1}$$

in which T_{g0} and $T_{g\infty}$ represent the glass transition temperatures of the monomer and fully cured network, respectively, and in which λ is effectively an adjustable parameter ($0 \leq \lambda \leq 1$) that in theory is determined by the heat capacity characteristics of the monomer and cured network.[S1] According to eq. S4-1, the glass transition temperature of a cyanate ester network is independent of its cure history, a fact that has been verified experimentally for at least two different cyanate ester monomers.[S3,S4] As a result, for any cure process, be it a complex part cured in an oven or a simple non-isothermal DSC scan, the network T_g at any location and/or instant in time may be computed as long as the conversion at the same location and/or instant is known. For carefully performed DSC scans, an instantaneous measure of conversion is always available by integrating the heat flow and dividing by ΔH_0. Thus, even in systems such as ESR-255, the developing T_g may be determined once a technique such as the combined DSC/IR method described in Section S3 has been used to correctly measure ΔH_0 and the diBenedetto equation parameters have been computed.

Techniques for the determination of diBenedetto equation parameters for thermosetting polymers may be divided into two general cases. In the first case, which applies to most lower service temperature cyanate esters such as BADCy, and also applies to monomer **1** (that is, 1,3,5-tris(4-cyanatophenylmethyl)benzene), the parameters T_{g0} and $T_{g\infty}$ are easily determined by a method such as DSC, and only the parameter λ must be determined experimentally. In such cases, even a single T_g

measurement in combination with a conversion measurement on a partly cured system allows for a determination of λ, with more than one point needed for an estimate of uncertainty. In practice, however, the values of λ that we have determined for a variety of cyanate esters always fall in the range of 0.25 to 0.45, and regardless of how many data points are used, it appears that an uncertainty of 0.05 to 0.1 is commonly encountered due primarily to uncertainties in measuring both T_g and α. Moreover, in many cases a fairly narrow range of conversions (beyond the vitrification point) is actually of practical interest, thus there is not much to be gained from performing many measurements of T_g at low conversion. Instead, a few T_g and α pairs at high conversion may be used to determine λ through either a non-linear curve fitting approach, or, the following convenient form may be used in a linear regression (with intercept fixed at zero)

$$\frac{(T_{g\infty}-T_{g0})}{(T_g-T_{g0})} - 1 = \lambda\left[\left(\frac{1}{\alpha}\right) - 1\right] \qquad \text{S4-2}$$

For cyanate esters with high glass transition temperatures, however, $T_{g\infty}$ may not be directly measureable, because the network may undergo thermal degradation before the thermodynamic transitions associated with $T_{g\infty}$ can be observed in an actual heating experiment. As a result, multiple parameters appearing in the diBenedetto equation may need to be determined simultaneously. In such cases, having many measurements available is advisable since the optimization needed is both multi-variate and nonlinear. At present, the best approach to performing this kind of optimization with experimental data on thermosetting polymers remains an open question. As in the simpler problem, data at lower conversions does not add much to the robustness of the optimization. Thus, when collecting data, if the conversions are not controlled (as with a scheduled cure experiment), it may be necessary to collect a large number of data points just to ensure that enough of these points are available at high conversions to enable a useful determination.

S4.2 Methods for Determination of diBenedetto Parameters. Because the available quantities of the three monomers varied (**2** was produced only in low yield after many synthesis steps, while ESR-255 was produced in high yield from one step), and because the three monomers differed in availability of fully-cured glass transition temperature data, we chose to estimate diBenedetto parameters based on separate approaches judged best for each monomer. The level of information obtained thus differed quite a bit from monomer to monomer, with most parameters for **2** available as fairly broad ranges while parameters for ESR-255 were all available as point estimates with clearly determined uncertainties.

S4.2.1 for monomer 1 (1,3,5-tris(4-cyanatophenylmethyl)benzene). The glass transition temperature of the monomer was determined by DSC on heating from -70 °C to 100 °C at 10 °C / min. The glass transition temperature of the fully cured polymer was also determined DSC scans on the second heating scan of a cycle from 100 °C to 350 °C at 10 °C / min. All DSC scans were performed on a TA Instruments Q200 under 50 mL/min of flowing nitrogen. To determine a value for λ, the DSC scans of samples previously heated to 250 °C, 270 °C, and 290 °C for 30 minutes were utilized. These samples were heated to 350 °C at 10 °C / min as part of the standard procedure for chemical kinetics analysis (see Section S6), a technique which simultaneously measured the conversion of the as-cured samples. The observed heating scans showed no residual cure below the glass transition temperature, so no adjustment for *in-situ* cure was needed. The DSC scans of samples isothermally cured at lower temperatures showed residual cure but no apparent glass transition temperature on residual heating. These scans were used to exclude a range of possible values for λ on the basis that a glass transition would have been visible had λ fallen within the excluded range. For instance, when heated to 230 °C for 30 minutes, a conversion of around 0.82 for monomer **1** resulted. At a conversion of 0.82, a value of 0.25 for λ would have resulted in a glass transition temperature of 159 °C for the partly cured **1**, whereas a value of 0.35 for λ would have resulted in a glass transition temperature of 187 °C (based on the

known T_{g0} and $T_{g\infty}$ values, see Table S4-1). Since a T_g was definitely not observed between 153 °C and 178 °C in the residual heating scan under these conditions, a value of 0.25 for λ may be excluded, whereas a value of 0.35 for λ cannot be excluded (on the basis of this particular scan).

The individual estimates for λ based on single heating scans (found by solving the diBenedetto equation algebraically) were compared with the best fit value obtained by a weighted least squares method in which λ was varied in increments of 0.01, then in increments in 0.001 to refine the estimate. The weighting factor for each point was determined by the inverse square of the estimated uncertainty in the experimentally observed T_g value. For further comparison, a linear regression of the data using Eq. S4-2 was also performed. Lastly, the values of λ excluded on the basis of a lack of observed glass transition temperature signals in DSC scans were checked against the other estimates for consistency.

S4.2.2 for monomer 2 (3,5-Bis[(4-cyanatophenyl)methyl)]phenylcyanate). The glass transition temperature of the uncured monomer was determined using the technique described in S4.2.1. The fully cured glass transition temperature was apparent neither from DSC nor from TMA measurements, however, because **2** is a close structural analog of REX-371 (whose fully cured T_g was reported at 370 °C)[S1], as well as a small, model oligomer of PT-30 (fully cured T_g reported at 400 °C)[S5] the fully cured T_g may be assigned a probable value of 385 ± 15°C. Based on this information, constraints on the value of λ could be determined from the residual heating portion of isothermal DSC cure experiments in which no glass transition temperature was observed, as described in S4.2.1, but no glass transition temperatures of partly cured samples were available for an estimate for λ. Instead, the values of λ for the analogous monomers **1** and ESR-255 were simply averaged to determine a rough estimate, and this estimate was checked for consistency with the constraints obtained from the DSC data. Due to the many uncertainties in the estimation of diBenedetto parameters for this monomer and its reliance on

analogy with other known systems, we have noted in the main manuscript that estimates of diBenedetto parameters for **2** are not of the same quality as those for **1** and ESR-255.

S4.2.3 for ESR-255 (1,1,1-tris(4-cyanatophenyl)ethane). Due to the large available quantity of this monomer, a different technique for the estimation of diBenedetto parameters were employed. The three diBenedetto equation parameters T_{g0}, $T_{g\infty}$, and λ were estimated simultaneously using the Solver nonlinear optimization routine (with default settings) found in Microsoft® Excel 2010. Since a detailed study of the relative merits of various nonlinear techniques was judged to be well beyond the required scope of effort, and since values for T_{g0} and λ were easy to check for reasonableness, we judged that simply adapting the generic nonlinear optimization algorithm present in Solver was the best choice.

In order to generate data on partly cured systems, samples were heated at 10 °C / min using the DSC method analogous to that described in S4.2.1 to a chosen isothermal temperature and cured for 30 minutes, then cooled at 10 °C / min to 50 °C. After five minutes of isothermal quiescence (to remove transients from the DSC signal), the samples were subjected to modulated DSC by heating at 5 °C / min to 350 °C to measure residual cure (based on the non-reversing portion of the signal). A modulation amplitude of 1 °C and a modulation period of 60 s were used, along with a re-scanned baseline for both isothermal and modulated residual heating. All ΔH values were calibrated using the enthalpy of melting of ESR-255 as an internal standard, as described in Section S6. Note that because samples did not cure fully under these conditions, the conversion was determined based on the measurement of the heat evolved during the isothermal portion of the cure, using ΔH_0 = 110 kJ/eq. (based on the results described in Section S3). In other words, the formula used to determine conversion was

$$\alpha = \Delta H_{iso} / \Delta H_0. \qquad \text{S4-3}$$

As a check on consistency of the data, we did calculate the residual heat ΔH_r based on $\Delta H_{r,DSC}$ and ΔH_{xi} according to Eq. S3-2, then checked that the traditional Eq. S3-1 gave the same conversion values as those obtained via Eq. S4-3.

The isothermal 30-minute temperatures used to determine values of λ, T_{g0}, and $T_{g\infty}$ were 150, 220, 230, 240, 245, 250, 255, 260, 270, and 290 °C. For each data point, the value of T_g seen during the residual cure scan (from the reversible portion of the signal) was compared to the value predicted by the diBenedetto equation, and the parameters of the diBenedetto equation that minimized the sum of squared differences between predicted and observed values were determined using the Microsoft® Excel Solver algorithm. Note that the lower temperatures tended to give low conversions (and thus values of T_g not that different from T_{g0}, while temperatures of 270 and 290 °C did not produce a measurable T_g., hence 8 data points were used to find the values for the three unknown variables. T_{g0} was also determined using a separate DSC scan using the procedure described in S4.2.1 and compared to the value found by the Solver algorithm.

S4.3 Results and Discussion

S4.3.1 for monomer 1 (1,3,5-tris(4-cyanatophenylmethyl)benzene). The value of T_{g0} found by DSC was -16 °C. Table S4-1 provides the observed actual and minimum possible observed T_g values for the partly cured samples as a function of cure temperature, based on the reasoning described in S4.2.1, along with the resulting point estimate or range estimate for λ, and the observed value of $T_{g\infty}$. The estimated value of $T_{g\infty}$ was taken as the average of these values, or 320 ± 4 °C. The value of λ determined by the non-linear least squares was 0.300, in line with the average value of 0.31 ± 0.07 obtained from the three point estimates. The linear regression using Eq. S4-2 is shown in Figure S4-1. The value of λ was estimated at 0.29 using a weighted regression with weights proportional to the inverse of the uncertainty in the T_g measurement squared. An unweighted regression produced an estimate of 0.28 ±

0.02 for λ. Note that these values are all consistent with the constraints arising from the DSC scans in which no discernible T_g was observed. Taking all the methods into consideration, a value of 0.30 ± 0.05 for λ seemed reasonable. When considering the uncertainties in the model, it should be remembered that the uncertainties in many of the input parameters (e.g. DSC measurements) are not based on well-studied statistical distributions, and that the errors in the model parameters are correlated (e.g. an overestimate of $T_{g\infty}$ will produce an underestimate in λ), thus standard propagation of error calculations are not likely to be useful. Instead, more direct methods can be utilized. For instance, the error in predicting the T_g of partly cured systems may be estimated simply by examining the residuals in the best fit model, which in this case revealed an average deviation of just 5 °C.

Table S4-1

Estimated diBenedetto equation parameters from DSC scans of monomer **1**

Cure Temp. (°C)	α	$T_{g\ as\text{-}cured}$ (°C)	$T_{g\infty}$ (°C)	λ
230	0.82	none (158-168)*	320 ± 5	< 0.25 or > 0.28
250	0.92	246 ± 2	321 ± 2	0.29 ± 0.02
270	0.96	273 ± 8	318 ± 2	0.23 ± 0.08
290	0.98	304 ± 2	319 ± 2	0.38 ± 0.09

* the numbers indicate the temperature range over which a T_g was clearly not observed

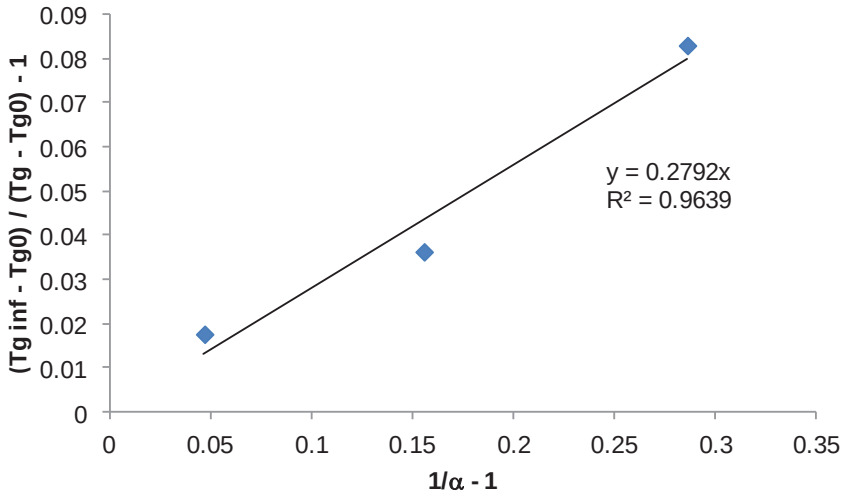

Figure S4.1 Regression plot using the linearized form of the diBenedetto equation (eq. S4-2)

S4.3.2 for monomer 2 (3,5-Bis[(4-cyanatophenyl)methyl)]phenylcyanate). The value of T_{g0} found by DSC was -23 °C, similar to that found for monomer **1**. As mentioned in S4.2.2, the values of $T_{g\infty}$ and λ were estimated simply by analogy with data on comparable cyanate esters as 385 °C and 0.31, respectively. The constrains on the values of λ found by DSC scans are listed in Table S4-2, and, in total, they reveal only that values of λ below about 0.29 are unlikely. A reasonable upper bound for λ based on comparable cyanate esters would be about 0.4. Hence, the uncertainty in λ is asymmetric. Since there are no partly cured T_g values to provide a direct estimate of the prediction error, we note that if the model predictions (listed in the Table) were typically more than about 5 °C too high, a T_g would have been visible where none was observed. Based on the difference in model predictions between λ = 0.3 and λ= 0.4, an underestimate of about 20 °C on average was possible. The uncertainty in $T_{g\infty}$ also results in a change of plus or minus 10 °C on average. If, for lack of a better simple alternative, the errors are assumed to combine randomly, then the total uncertainty ranges from an overestimate of about 12 °C to an underestimate of about 22 °C. Thus, the quality of these estimates is lower than for the other monomers, however the values are still quite reasonable to employ in studies of the evolution of the glass transition temperature during cure so long as the errors and assumptions are noted. One such assumption is that the system cured fully when heated to 350 °C in the DSC, which, given the expected value of $T_{g\infty}$, may not be true. However, a major overestimation of T_g due to invalidity of this assumption is unlikely, as there is a good chance it would have produced at least one clearly seen T_g value where in fact none was seen.

Table S4-2

Estimated diBenedetto equation parameters from DSC scans of monomer **2**

Cure Temp. (°C)	α	$T_{g\ as\text{-}cured}$ (°C)	$T_{g\ model}$ (°C)**	λ
230	0.78	none (155-185)*	190	< 0.22 or > 0.29
250	0.90	none (155-244)*	279	< 0.08 or > 0.21
270	0.95	none (155-265)*	326	< 0.04 or > 0.12
290	0.98	none (155-255)*	360	< 0.02 or > 0.04

* the numbers indicate the temperature range over which a T_g was clearly not observed
** based on $T_{g\infty}$ = 385 °C and λ = 0.31.

S4.3.3 for ESR-255. Table S4-3 shows the observed and predicted (based on the best fit model) T_g values for partly cured ESR-255 as a function of isothermal cure temperature. The best fit model parameters obtained by the Solver algorithm were T_{g0} = -9 °C, $T_{g\infty}$ = 558 °C, and λ = 0.32. Figure S4-2 illustrates the agreement between the fitted model and the data. Note that T_{g0} was separately measured at 8 ± 3 °C, hence the fitted model tends to underestimate the T_g at low conversions. Although the value of λ is similar to what was found for monomer **1**, the value of $T_{g\infty}$ seems remarkably high. By heating a disc sample to decomposition at 50 °C/min in a TMA under nitrogen, a loss peak was observed at 419 °C (see Figure S5-7). Such an experiment should be attempted only with caution and with strong measures to contain the gaseous decomposition products. The results indicate that the T_g of the fully cured network in the absence of thermal degradation, which is what the diBenedetto parameter represents, must be at least 419 °C. Indeed, considering that the removal of just one flexible methylene group from monomer **1** increased the $T_{g\infty}$ of the network by 50 – 80 °C, a further increase of 160 – 190 °C caused by the removal of two more such groups (which yields ESR-255) is not unreasonable. The average deviation between the predicted and observed glass transition temperatures using these model parameters was 10 °C, hence, for T_g values below about 300 °C, the model provides a good empirical predictive capability.

Table S4-3

Estimated diBenedetto equation parameters from DSC scans of ESR-255

Cure Temp. (°C)	α	$T_{g\ as\text{-}cured}$ (°C)	$T_{g\ predicted}$ (°C)
150	0	8 ± 3	-10
220	0.17	22	25
230	0.19	24	30
240	0.25	34	45
245	0.34	62	71
250	0.50	122	129
255	0.60	198	174
260	0.80	304	310

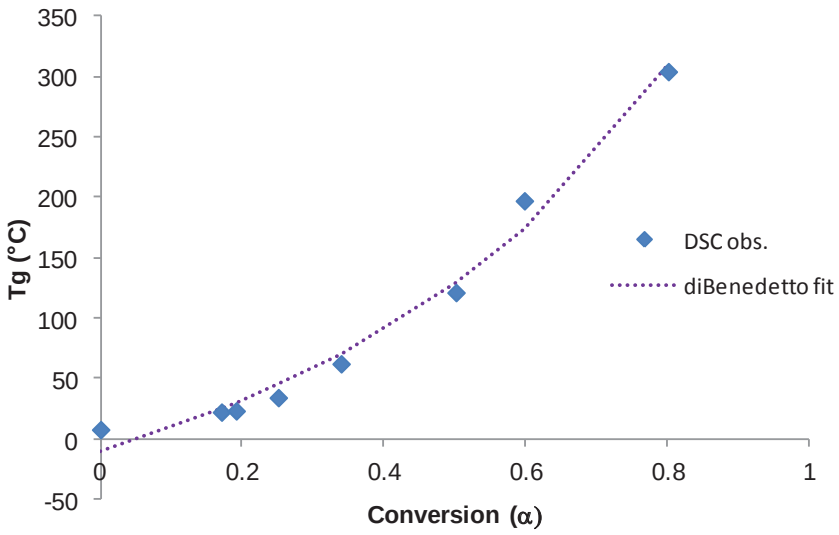

Figure S4.2. Glass transition temperature as a function of conversion for ESR-255

S5. TMA Data on "As Cured", "Fully Cured", and "Wet" Samples

Figures S5-1 through S5-3 show the dynamic TMA (storage and loss components of stiffness along with their ratio (tan delta), for monomer **1**, monomer **2**, and ESR-255, respectively. Note that the heating rate used in these experiments was a very rapid 50 °C / min., a rate that is necessary to avoid significant *in-situ* cure of the samples prior to reaching the glass transition temperature. Above the glass transition temperature, *in-situ* cure is unavoidable, and its effects are evident in the TMA data plots. For monomers **1** and **2** the effects are subtle, such as asymmetric peak shapes and a less than expected drop in the storage component of stiffness on passing through T_g, indicating that *in-situ* cure is not severe. For ESR-255, however, significant *in-situ* cure begins right at the glass transition temperature, owing to the comparatively low conversion. The *in-situ* cure causes the T_g to rise faster than the sample heating rate, which leads to a reversal of the signal trend, that is, the storage actually increases rapidly, and the peak in tan delta coincides with, rather than lags, the peak in the loss component (a lagging tan delta indicates normal de-vitrification, a leading tan delta indicates vitrification, and, typically, a coincident tan delta indicates de-vitrification followed almost immediately by re-vitrification). Remarkably, the glass transition temperature of ESR-255 in the solid state increased faster than 50 °C / min. Through the diBenedetto equation, one may calculate that a conversion rate of 5×10^{-4} / s is sufficient to raise T_g at the required rate, a rate about seven times higher than the observed rate seen in the kinetic data for ESR-255 at 250 °C and a similar conversion.

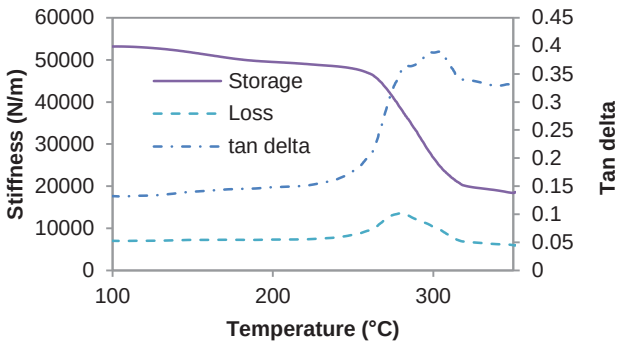

Figure S5-1. Dynamic TMA of "as cured" monomer **1**.

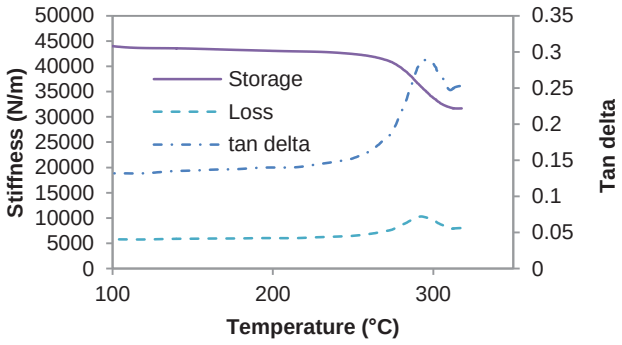

Figure S5-2. Dynamic TMA of "as cured" monomer **2**.

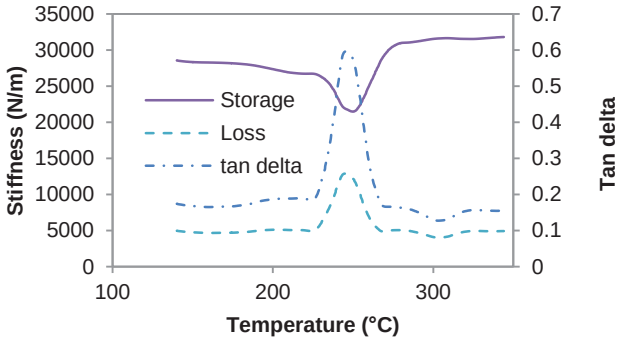

Figure S5-3. Dynamic TMA of "as cured" ESR-255.

Figures S5-4 through S5-6 present the corresponding dynamic TMA data for the "fully cured" monomer **1**, monomer **2**, and ESR-255, respectively. Note that full cure is achieved by first heating these samples at a much slower 10 °C / min to 350 °C, in effect facilitating rather than preventing, *in-situ* cure. Only in the case of monomer **1** is a T_g visible, at 338 °C (loss peak). Figure S5-7 shows the dynamic TMA of ESR-255 heated to decomposition. When the storage finally begins to drop, with a loss peak at 419 °C, decomposition is already well under way. (Please note: such an experiment should be done only with caution and careful provision for the safe and rapid removal of decomposition products.) Thus, it is not possible to determine the (theoretical) softening point of the network in the absence of degradation; only a lower limit for the softening point was found. Although the softening point of ESR-255 has been reported previously,[S6] the extent of cure in the samples was not simultaneously reported.

Figures S5-8 through S5-10 show the dynamic TMA (first heating) of the "wet" monomer **1**, monomer **2**, and ESR-255, respectively. Note that "wet" refers to having been immersed in 85 °C water for 96 hours. As is typical for "wet" samples, bubbles formed soon after the T_g was reached, causing significant disturbances. Nonetheless, the actual glass transition was visible just prior to the onset of the disturbances.

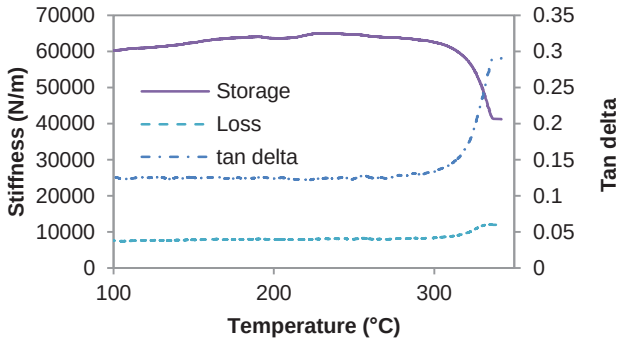

Figure S5-4. Dynamic TMA of "fully cured" monomer **1**.

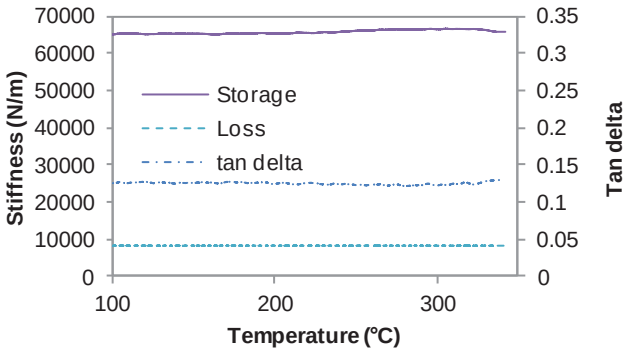

Figure S5-5. Dynamic TMA of "fully cured" monomer **2**.

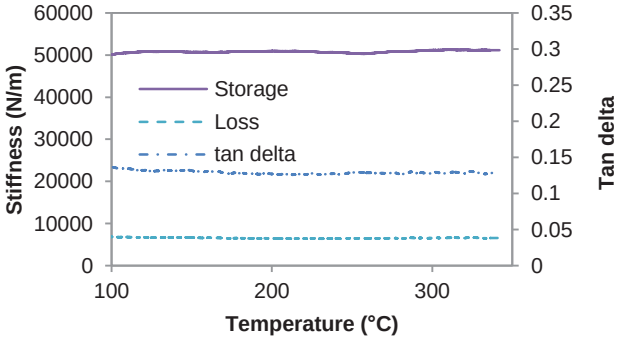

Figure S5-6. Dynamic TMA of "fully cured" ESR-255.

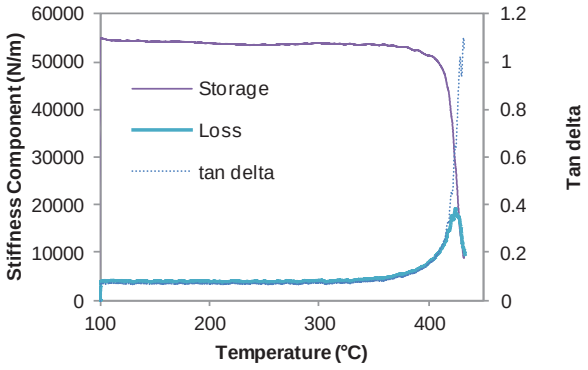

Figure S5-7. Dynamic TMA of ESR-255 heated to decomposition.

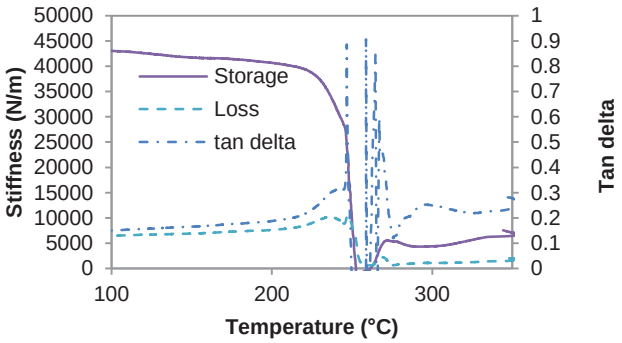

Figure S5-8. Dynamic TMA of "wet" monomer **1**.

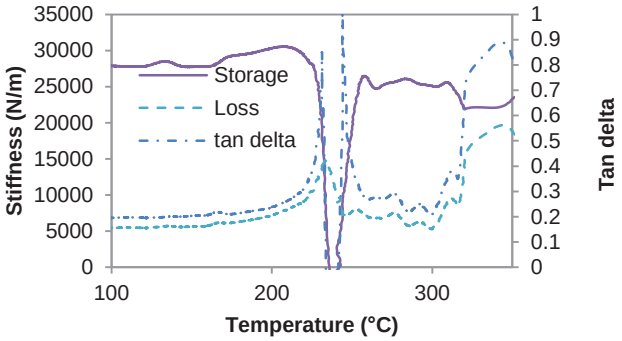

Figure S5-9. Dynamic TMA of "wet" monomer **2**.

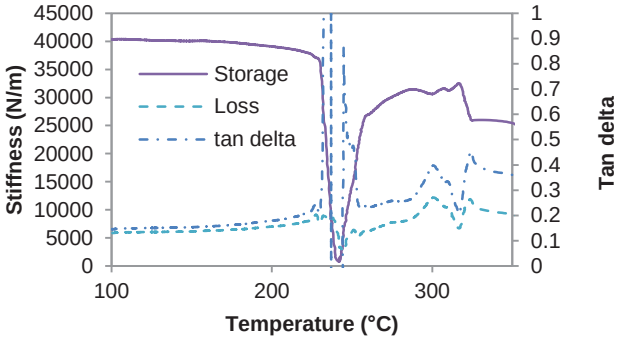

Figure S5-10. Dynamic TMA of "wet" ESR-255.

S6. Detailed Information on the Investigation of Cure Kinetics

S6.1 Introduction. The analysis of cure kinetics generally followed the pattern used in our previous work,[S7] with some notable extensions in order to handle more complex data. For those readers familiar with our previous efforts, Section S6.2 summarizes these efforts in terms of the minor changes and expansions from the previous work. Section S6.3 details the treatment of the raw DSC data to extract the rate of conversion as a function of time including baselines (S6.3.1), isothermal data (S6.3.2), estimation of residual cure (S6.3.3) and combined error analysis (S6.3.4). Section S6.4 describes the analytical methods employed to determine the rate constants, for both individual curves (S6.4.2) and sets of data with temperature-independent exponents (S6.4.3). In Section S6.5, alternative analyses are utilized in order to provide for an estimation of uncertainty, since traditional propagation of error techniques are too unwieldy to be practical for such a complex, nonlinear multi-variate problem. The final data sets are all tabulated in Section S6.6. Note that kinetic parameters were calculated only for samples that reached a clearly defined maximum in their cure rate within the allotted time. In the case of ESR-255, for which only the highest temperatures met the above criterion, additional data sets with longer cure times (4 hours at 250 °C, from the DSC/IR studies reported in Section S3, and 24 hours at 210 °C, from the studies of purity reported in Section S8), were used to supplement the data.

S6.2 Summary of Changes Relative to Method Published in Guenthner *et al*. (Polymer, 2011, 52, 3933-3942).

1. A two-level nested iteration is used to find k_1', k_2', m, and n, relaxing the assumption that $k_1' << k_2'$ used previously. The starting point for the iteration is the same, namely the assumption that $m / (m + n) = \alpha_{max}$, but now the quantity $m / (m + n)$ is adjusted iteratively to match the model α_{max} (which differs slightly from the value of $m / (m + n)$ due to k_1' being non-negligible) to the

experimental α_{max}. This expansion allows for determination of model parameters when k_1' is much larger compared to k_2'.

2. The conversion ranges used in the model are now based on the observed maxima (and in some cases minima) in the conversion rate as a function of conversion curve, rather than on fixed values of conversion. Note that these new criteria are designed to match the previous, fixed values in cases where K_1', << k_2' and the maximum rate of conversion is near $\alpha = 0.5$, as was true in all samples previously analyzed, but is not true in all of the cases reported herein. Hence, the new criteria allow for consistent analysis across a wider range of parameters, particularly it allows for consistent analysis when k_1', is non-negligible and m and n are well above one.
3. The baselines for determining the rate of conversion are now determined by re-scanning the sample through the entire procedure once residual cure is complete. This change was implemented in order to match methods previously reported by others, and its validity was confirmed by the analysis of baseline effects reported in Section S6.3.1. Note that for non-isothermal segments, the re-scanned data is offset as described in S6.3.1 to construct the baseline.

Note that the previously reported kinetic data can thus be regarded as simply a special case of the current analysis technique, one in which k_1' << k_2', $\alpha_{max} = 0.5$, and the re-scanned and internal baselines are not significantly different.

S6.3 Treatment of DSC Data

S6.3.1. Baselines. As noted in S6.2, the DSC data were converted to conversion rates using re-scanned baselines, that is, the entire DSC method was repeated after the completion of cure in order to generate the baseline values. Since this technique has been shown to work well by others,[S3] we investigated the

effects of using a re-scanned baseline in order to validate (and modify, if necessary) the technique, as well as to understand the measurement uncertainties related to the choice of baseline.

We identified two main concerns with the use of re-scanned baselines. The first, referred to as baseline drift, is that, in a method that takes a few hours to run, a slow drift of the baseline over time may lead to significant error. To investigate this effect, we examined the heat flow values measured during the initial, five-minute isothermal segment of the DSC method at 120 °C, a temperature at which the sample was completely melted and no cure took place. To minimize the effect of transients, only the last minute of the segment was used. Table S6-1 shows the differences in the heat flow values recorded on the initial scan compared to those recorded on the re-scan. A baseline drift would be expected to produce differences that varied in a random way among samples. Another possible effect, baseline shift, however would be expected to produce differences that varied in systematic ways. The most likely cause of what we term "baseline shift" is solidification of the sample. For the lower cure temperatures, the sample does not solidify during the isothermal cure segment, but does solidify during residual cure. For the higher temperatures, the sample solidifies during the isothermal cure segment. If a systematic baseline drift took place, it would be present at about the same value for both the 120 °C comparison and the "end of isothermal cure" comparison, for all samples. However, if a shift due to solidification were present, then for samples cured at higher temperatures, the difference should be larger in the 120 °C comparison than in the "end of isothermal cure" comparison, since solidification will have taken place prior to both of the measurements used in the "end of isothermal cure" comparison.

To help the reader identify the relevant data, we have marked samples that solidify between the initial scan and the re-scan with an "x" in Table S6-1. When an "x" is present in the first but not the second column, then a systematic drift should result in similar values in both columns, whereas a solidification-induced shift should result in smaller values in the second column. Table S6-1 also includes

the projected "worst case" difference in measured conversions after the isothermal cure segment, as well as in the maximum conversion rate, that result from assuming that the baseline drift or shift, as indicated by the differences in the 120 °C segment, either are or are not valid corrections to the data. Note that, during the isothermal segments, changes in sample heat capacity should not contribute to differences in the measured heat flow.

Table S6-1

Parameters Related to Investigation of Re-Scanned DSC Baseline (Isothermal Segments)

Sample ID	Difference in heat flow (initial isothermal segment), mW[a]	Difference in heat flow (end of isothermal cure segment), mW[a]	Difference in conversion after isothermal cure (drift/shift vs. no drift/shift assumed) [b]	Relative change in max conversion rate (drift/shift vs. no drift/shift assumed) [a]
Monomer 1 – 210 °C	-0.0161 x	n/a[c] x	-1.8%	-1.0×10^{-5} /s (-3.6%)
Monomer 1 – 230 °C	-0.0129 x	n/a[c] x	-1.1%	-5.9×10^{-6} /s (-0.7%)
Monomer 1 – 250 °C	-0.0108 x	-0.020	-1.2%	-6.4×10^{-6} /s (-0.3%)
Monomer 1 – 270 °C	-0.0124 x	-0.011	-1.2%	-6.6×10^{-6} /s (-0.2%)
Monomer 1 – 290 °C	-0.0128 x	-0.007	-1.2%	-6.6×10^{-6} /s (-0.1%)
Monomer 2 – 210 °C	-0.0099 x	n/a[c] x	-0.7%	-3.8×10^{-6} /s (-5.1%)
Monomer 2 – 230 °C	-0.0172 x	n/a[c] x	-2.4%	-1.3×10^{-5} /s (-2.4%)
Monomer 2 – 250 °C	-0.0168 x	-0.039	-1.5%	-8.5×10^{-6} /s (-0.7%)
Monomer 2 – 270 °C	-0.0309 x	-0.027	-2.3%	-1.3×10^{-5} /s (-0.5%)
Monomer 2 – 290 °C	-0.0349 x	-0.024	-2.4%	-1.3×10^{-5} /s (-0.2%)
ESR-255 – 230 °C	-0.0116 x	n/a[c] x	-0.7%	-4.1×10^{-6} /s (-4.3%)
ESR-255 – 230 °C	-0.0033 x	n/a[c] x	-0.3%	-1.7×10^{-6} /s (-1.0%)
ESR-255 – 250 °C	-0.0184 x	n/a[c] x	-1.1%	-6.3×10^{-6} /s (-1.3%)
ESR-255 – 270 °C	-0.0428 x	-0.040	-3.3%	-1.8×10^{-5} /s (-1.7%)
ESR-255 – 290 °C	-0.0238 x	-0.086	-2.1%	-1.1×10^{-5} /s (-0.5%)
ESR-255 – 250 °C 4h	-0.0253 x	-0.007	-16.7%	-1.2×10^{-5} /s (-2.8%)

[a] value on re-scan minus value on first scan

[b] (value assuming drift/shift minus value assuming no drift / shift) / value assuming no drift/shift

[c] heat flow signal did not reach a constant value during isothermal cure (incomplete cure)

"x" indicates sample vitrified (i.e. T_g surpassed the isothermal temperature) between measurements

The differences seen in Table S6-1 do seem to show systematic effects. In particular, the samples cured at the higher temperatures (or the longest times), which result in the highest extent of solidification, show the expected effects of a baseline shift due to solidification. Note that the sample cure rates at the end of the isothermal segment, which are not quite equal to zero, may also affect the

results. The ESR-255 sample that was cured isothermally for four hours as part of the DSC/IR experiments described in Section S3 also provided a useful set of data. If baseline drift were a major issue, one would expect this sample to show a significantly larger difference than the others, whereas in fact the differences are quite similar. Thus, while baseline drift can be ruled out as a source of concern, baseline shift due to solidification cannot be ruled out.

Although it cannot be ruled out as a source of concern, Table S6-1 shows that, for 30 minute isothermal cure segments, the baseline shift issue is not a major source of error. The projected difference in conversion results from assuming a constant error in the heat flow rate, but, in the case of a shift due to solidification, such a difference will only affect the data up to the point of solidification. For samples cured at the higher temperatures, this point is reached very early in the isothermal cure segment, such that the probable error from neglecting to account for baseline shift is about an order of magnitude less than the worst-case estimate shown in Table S6-1. For the ESR-255 / four hour cure sample, similarly, the large error in conversion will only occur if the sample does not solidify during the entire four hour isothermal cure. Since, in fact, the sample solidifies after only 30-60 minutes, the actual error in conversion is more likely to be just 2-4%. As will be shown in discussion of errors (S6.3.4), the projected errors in Table S6-1 are generally a small component of the errors present in the measurement. Thus, although baseline shift due to solidification cannot be ruled out, it can be safely ignored without significant loss of data quality, so long as either 1) isothermal cure times are limited to 30 minutes, or 2) solidification of the sample takes place in about 30 minutes if a longer isothermal time is used.

For non-isothermal segments, not only are baseline drifts and shifts due to solidification possible, but also changes in sample mass or heat capacity can also contribute to apparent offsets in the re-scanned baseline. As with the isothermal data, the effects of drift should be essentially independent

of sample condition, whereas baseline shifts should be more prominent in samples that solidify between the initial scan and the re-scan. Though mass loss is expected to be negligible in the sealed DSC samples, heat capacity changes might also be expected to play a role in samples that exhibit significant residual cure. Table S6-2 lists the apparent offset in the baseline (determined by considering the maximum amount the re-scanned heat flow would need to be offset to avoid negative values of residual cure, as illustrated in Figure S6-1) for the different samples studied. Samples that solidify between the initial scan and re-scan are indicated by an "x" in Table S6-2 as in Table S6-1. In most cases, samples that have solidified prior to the initial scan show much smaller offsets than do those that solidify between the scans.

The effect of ignoring the apparent offset in the baseline on conversion is also shown in parenthesis in the entries in Table S6-2. Unlike the case for the isothermal segments, the apparent offsets do make a significant difference in the calculation of conversions, potentially up to about 10%. Also, unlike the isothermal cases, if a baseline shift does occur due primarily to solidification, for these samples it generally would have taken place at least halfway through the non-isothermal scan (vitrification is approximately synchronous with the peak of the residual cure for samples not already solidified), and thus most of the potential error (which is based on the assumption of an incorrect heat flow throughout the entire segment) will likely be realized. Hence, these errors are too large to ignore, and, therefore, in the treatment of the non-isothermal data we have assumed that a baseline shift does occur and made use of the apparent offset in calculating the residual enthalpy of cure.

Table S6-2

Apparent Offset in Re-scanned Baseline (Non-isothermal Segments) and Its Effect on Conversion Estimates

Cure Temperature (°C)	Monomer 1	Monomer 2	ESR-255
210	+0.073 (5.7%) x	-0.213 (9.6%) x	-0.233 (10.0%) x
230	-0.010 (0.6%) x	-0.016 (1.0%) x	-0.145 (9.2%) x
250	-0.004 (0.3%)	+0.049 (2.9%)	-0.276 (11.5%) x
270	+0.003 (0.2%)	+0.047 (2.2%)	-0.090 (4.6%)
290	-0.005 (0.3%)	+0.088 (4.0%)	-0.038 (2.2%)

"x" indicates the sample vitrified (i.e. T_g surpassed the cure temperature) between measurements

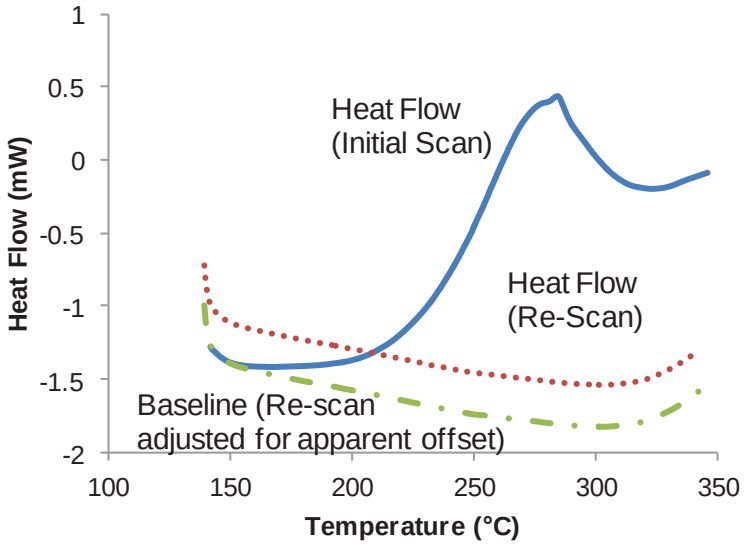

Figure S6-1. Illustration (using residual scan of ESR-255 cured at 250 °C for 30 minutes) of the apparent offset needed when constructing a baseline from heat flow data generated during a re-scan of the sample (non-isothermal segments only). The offset is calculated by subtracting the re-scanned data from the initial data, noting the minimum (most negative or least positive) value.

S6.3.2 Issues with isothermal data. The primary issue affecting the isothermal data is the determination of conversion rates at the start of the isothermal segment. Although heating rates approaching 100 °C / min. are attainable in the DSC, this means that the "jump" needed to reach the

isothermal cure temperature can take up to about two minutes, followed by a short period of equilibration during which transient signals will affect the data. Particularly during the last 30 seconds or so of the "jump" for samples cured at high temperatures, a significant amount of cure does take place and cannot be ignored without significant loss of data quality. Fortunately, the use of the re-scanned baseline provides a convenient way to estimate the heat flow during the initial "jump" and transient periods. However, because the "jump" involves very high heating rates, the DSC signal during the jump will be dominated by the heat capacity term, which is proportional to the heating rate. Hence, during the "jump" and initial transient period, which we defined as any period in which the heating rate exceeded 0.1 °C / min., the baseline was constructed by finding the re-scanned data points with the matching heating rate, rather than the matching elapsed time as was done for the remaining isothermal data.

The use of the re-scanned baseline in the manner just depicted can lead to slightly negative apparent values for the rate of cure. In order to correct this problem, we identified the latest point in the data (always well before the end of the "jump") in which an apparent cure rate of zero or less was computed. We then set the cure rate for all times up to this point to zero, essentially excluding it from consideration. Furthermore, the dynamics of the transients are likely not reproduced exactly during the re-scan, though, typically these transients produce sinusoidal patterns superimposed on the data, and therefore, if averaged over time (as in integration to determine conversion) the transient effects are significantly reduced. At lower cure rates, the transient effects are important for a longer time period. Hence, we believe the best method for dealing with the transients is to exclude from further analysis the cure rate data for the first 10% of conversion beyond the initial minimum seen in the rate (often at zero), with the exception of integrating the heat flow values in order to estimate the conversion at the start of the useable rate data. Using a cut-off criteria based on conversion automatically compensates

for the aforementioned effects of temperature on the length of time that transients are important, but also necessitates the integration of the heat flow during the transient period.

As mentioned in the discussion on baselines (S6.3.1), for the isothermal data, any apparent baseline shifts due to solidification of the sample are not taken into account. In addition to subtraction of baseline, there are issues relating to how to calibrate (or scale) the heat flow data. The weighing of mg scale DSC samples typically involves errors of at least a few per cent, and for isothermal cure studies on cyanate esters it is important not to use large samples due to the need to rapidly remove the considerable quantities of heat generated during rapid cure. Fortunately, for the highly crystalline monomers under study, the enthalpy of melting can be measured to within about 1%, and, since it was measured many times (see the tables in Section S7), it was used as an internal standard to correct for small weighing errors.

S6.3.3 Issues with non-isothermal data. For the non-isothermal data, the only analysis performed is an integration of the residual heat flow to determine the residual enthalpy of cure and, hence, conversion at the end of the isothermal cure segment. For this data collection, the initial transient involves quenching the sample and holding at low temperatures. We did not attempt to integrate the heat flows during the quench, since, for samples cured at high temperature, significant cure tended to cease long before the end of the isothermal period, while, at low cure temperatures, significant cure ceased almost immediately once the quench began. Since, as mentioned in S6.3.2, the main issue with transients is loss of accurate heat flow data rather than integrated errors, and since the only operation performed on non-isothermal data was integration, we did not investigate transient effects in detail. In determining the offset needed to construct the baseline, there is, as a consequence of the method used, a single point at which the heat flow equals zero (see Figure S6-1). We simply assumed that this point represented the start of residual cure and did not integrate any signals prior to this point during the

segment. Since this point typically was well past the start of the segment (and typically became later and later in the segment with increasing cure temperature), it effectively excludes portions of the data affected by transients from consideration.

Note that, as explained in Section S6.3.1, apparent baseline shifts are not ignored in the non-isothermal data, due to the magnitude of the potential errors involved. Including the shifts does seem appropriate as, at lower isothermal cure temperatures, it tends to result in a lower apparent onset temperature for residual cure, while at higher temperatures, it tends to result in a higher apparent onset temperature for residual cure. In addition, as with the isothermal cure data, the measured enthalpy of melting was used as an internal standard to calibrate the heat flow values as explained at the end of Section S6.3.2.

S6.3.4 Error estimates. Since, as outlined above, there are significant potential issues with the handling of the raw DSC data, we believe that it is important to attempt to understand the potential errors involved. In Tables S6-1 and S6-2, we have included "worst-case" error estimates for the effects on measured conversions at the end of the isothermal cure step and maximum rates of cure during the isothermal step. The effect of our treatment of transients, though, is much more difficult to assess, other than to note that, based on the appearance of what seem to be artificial "bumps" in the otherwise smooth conversion rate curves (see Figures S6-10 through S6-12, and note that these data were collected and shown but not used in subsequent analysis), the effect of transients appears to extend consistently through the first 4-7% of conversion. The magnitude of these "bumps" would be consistent with errors in conversion rates of around 10%, and hence total errors in integrated conversion of less than 1%.

Although we were able to obtain some rough estimates of the effects of individual sources of error, many of these errors are not likely to involve normal probability distributions. Baseline shifts, for

instance, either do or do not occur, and although their estimated effects involve some random errors, the actual error in the baseline estimate is more likely to be 10% of the computed offset (for a properly corrected shift) or 90% of the computed offset (for an improperly corrected shift) than say, 50% of the computed offset, resulting in a complex bimodal probability distribution. Therefore, propagation of error calculations cannot be performed in a straightforward way; a better approach to estimating the overall error is to look at the variability in composite measurements.

Fortunately, the total enthalpy of cure for each monomer should be independent of cure temperature. Even for ESR-255, which cannot be fully cured in the DSC (see Sections S2 and S3), the enthalpy of cure up to 350 °C is still likely to be independent of the earlier isothermal cure temperature, provided that the isothermal cure temperatures used are well below 350 °C. Even better, for cyanate esters, the total enthalpy of cure is almost always in the range of 100 – 110 kJ/eq. for uncatalyzed samples, and is available from non-isothermal measurements, thus, an assessment of accuracy as well as precision is available by comparing the total enthalpy of cure for these samples. Again, even for ESR-255, the extent of cure for ramps to 350 °C is known from the IR data, and can be combined with the known enthalpy of cure of cyanate esters to provide an assessment of accuracy. Lastly, if we wish to determine whether or not a particular factor contributes significantly to the total error, we can in many cases check the effect on the variation in the total enthalpy of cure. If a particular change (such as ignoring a baseline shift) does not affect the variation in the total enthalpy of cure, then it is likely not a significant source of error. In addition to composite measurements, in some cases we have data sets that are, practically speaking, replicates. For instance, the 250 °C isothermal cure data for ESR-255 that was collected as part of the IR/DSC determination of conversion (Section S3) can be compared to the data generated using the standard cure kinetics procedure at the same temperature to get a sense of the level of reproducibility of the data.

Table S6-3 shows the total enthalpy of cure for each of the samples analyzed for cure kinetics, plus the replicated ESR-255 data at 250 °C. The first numerical column shows the values for the data set as treated; subsequent columns show the effect of possible variations, namely, including a correction for baseline shift in the isothermal data, not offsetting the re-scanned baseline in the non-isothermal data, and not making use of the heat of melting as an internal calibration, respectively. For each monomer tested, the average and standard deviation are shown. The average values are also compared to those found from non-isothermal DSC runs (the standard method for estimating enthalpies of cure). For ESR-

Table S6-3

Enthalpies of cure of cyanate ester monomers for various DSC data treatment scenarios

Sample ID	ΔH_{cure} – as-measured (kJ/eq.)	ΔH_{cure} – if baseline shift in isothermal segments is included (kJ/eq.)	ΔH_{cure} – if offset in non-isothermal segment baseline is not included (kJ/eq.)	ΔH_{cure} – if internal calibration is ignored (kJ/eq.)
Monomer 1 – 210 °C	118.9	116.7	125.7	94.0
Monomer 1 – 230 °C	123.0	121.7	123.7	154.5
Monomer 1 – 250 °C	127.1	125.6	126.7	123.1
Monomer 1 – 270 °C	128.7	127.2	129.0	124.0
Monomer 1 – 290 °C	127.8	126.3	127.4	122.2
Average (Isothermal runs)	125.1 ± 4.1	123.5 ± 4.3	126.5 ± 2.0	123.6 ± 21.5
Non-isothermal DSC	119.3	n/a	106.6	122.7
Monomer 2 – 210 °C	127.1	126.3	115.0	130.5
Monomer 2 – 230 °C	123.2	120.2	121.9	117.9
Monomer 2 – 250 °C	119.4	117.6	122.9	125.1
Monomer 2 – 270 °C	113.1	110.5	115.6	117.3
Monomer 2 – 290 °C	128.0	124.9	133.1	129.1
Average (Isothermal runs)	122.1 ± 6.1	119.9 ± 6.3	121.7 ± 7.3	124.0 ± 6.2
Non-isothermal DSC	105.7	n/a	145.6	100.4
ESR-255 – 230 °C	102.6	101.8	92.3	101.1)
ESR-255 – 230 °C	100.2	99.9	91.0	109.4
ESR-255 – 250 °C	99.4	98.3	88.0	91.4
ESR-255 – 270 °C	95.2	92.0	90.8	85.2
ESR-255 – 290 °C	97.8	95.7	95.7	105.7
Average (Isothermal runs)	99.1± 2.8	97.6 ± 3.8	91.6 ± 2.8	97.9 ± 11.5
Non-isothermal DSC	93.1	n/a	80.1	92.6
ESR-255 – 250 °C 4h (IR)	95.5	79.5	84.4	85.0

* from the data set used to determine diBenedetto equation parameters

255, the enthalpy shown is for cure to 350 °C rather than complete cure (the DSC/IR technique in Section S3 indicates that the total enthalpy of cure should be about 14 kJ/eq. higher than the listed enthalpies).

The key result indicated by the data in Table S6-3 is that, of the four methods, the as-treated data provided the least variation between isothermal and non-isothermal methods, the least variation among the different monomers, which should have similar enthalpies of cure, and either the lowest or second to lowest variation within each set of isothermal kinetics data for a given monomer. Of the 19 samples investigated, the only sample for which an alternate method appears to give a more reliable estimate of the enthalpy of cure is monomer **1** cured isothermally at 210 °C. This particular sample was notable (see Table S6-2) for having the largest positive offset in the non-isothermal baseline of any of the samples listed in the table, an offset that is an order of magnitude larger than any of the others for monomer **1**. This sample features the shallowest quench depth of any sample (87 °C). Moreover, in this sample, the conditions at the end of isothermal cure (conversion near 50% and hence auto-catalysis having maximum influence) are the most difficult for readily quenching the reaction. It thus appears that in this particular case, complete quenching was not achieved, meaning that the minimum observed DSC signal with respect to the re-scanned value did not reflect true baseline (no residual cure) conditions, since cure was likely not completely stopped at the start of the residual heating scan. As a result, the computed offset for the baseline was artificially positive, leading to a residual enthalpy of cure that was too low and an error of approximately 5% in the total enthalpy of cure. Since this particular shortcoming in the as-used baseline construction method affected only 1 of 19 samples, was associated with clear indicators of anomalous conditions, and resulted in an error that was similar in magnitude to the apparent uncertainty of the measurement in general, we believe it is more appropriate to retain an identical data treatment method for all samples rather than to employ complex criteria in order to eliminate this occasional source of error.

From Table S6-3 it can also be seen that the isothermal methods (which include a non-isothermal segment with the same temperature ramp rate and range as the purely non-isothermal methods) yield slightly larger values of the enthalpy of cure using the as-treated data. This result makes sense given that the isothermal method always involves additional opportunities for the sample to cure compared to the purely non-isothermal data, although the same result could also be due to systematic errors such as an overestimation of heat flow when transient signals affect the isothermal data. In contrast, any data sets that show a lower enthalpy of cure for the isothermal method most likely involve errors in data treatment. Such data sets are, however, only generated when the offset in the non-isothermal segment baseline is ignored. Further, for the purely non-isothermal methods, ignoring the offset in the baseline results in large differences in cure enthalpies for the three monomers studied (even accounting for the incomplete cure of ESR-255), a situation which is highly unlikely in reality. Ignoring the internal calibration of heat flows by measurement of the enthalpy of melting at times results in large variations within monomers, but, on average, yields results very similar to the other methods. This feature is a good indicator that the errors introduced in weighing the samples (that are corrected via the internal calibration) are indeed unbiased, and hence, in non-crystalline monomers that do not afford such internal calibration, replication of samples can be used effectively to reduce this source of error, which appears to average around 10%.

In summary the total enthalpy of cure data indicate a precision of around 3-5% in measurements obtained directly from DSC data without the use of kinetic models. Comparisons among different monomers also indicate a relative error of around 5% in the measured data, while comparisons of the measured enthalpies of cure to the expected value of 110 kJ/eq. indicate that, in terms of absolute accuracy (which is difficult to gauge with newly synthesized materials), the errors may be as high as 10% on average. These results illustrate, as previously pointed out by Hamerton[S8] and others,

the importance of carefully considering issues relating to baseline construction in the treatment of DSC chemical kinetics data.

S6.3.5 Step-by-step implementation of DSC cure kinetics method. Figure S6-2 illustrates the steps in the DSC program, which are as follows: A) ramp at 5 °C/min to 120 °C in order to melt the monomer B) isothermal for 5 minutes (check for baseline drifts and shifts) C) jump to isothermal cure temperature (approx. 100 °C / min.) D) isothermal cure for 30 minutes E) quench to 120 °C (note that in reality the quench, at approx. 100 °C / min only reaches minimum temperatures near 135 °C before the program set-point again induces heating) F) heat at 10 °C / min. to 350 °C (residual cure). Following this program the DSC is cooled (step G) to 120 °C and steps B through F (labeled B' through F') are repeated in order to generate the re-scanned baseline.

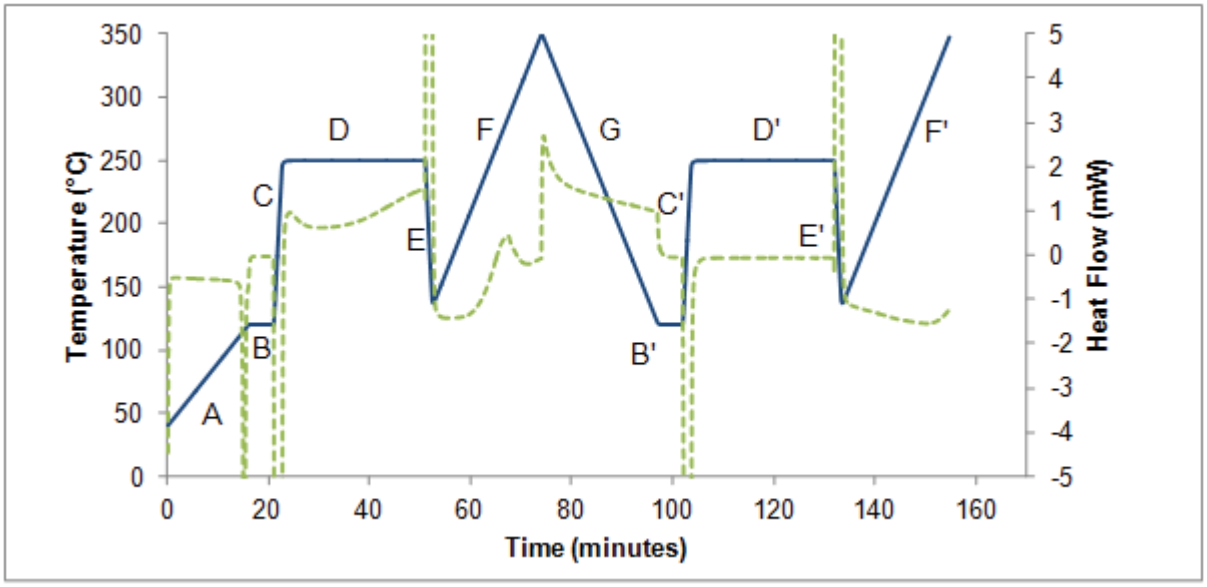

Figure S6-2. Illustration of DSC isothermal kinetics program (see text at start of S6.3.5 for detailed description of steps) showing temperature (solid line, left axis) and measured heat flow (dashed line, right axis) for the ESR-255 sample with an isothermal cure temperature of 250 °C.

To prepare the data for kinetics analysis, perform the following steps:

1. *Subtract baseline*. Subtract heat flow values found in steps C, D, and F from their matching re-scanned baseline values (C', D', and F', respectively). For step C, match values on the basis of heating rate, for step D, match values on the basis of elapsed time, and for step F, match values on the basis of temperature. Note that the boundary between sections C and D (as well as C' and D') is defined as the point in time when the heating rate falls below 0.1 °C / min. Herein the resultant sets of heat flow difference data are denoted ΔC, ΔD, and ΔF.

2. *Offset non-isothermal data to correct for baseline shift*. Find the minimum (most negative) value in ΔF (referred to as ΔF_{min}). Subtract ΔF_{min} from all values in ΔF. The resultant set of values is referred to as ΔF_{offset}. Note that the minimum value of ΔF_{offset} should be zero.

3. *Discard unreliable data*. Find the latest point in time for which an associated value in $\Delta C \leq 0$. Set all values in ΔC associated with a prior time to zero. Set any values remaining in ΔC or in ΔD that are ≤ 0 to zero. Find the earliest point in time for which an associated value in ΔF_{offset} equals zero. Set all values in ΔF_{offset} associated with a prior time to zero.

4. *Calibrate heat flow data*. Measure the enthalpy of melting of the sample, and multiply all the newly adjusted values in ΔC, ΔD, and ΔF_{offset} by the ratio of the known enthalpy of melting for the material to the measured enthalpy of melting. The resulting heat flows (as functions of time, and normalized by weight) are referred to as $q_C(t)$, $q_D(t)$, and $q_{Foffset}(t)$.

5. *Integrate heat flows*. Integrate the heat flows $q_C(t)$ and $q_D(t)$, as a function of time (define the reference time $t' = t - t_0$, where t_0 is the time associated with the first non-zero value of q_C) to generate the isothermal enthalpy of cure $H_{iso}(t')$. Integrate the heat flow $q_{Foffset}(t)$ over its entire range to compute the residual enthalpy of cure H_{res}. For fully curable samples, define the total enthalpy of cure

(H_0) as the maximum value of $H_{iso}(t')$ + H_{res}, or, for samples such as ESR-255 that cannot be fully cured without thermal degradation, use a previously determined value for H_0 (for ESR-255, 110 kJ/eq., that is, 866 J/g).

6. *Generate conversion and conversion rate data sets*. At intervals of every 0.25 minutes (or 0.125 minutes for samples that reach 50% conversion in under 3 minutes) starting at t' = 0, average the values of $q_C(t')$ and/or $q_D(t')$, divided by H_0, over a window of 0.1 minute centered on t' to generate conversion rate ($d\alpha/dt$) data. At the same intervals, divide (without averaging over a window), the last available (prior to t') value of $H_{iso}(t')$ by H_0 to obtain conversion (α) data. The result should be a set of values of $d\alpha/dt$ and α at regular intervals of t', referred to herein as "isothermal kinetics data"

S6.4 Analysis of Isothermal Kinetics Data using Kamal Model

S6.4.1 Introduction. In previous work[S7] we have analyzed cyanate ester isothermal kinetics data using the Kamal model,[S9] namely

$$\frac{d\alpha}{dt} = k_1'(1-\alpha)^n + k_2'\alpha^m(1-\alpha)^n \qquad \text{(S6-1)}$$

in combination with a modified version of Kenny's graphical method,[S10] and found an excellent and reliable fit to the data. The previously developed method, however, was limited to data in which the catalytic rate constant k_1' was much smaller than the auto-catalytic rate constant k_2'. We then found parameters for a version of the Kamal model in which the exponents are assumed to remain constant (at the average values of m and n obtained over all temperatures investigated), namely

$$\frac{d\alpha}{dt} = k_1(1-\alpha)^{\bar{n}} + k_2\alpha^{\bar{m}}(1-\alpha)^{\bar{n}} \qquad \text{(S6-2)}$$

(note the differences in notation) and utilized it to compute the activation energy of the auto-catalytic component for the monomers under study. Note that because of correlations among model parameters

and actual reaction rates (i.e. a different value of m or n will give a different reaction rate for the same value of k_2'), meaningful values of activation energy require exponents that are constant with respect to temperature.

In what follows, we expand the previously developed method to include the more general case in which the auto-catalytic parameter is merely significant, that is, $k_1' < k_2'$ or $k_1' \sim k_2'$. The goal of the analysis, however, remains the determination of significant comparative parameters in order to better understand structure-property relationships. Because catalysis of cyanate esters depends on impurities rather than on network structure, and may involve many different reaction mechanisms, the catalytic rate constant conveys information of limited usefulness for structure property relationships. However, because cyanate esters (when cured under appropriate conditions) form networks with a single, well-defined network structure based on cyanurate linkages, and because it is the catalytic effect of these cyanurate groups that is responsible for auto-catalysis, the auto-catalytic rate constant provides a useful means of comparing the effect of monomer structure on cure chemistry involving a mechanism that is common to all monomers. Our approach is thus designed to emphasize the extraction of meaningful data relating to rates of auto-catalysis.

Section S6.4.2 covers the analysis of individual isothermal kinetics data sets to find the best fit parameters of Eq. S6-1, while in Section S6.4.3, the determination of the rate constants in the Kamal model with temperature-independent exponents (Eq. S6-2) is described.

S6.4.2 Kamal model parameters for individual isothermal kinetics data curves. In the Kamal model, there are four parameters to be determined. In Kenny's graphical method, two of these parameters are determined via linear regression, while a third (the catalytic rate constant) is determined by matching a key feature of the data (the initial reaction rate) to the model prediction (which depends only on a single parameter), with the fourth parameter determined by visual judgment of which value yields the

straightest line for linear regression. Since Kenny's graphical method was developed before the advent of powerful desktop computers, the visual method, despite its subjectivity, was needed to enable the analysis to be completed in a reasonable period of time in practical settings. In the previously developed approach, we replaced the subjective visual analysis with a single-parameter iteration that is now easily carried out in a few seconds on a desktop computer. The iteration relied on matching another key feature of the data, the conversion at which the reaction rate is maximum (α_{max}), which when $k_1' << k_2'$, is used as the basis of a simple constraint among two model parameters that replaces the "straightest line" constraint.

In expanding the model to more general situations, there are two key complications. The first is that the parameter α_{max} is no longer given by a simple analytical formula, however, a more complex procedure can still be used in which the model α_{max} is matched to the experimental value via a second level of iteration (the resulting procedure thus involves a two-level, nested iteration using two data features to determine two model parameters, with two others determined by linear regression). The second is that the shape of the reaction rate curve as a function of conversion may be more complex, starting at a non-zero value at zero conversion, and then either rising through a single maximum, or, if m ~ n >> 1, falling to an initial local minimum then rising through a maximum as conversion increases. In the latter case, the range of conversions in which auto-catalysis dominates is between the early local minimum (herein referred to as α_{min}) and α_{max}. Our method is therefore designed to focus on modeling reaction rates for conversions between α_{min} and α_{max}, (with α_{min} = 0 in many cases). The flow chart in Figure S6-3 summarizes the method.

The outer iteration loop is primarily designed to match the model value of α_{max} to the experimental value. To accomplish this task, an intermediate parameter $\alpha_{max\text{-}k2}$ is defined as equal to the ratio m / (m+n). This parameter represents the conversion at which the reaction rate due to auto-

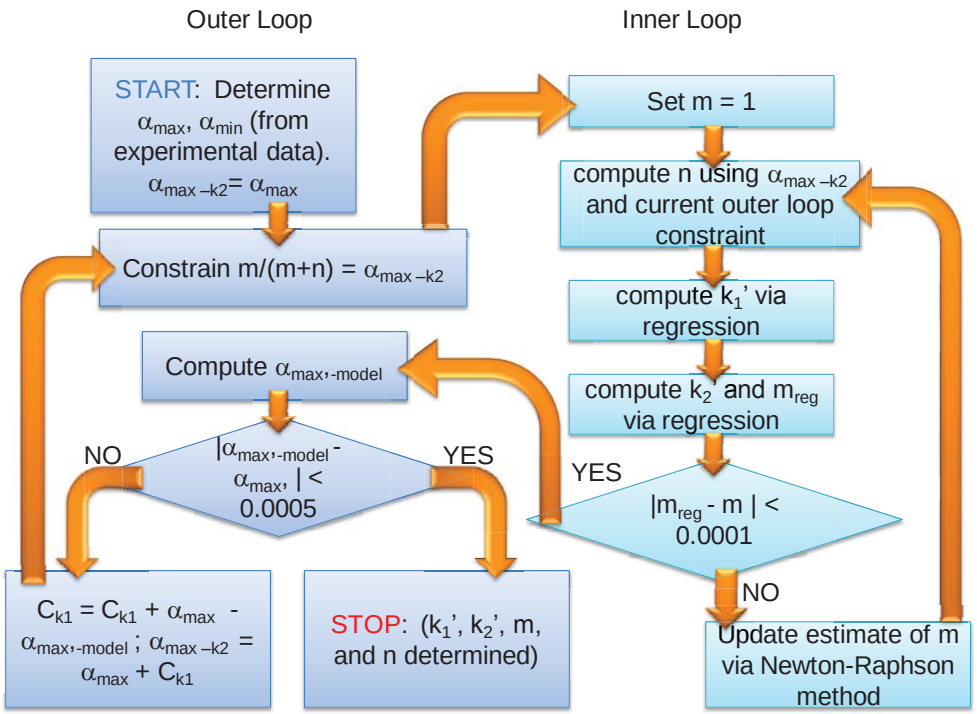

Figure S6-3. Flow chart illustrating the procedure for fitting individual isothermal kinetics data to Kamal model parameters using a modified version of Kenny's graphical method.

catalysis is maximum. When $k_1' = 0$, $\alpha_{max\text{-}k2}$ and α_{max} coincide exactly. The outer loop iteration works on the principle that if k_1' is not too large, $\alpha_{max\text{-}k2}$ and α_{max} will be fairly close to one another, and approximately related by $\alpha_{max\text{-}k2} = \alpha_{max} + C_{k1}$, where the offset C_{k1} is likely most strongly a function of k_1'/k_2'. To initialize the outer loop, the initial guess $C_{k1} = 0$ (that is, $\alpha_{max\text{-}k2} = \alpha_{max}$) is used. The inner loop then operates, as described later) by choosing a value of m, using the guess for $\alpha_{max\text{-}k2}$ to compute n, then computing k_1', k_2', and the updated guess for m, until the inner loop converges. After convergence, the reaction rate is calculated for all values of α with a resolution of 0.001 based on the converged inner loop values of k_1', k_2', m, and n. From the set of reaction rate values, the value of α associated with the largest computed reaction rate, that is, $\alpha_{max\text{-}model}$, is selected. The model and observed values of α_{max} are

then compared, and a new estimate for C_{k1} is computed according to the simple formula, $C_{k1} = C_{k1} + \alpha_{max} - \alpha_{max\text{-}model}$. The updated value of C_{k1} is then used to generate a new value of $\alpha_{max\text{-}k2}$ and repeat the inner loop based on the updated constraint between m and n. The process continues until the absolute value of C_{k1} is less than 0.0005, a criterion that was always met within four iterations of the outer loop. Note that, in order to improve the estimation of α_{max}, the experimental value is refined by fitting a cubic polynomial to the five data points spanning the experimentally observed maximum at the mid-point and using the maximum of the interpolating polynomial.

Figure S6-4 illustrates the process using the data for ESR-255 cured at 270 °C. Figure S6-4 shows the polynomial interpolation, which is used to refine the estimate of α_{max} from 0.549 (with resolution of about 0.016) to 0.546 (with a resolution of about 0.001). For the initial guess, $\alpha_{max\text{-}k2} = 0.546$, which, after operation of the inner loop, generates the model curve, shown compared to experimental data in Figure S6-5. After the first operation of the inner loop, $\alpha_{max\text{-}model} = 0.523$, hence C_{k1} is then updated from zero (the initial guess) to 0.023. This generates $\alpha_{max\text{-}k2} = 0.569$ for the next iteration, which, after operation of the inner loop with the updated constraint between m and n, generates slightly different values for k_1', k_2', m, and n, and $\alpha_{max\text{-}model} = 0.543$. C_{k1} is then incremented from 0.023 to 0.026, and the process repeated. The outer loop converges at $C_{k1} = 0.027$, or $\alpha_{max\text{-}k2} = 0.573$. The set of k_1', k_2', m, and n for which $m / (m+n) = 0.573$ are then used as the "best fit" model parameters.

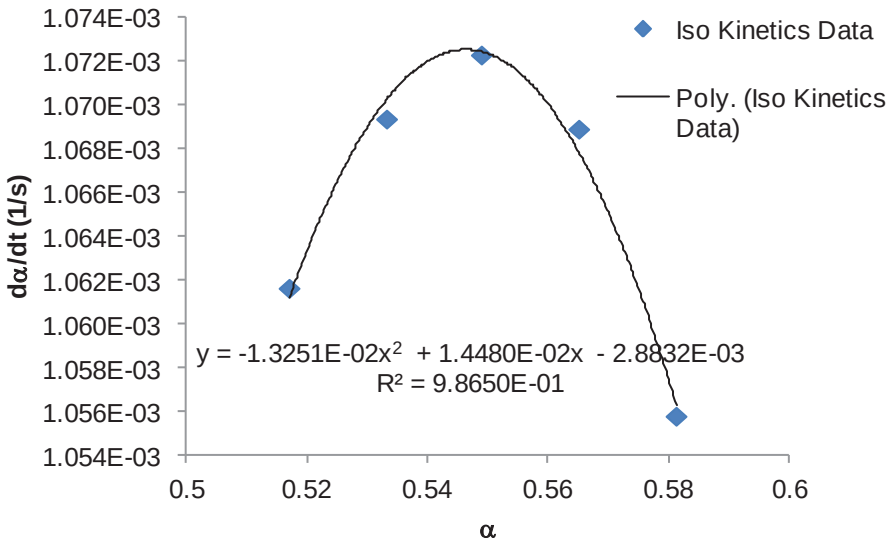

Figure S6-4. Isothermal kinetics data near the maximum reaction rate for ESR-255 cured at 270 °C, illustrating the use of polynomial interpretation to improve the experimental estimate of α_{max}.

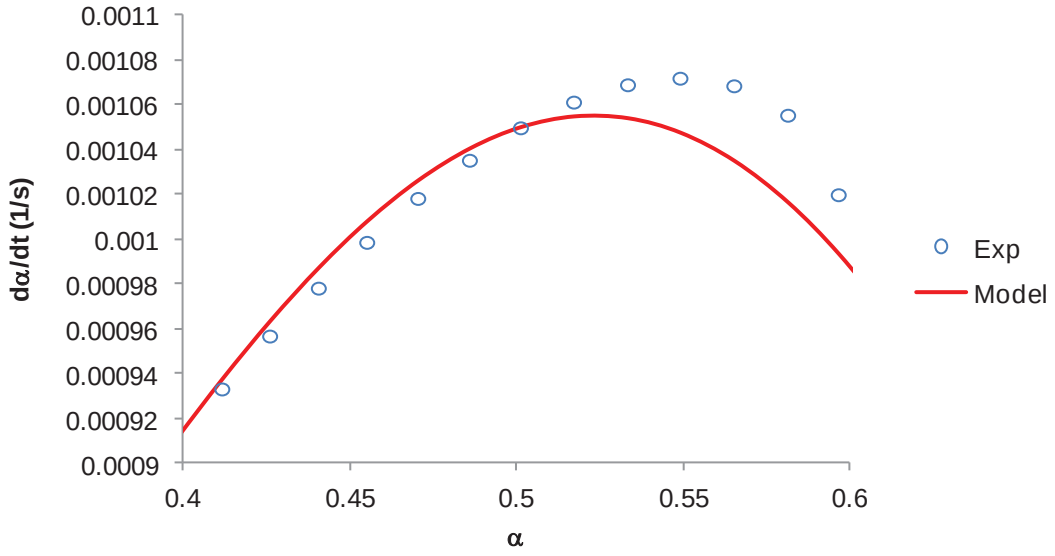

Figure S6-5. Model and experimental isothermal kinetics data near the maximum reaction rate for ESR-255 cured at 270 °C, after the first iteration of the outer loop, α_{max} = 0.546, $\alpha_{max\text{-}k2}$ = 0.546, and the resulting $\alpha_{max\text{-}model}$ = 0.523. The updated estimate for C_{k1} (initially zero) is thus 0.023, and the updated estimate for $\alpha_{max\text{-}k2}$ = 0.569. After further iterations, the loop converges at $\alpha_{max\text{-}k2}$ = 0.573.

For the inner loop, the main consequence of having k_1' values comparable to k_2' values is the effect on curve shape. As mentioned previously, the key conversion range for fitting data lies between the parameters α_{min} and α_{max}, with α_{min} = 0 in some cases, rather than always starting at zero conversion. To reflect this, the procedure developed previously for finding k_1', k_2', m, and n is updated so that, rather than performing regressions over fixed conversions, the conversion ranges are always computed relative to α_{min} and α_{max}. The determination of k_1' also becomes more complex, and changes with each iteration of the loop when α_{min} does not equal zero. In practice, however, the inner loop is easily automated.

To start the inner loop, a value of the parameter m is chosen as a starting guess (in these cases, m = 1 was used). Based on the current value of $\alpha_{max\text{-}k2}$ from the outer loop, the relation $\alpha_{max\text{-}k2}$ = m / (m + n) is used to compute the value of n. To compute k_1', a linear regression of all data points within and adjacent to the interval α_{min} + 0.1 to α_{min} + 0.15 is performed. The predicted value of the regression at α_{min}, that is, $(d\alpha/dt)_{min\text{-}model}$, is then used to compute k_1' using the assumption that the effect of auto-catalysis at the low conversions involved is small and positive, and approximately large enough to just compensate for the slight underestimate of the experimental, $(d\alpha/dt)_{min}$ due to performing the regression on data with a slight upward curvature. In practice, this assumption works very well. Hence, the auto-catalytic part of the rate formula is assumed negligible and the formula is thus $k_1' = (d\alpha/dt)_{min} / (1 - \alpha_{min})^n$. Since this formula does not involve k_2', it can be updated along with m and n at the start of each pass through the inner loop. Note that when α_{min} = 0, k_1' becomes simply the intercept of a linear regression of the data from α = 0.10 to α= 0.15, thereby guaranteeing that data from α < 0.1, which is subject to the effect of transients, is never used in the computation of k_1'. Figure S6-6 illustrates how k_1' is computed when $\alpha_{min} \neq 0$, showing how the selected method more accurately estimates the scale of the auto-catalytic effect compared to alternative approaches.

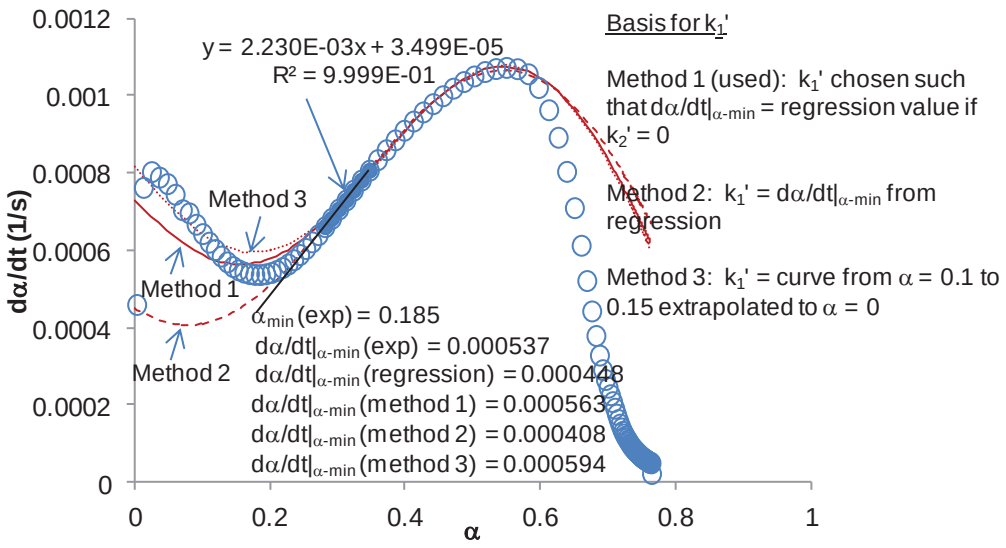

Figure S6-6. Comparison of proposed methods for determination of k_1' based on the resultant model curves (solid lines) compared to experiment (symbols) for ESR-255 cured at 270 °C. Method 1, which is described in detail in the text, provides the best agreement between the model and experiment with regard to the auto-catalytic reaction rate, as quantified by the difference between maximum (near 50% conversion) and minimum (18.5% conversion) reaction rates. Since the maximum rate is the same for all models, the value of the reaction rate ($d\alpha/dt$) at the minimum represents the discriminating characteristic. The difference between model and experiment was 5% for method 1, 24% for method 2, and 11% for method 3.

Once m, n, and k_1' are computed, the second part of the inner loop computes k_2' and updates the estimate of m. To do this, a linear regression based on the following rearrangement of Eq. S6-1 is used:

$$ln\left[\frac{\frac{d\alpha}{dt}}{(1-\alpha)^n} - k_1'\right] = \ln k_2' + m \ln \alpha \qquad \text{(S6-3)}$$

A linear regression of the left-hand side of Eq. (S6-3), which contains only parameters available from the earlier part of the inner loop, as a function of ln α yields an estimate of k_2' from the intercept and a second estimate of m (herein referred to as m_{reg}). The regression is carried out over the conversion range from α_{min} + 0.1 to α_{max}. To complete the loop, the objective function m_{reg} – m is computed, and the Newton-Raphson algorithm is utilized (as part of the Microsoft® Excel Goal Seek function) to generate an updated estimate for m. The updated estimate for m is then fed back into the inner loop, and the procedure repeated until the objective function converges to within 0.0001. Once converged, the parameters k_1', k_2', m, and n are passed back to the outer loop to compute $\alpha_{max\text{-}model}$ and continue on with the outer loop as described earlier. Figure S6-7 shows an example of the regression used in the inner loop. The resultant model parameters for each of the individual isothermal kinetics data sets collected as part of this work are tabulated in Section S6.6.

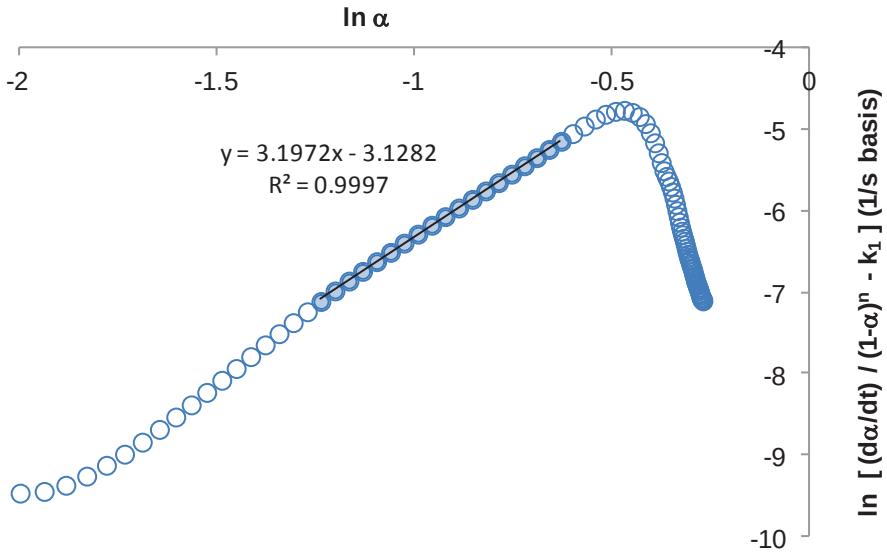

Figure S6-7. Linear regression used to determine ln k_2' and m_{reg}, for ESR-255 cured at 270 °C. The filled circles represent the subset of experimental data points used to compute the regression parameters.

S6.4.3 Kamal model with temperature-independent exponents. In order to compute activation energies, it is important to have a rate constant that allows for quantitative comparisons of the actual reaction rate. Although such a point might seem trivial, in fact, some care must be exercised to make sure that comparability is maintained. In analyzing individual isothermal kinetics data, for instance, the value of the constant k_2' that best describes the data (found through the procedure described in Section S6.4.2) changes based on the value of the reaction exponents m and n that are simultaneously determined to best describe the data. As a result, in two data sets where m and n differ, the ratio of the rate constants does not provide a direct measure of the ratio of reaction rates. To avoid this issue when calculating activation energies from a traditional Arrhenius plot, it is necessary to use temperature-independent rate constants, which are herein denoted as $\bar{m}$ and $\bar{n}$. The values of these exponents were determined by averaging the values of m and n found in all available sets of isothermal kinetics data for a given compound within the temperature range of 210 – 290 °C. With these two parameters fixed, the individual isothermal kinetics data sets were then re-analyzed to determine a new set of rate constants (herein denoted k_1 and k_2) that were suitable for computation of activation energies.

Since only two parameters needed to be determined, a single linear regression based on the following form of Eq. (S6-2) was utilized:

$$\frac{\frac{d\alpha}{dt}}{(1-\alpha)^{\bar{n}}} = k_1 + k_2\alpha^{\bar{m}} \qquad \text{(S6-4)}$$

A plot of the left-hand side as a function of $\alpha^{\bar{m}}$, using the data over a conversion range from α_{min} + 0.1 to α_{max} yields a slope of k_2 and an intercept of k_1. Figure S6-8 illustrates this regression. In Figure S6-9, the resultant model isothermal kinetics curve is compared to the data as well as the individually fitted curve found by the method in Section S6.4.2, for the ESR-255 sample cured at 270 °C. As expected,

having only two adjustable parameters reduces the quality of the fit slightly, however, the key features of the data, including, most importantly, the scale of the auto-catalytic effect, are still modeled well. The resultant data sets for all of the isothermal kinetics data collected as part of this work are tabulated in Section S6.6, along with the resultant activation energies (the plots are shown in Figure 6 of the main manuscript).

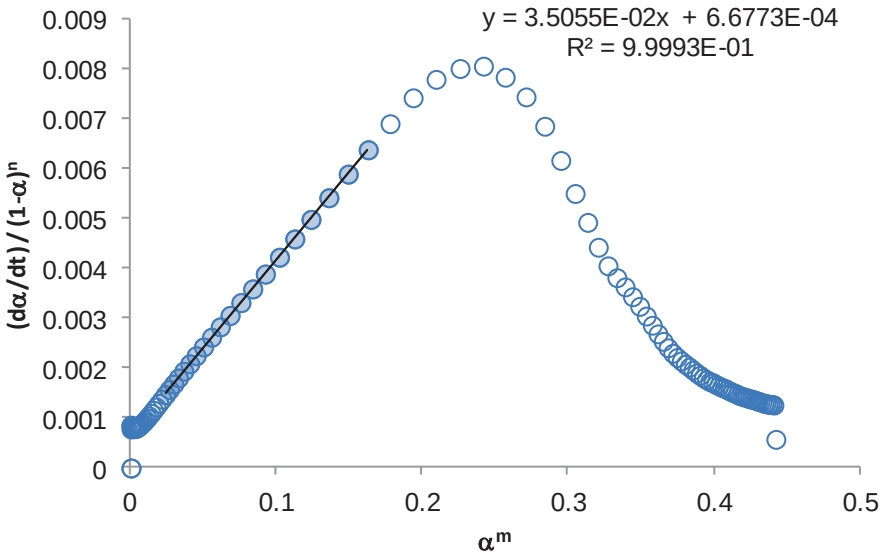

Figure S6-8. Regression used to calculate k_1 and k_2 from experimental data on ESR-255 cured at 270 °C. Note that only the filled symbols are used as experimental input data points for the regression.

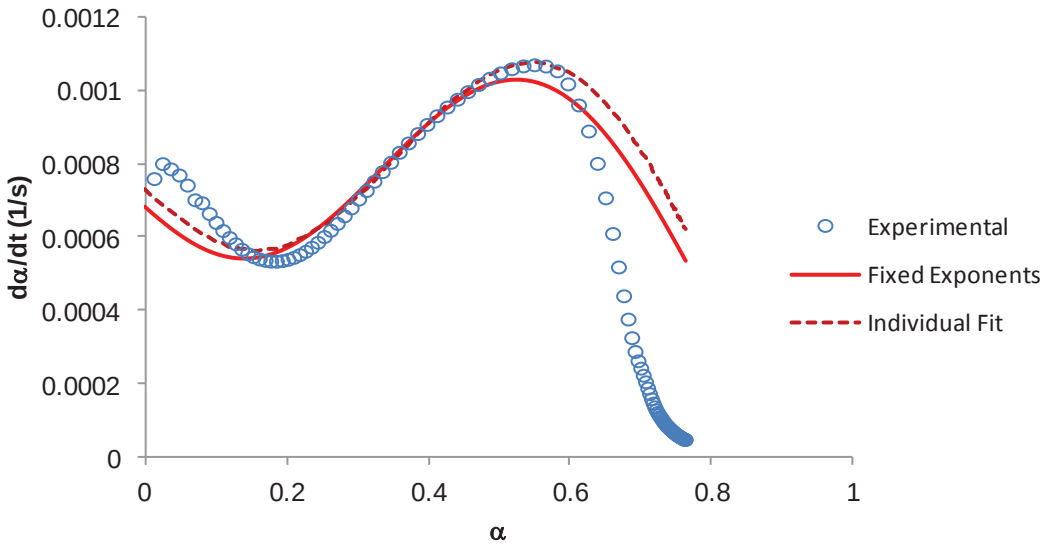

Figure S6-9. Comparison of experimental and model kinetic data (both individual curve fit and fit with temperature-independent exponents) for ESR-255 cured at 270 °C.

S6.5 Alternative Analyses for Error Estimates. Although the regressions used enable estimation of the errors in individual parameters for a given regression, these errors (which we have published for some data sets previously),[S11] do not reflect the propagation of error through the complex process of generating the nonlinear model. As with the treatment of DSC data, a more informative approach to estimating the errors is to examine the variability of results that, if error were not present, would be expected to show no variation. For the model exponents m and n, the variability in the individual data sets, which was 10-20%, represents a reasonable estimation of error. For the rate constants, the standard error in the Arrhenius plot provides one means of estimation, and appears to be around 5% as shown in Figure 6 of the main manuscript.

An additional technique that we have found useful in the past[S7] has been to overlay the individual rate curves with a vertical scaling factor. This scaling factor represents the relative rate of

reaction as a function of temperature without the need to invoke any particular model. An Arrhenius plot of the scale factor then provides both an alternative estimate of the activation energy, which allows for an error estimate of this parameter, which the standard error of the plot provides another indication of the relative error in the rate constants. Figures S6-10 through S6-12 show the overlaid data for the three monomers studied. It is clear that at both low conversions (at low temperatures) as well as high conversions beyond α_{max}, the curves do not overlay well. Within the analysis region, the overlay is best for ESR-255, followed by monomer **1**, then monomer **2**. The Arrhenius plots of the scale factors are shown in Figure S6-13. The activation energies from the scale factors, like the rate constants, exhibit a standard error of around 5%. These activation energies, however, differ from those found by modeling by only 1% for ESR-255, 6% for monomer **1**, and 11% for monomer **2**. Thus the level of disagreement appears to correlate with the lack of superposition in the relative rate curves. Note that these error estimates include both the error in extracting the conversion rates from the raw DSC data (3-5%) as well as additional errors introduced by the assumption of constant activation energy. The similarity of error magnitudes suggests that the latter assumption introduces a relatively small error into the process, while the differences in reported activation energy using the two techniques suggest that the model-based approach also introduces a comparatively small source of error.

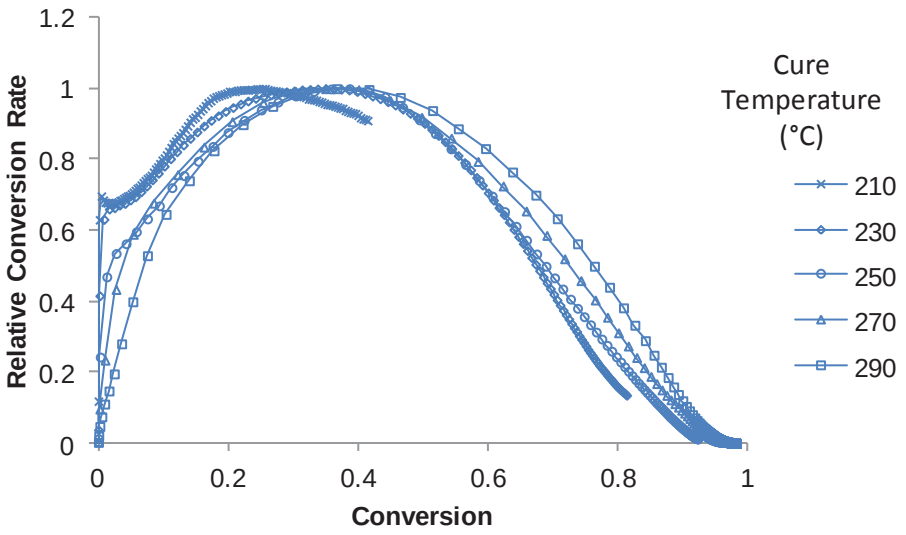

Figure S6.10. Relative reaction rate overlay for isothermal cure of monomer **1**.

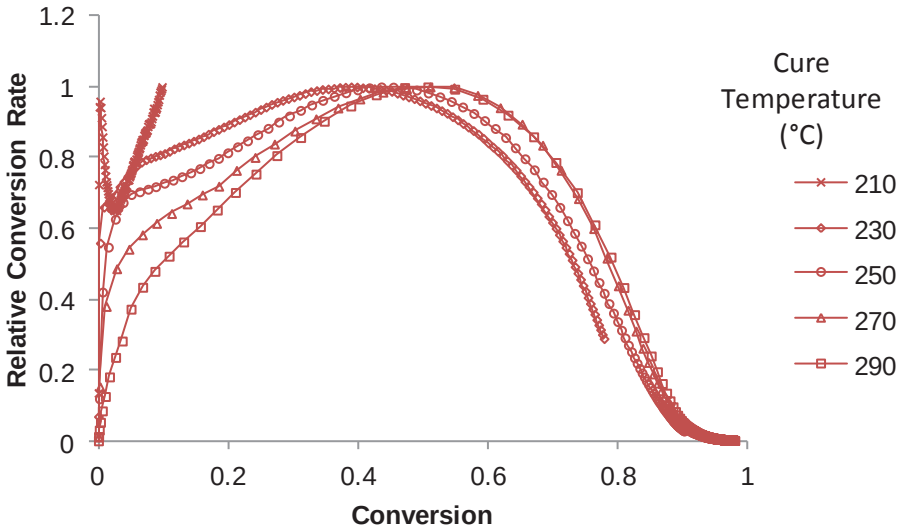

Figure S6.11. Relative reaction rate overlay for isothermal cure of monomer **2**.

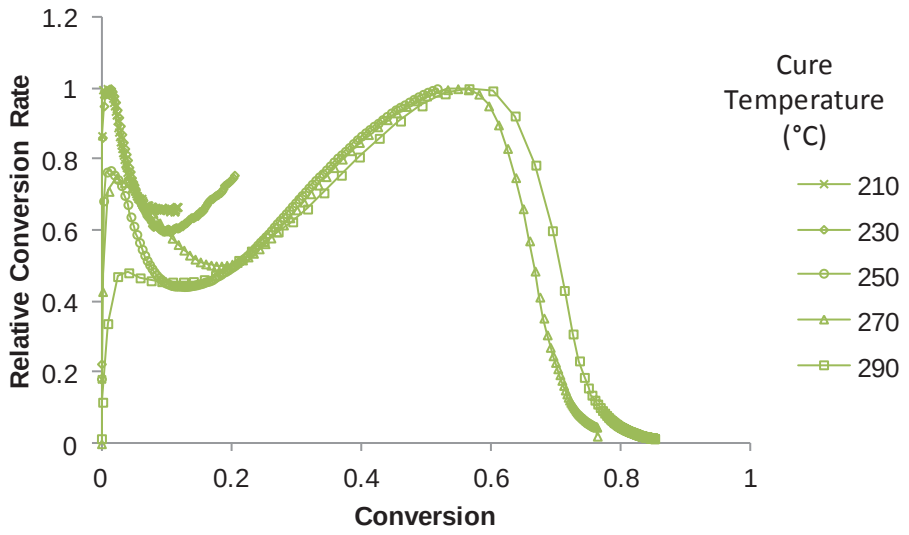

Figure S6.12. Relative reaction rate overlay for isothermal cure of ESR-255.

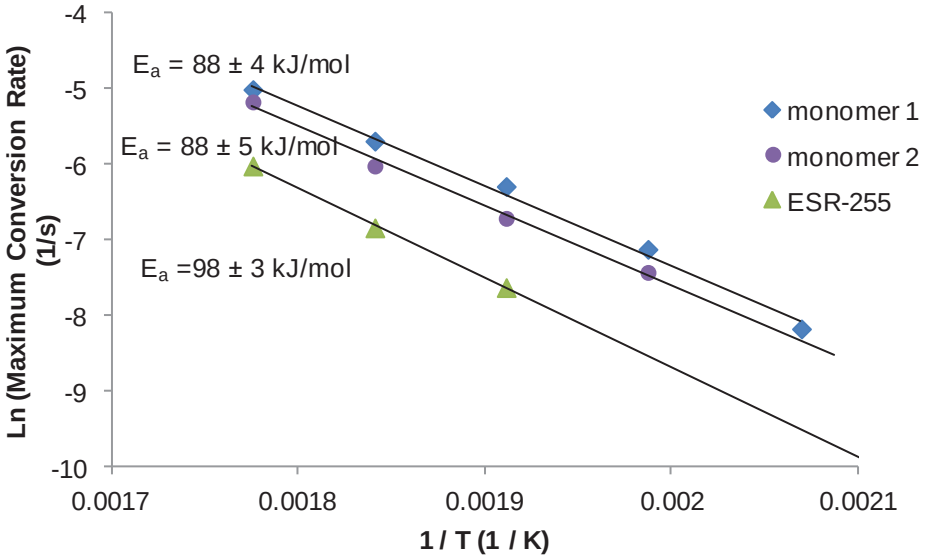

Figure S6-13. Arrhenius plot based on maximum observed conversion rates (no model) in isothermal kinetics data.

S6.6 Tables of Kinetic Model Parameters

Table S6-4

Individual isothermal kinetic model parameters for monomer **1**

Cure Temperature	k_1' (1/s)	k_2' (1/s)	m	n
210 °C *	0.000202	0.00528	1.588	3.535
230 °C	0.000472	0.00271	1.023	1.251
250 °C	0.000889	0.00888	1.162	1.485
270 °C	0.00170	0.0179	1.191	1.625
290 °C	0.00224	0.0291	1.031	1.356

*not used in computation of average exponents due to the large discrepancy with other data sets.

Table S6-5

Individual isothermal kinetic model parameters for monomer **2**

Cure Temperature	k_1' (1/s)	k_2' (1/s)	m	n
210 °C *	n/a	n/a	n/a	n/a
230 °C	0.000438	0.00228	1.326	1.249
250 °C	0.000794	0.00522	1.433	1.206
270 °C	0.00125	0.00836	1.314	0.940
290 °C	0.00189	0.0221	1.234	0.978

* sample did not reach maximum cure rate during test, therefore, no parameters were calculated

Table S6-6

Individual isothermal kinetic model parameters for ESR-255

Cure Temperature	k_1' (1/s)	k_2' (1/s)	m	n
210 °C *	0.0000496	0.00124	2.165	2.198
230 °C **	n/a	n/a	n/a	n/a
250 °C ***	0.000227	0.0216	3.333	2.566
270 °C	0.000729	0.0437	3.197	2.382
290 °C	0.00115	0.0390	2.551	1.773

* sample did not reach maximum cure rate during 30 minute test, therefore no parameters were calculated from the 30 minute data set, but data from a 24 hour isothermal test was available and used, though not for calculation of average exponents due to the large discrepancy with other data sets

** sample did not reach maximum cure rate during 30 minute test, therefore no parameters were calculated

*** sample did not reach maximum cure rate during 30 minute test, therefore no parameters were calculated from the 30 minute data set, but data from a 4 hour isothermal test was available and used

Table S6-7

Isothermal kinetic model (temperature-independent exponent) parameters for monomer **1**

Cure Temperature	k_1 (1/s)	k_2 (1/s)	$\bar{m}$	$\bar{n}$
210 °C	0.000194	0.00110	1.102	1.429
230 °C	0.000494	0.00319	1.102	1.429
250 °C	0.000834	0.00823	1.102	1.429
270 °C	0.00165	0.0147	1.102	1.429
290 °C	0.00256	0.0315	1.102	1.429

Table S6-8

Isothermal kinetic model (temperature-independent exponent) parameters for monomer **2**

Cure Temperature	k_1 (1/s)	k_2 (1/s)	$\bar{m}$	$\bar{n}$
210 °C *	n/a	n/a	n/a	n/a
230 °C	0.000441	0.00203	1.327	1.093
250 °C	0.000739	0.00458	1.327	1.093
270 °C	0.00115	0.0100	1.327	1.093
290 °C	0.00194	0.0260	1.327	1.093

* sample did not reach maximum cure rate within the 30 minute test time, therefore no parameters were calculated

Table S6-9

Isothermal kinetic model (temperature-independent exponent) parameters for ESR-255

Cure Temperature	k_1 (1/s)	k_2 (1/s)	$\bar{m}$	$\bar{n}$
210 °C *	0.0000753	0.00241	3.027	2.240
230 °C **	n/a	n/a	n/a	n/a
250 °C ***	0.000189	0.0139	3.027	2.240
270 °C	0.000668	0.0351	3.027	2.240
290 °C	0.00133	0.0796	3.027	2.240

* sample did not reach maximum cure rate during 30 minute test, therefore no parameters were calculated from the 30 minute data set, but data from a 24 hour isothermal test was available and used

** sample did not reach maximum cure rate during 30 minute test, therefore no parameters were calculated

*** sample did not reach maximum cure rate during 30 minute test, therefore no parameters were calculated from the 30 minute data set, but data from a 4 hour isothermal test was available and used

S7. Van't Hoff Determinations of Purity by DSC

Tables S7-1 through S7-3 contain the melting endotherm characteristics for all DSC runs of monomer **1**, monomer **2**, and ESR-255, respectively. These runs include the isothermal kinetics investigations for all monomers as well as the runs used to determine the diBenedetto parameters for ESR-255. The tabulated data include the melting point, enthalpy of melting, and van't Hoff purity (as determined by the TA Instruments Universal Analysis software package). The averages are also shown. Note that, as mentioned in Section S6, the enthalpy of melting was used as an internal standard to calibrate the heat flow data, because, as the tables show, small weighing errors resulted in variations in the heat flow values. The tables show clearly that ESR-255 exhibited the highest van't Hoff purity, followed by monomer **2**, and, at a slightly lower value, monomer **1**. The van't Hoff method is based on melting point depression, and therefore may not quantitatively represent the actual impurity levels present. Nonetheless, measurements of both as-received (99.4% purity) commercial BADCy as well as BADCy with 2% added impurity show van't Hoff purities near 99.5% and 98%, respectively.

Table S7-1

Melting endotherm characteristics of monomer **1** samples

Sample Type	Melting Point (°C)	ΔH_m (J/g)	Van't Hoff purity
Kinetics – 210 °C iso	100.6	57.3	96.17%
Kinetics – 230 °C iso	100.6	91.0	93.25%
Kinetics – 250 °C iso	100.6	70.2	95.28%
Kinetics – 270 °C iso	100.6	69.8	95.13%
Kinetics – 290 °C iso	100.4	69.3	95.60%
Standard non-isothermal	101.1	75.2	94.90%
Average*	100.7 ± 0.1	72.1 ± 4.5	95.06 ± 0.40%

*Shown with the uncertainty in the estimate of the mean, not the standard deviation

Table S7-2

Melting endotherm characteristics of monomer **2** samples

Sample Type	Melting Point (°C)	ΔH_m (J/g)	Van't Hoff purity
Kinetics – 210 °C iso	122.4	129.7	96.08%
Kinetics – 230 °C iso	122.0	121.0	96.17%
Kinetics – 250 °C iso	121.6	132.5	96.50%
Kinetics – 270 °C iso	122.2	124.2	96.61%
Kinetics – 290 °C iso	122.0	131.1	94.85%
Standard non-isothermal	123.3	120.0	97.38%
Average*	122.3 ± 0.2	126.4 ± 2.2	96.27 ± 0.34%

*Shown with the uncertainty in the estimate of the mean, not the standard deviation

Table S7-3

Melting endotherm characteristics of ESR-255

Sample Type	Melting Point (°C)	ΔH_m (J/g)	Van't Hoff purity
DiBenedetto fit – 150 °C iso	116.0	74.0	99.51%
DiBenedetto fit – 220 °C iso	115.2	69.9	99.44%
DiBenedetto fit – 230 °C iso	115.3	71.6	99.64%
DiBenedetto fit – 240 °C iso	115.9	66.9	99.29%
DiBenedetto fit – 245 °C iso	115.2	74.3	99.41%
DiBenedetto fit – 250 °C iso	115.3	61.7	99.14%
DiBenedetto fit – 255 °C iso	115.5	73.1	99.34%
DiBenedetto fit – 260 °C iso	115.5	71.4	99.17%
DiBenedetto fit – 270 °C iso	115.5	70.2	99.14%
DiBenedetto fit – 290 °C iso	115.2	69.3	99.41%
Kinetics – 210 °C iso	115.0	73.5	99.61%
Kinetics – 230 °C iso	114.9	80.1	99.65%
Kinetics – 250 °C iso	115.2	67.9	99.54%
Kinetics – 270 °C iso	115.1	65.9	99.46%
Kinetics – 290 °C iso	114.9	79.1	99.44%
Kinetics – 210 °C iso 24 hrs	115.6	71.7	99.38%
Standard non-isothermal	115.5	71.5	99.36%
Monomer T_g check	115.2	74.9	99.38%
Monomer / full cure T_g check	114.9	76.2	99.41%
Average*	115.3 ± 0.1	71.7 ± 1.0	99.41 ± 0.03%

*Shown with the uncertainty in the estimate of the mean, not the standard deviation

S8. Data on Monomer 1 Purified at Small Scale by Flash Chromatography

S8.1 Introduction. Since, for cyanate esters, the cure kinetics depend strongly on the concentration of catalytic impurities, and since the cure kinetics may affect the ultimate conversion (and hence the glass transition temperature) achieved during cure, it is reasonable to examine what role, if any, the known differences in impurity levels play in determining the cure kinetics and properties of the cyanate esters under study. Given that the impurity profiles of cyanate esters synthesized via unique multi-step routes likely differ in many different ways, a comprehensive investigation was judged beyond the scope of this work, and a simpler approach was sought. For the simplified approach, we took a small quantity of monomer **1**, which had the lowest van't Hoff purity, and passed it through a flash chromatography unit using a mixture of ethyl acetate and hexane. The main fraction collected exhibited a van't Hoff purity of 99.6%, which is almost identical to that of ESR-255, the monomer with the highest measured van't Hoff purity. We could thus compare monomer **1** and ESR-255 having equivalent van't Hoff purity values, as well as check the effect of purification on the properties of monomer **1**.

S8.2 Results. Table S8-1 compares the melting endotherm and isothermal cure kinetics parameters at 210 °C of monomer **1** at regular and high purity, along with ESR-255, with the latter two samples cured using an isothermal period of 24 hours and analyzed according to the methods presented in Section S6. A 24 hour period, rather than 30 minutes, was chosen in order to allow for analysis over the widest possible range of conversion, as well as to provide insight into the physical properties of the monomers, which were measured on samples cured at 210 °C for 24 hours. The total heat flow data from the residual heating scans, which were completed using modulated DSC, are shown in Figure S8-1. In this case, however, no features that could clearly be assigned to a glass transition temperature were present in the reversible heating curves, and the irreversible heating curves were no different in appearance than the total heating curves shown in Figure S8-1. In these situations, Kasehagen *et al.*,[S12] for example,

have pointed out that the onset of significant residual cure is a good indicator of the "as cured" glass transition temperature, since the rate of reaction is expected to jump significantly once de-vitrification takes place.

Table S8-1

DSC Parameters of Monomer **1**, Highly Purified Monomer **1**, and ESR-255

Parameter	Monomer 1 (pre-column)	Monomer 1 (post-column)	ESR-255 (no column)
T_m (°C)	100.7*	102.8	115.3*
ΔH_m (J/g)	72.1*	71.2	71.7*
van't Hoff purity	95.06%*	99.61%	99.41%*
k_1' (1/s)	0.000202	0.000207	0.0000496
k_1' (1/s)	0.00528	0.000500	0.00124
m	1.588	0.713	2.165
n	3.535	0.841	2.198
k_1 (1/s)	0.000194	0.000230	0.0000753
k_2 (1/s)	0.00110	0.00110	0.00241
$\bar{m}$	1.102	1.102	3.027
$\bar{n}$	1.429	1.429	2.240

*average of all DSC runs (see Tables S7-1 and S7-3 for error estimates)

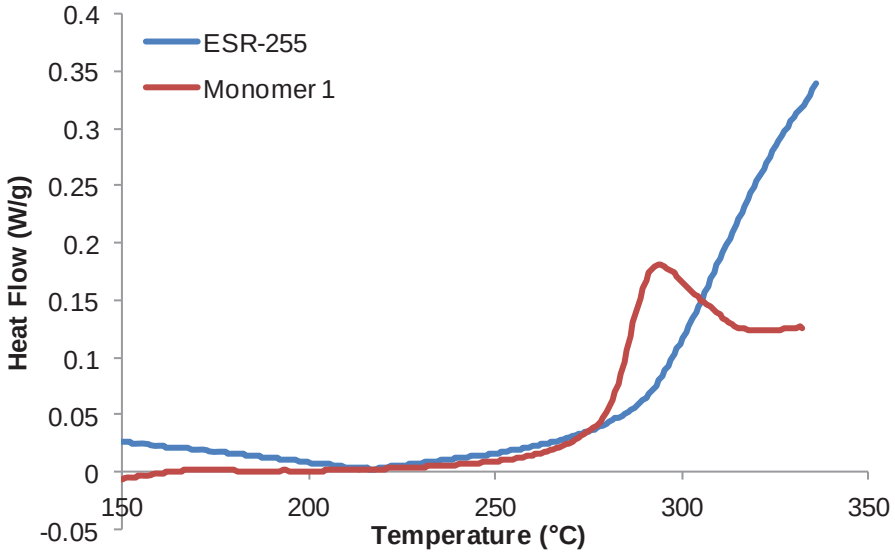

Figure S8-1. Modulated DSC of highly purified **1** and ESR-255 after 24 hours at 210 °C.

Interestingly, Table S8-1 shows that the regular and high purity versions of monomer **1** differ only modestly in cure kinetics. Note that the rate constants are only comparable when the exponents are the same, thus the catalytic rate constant is only 15% higher after purification while the auto-catalytic rate constant is unchanged. The very large difference in the individual fit exponents, though, does indicate that some aspects of the cure reaction are affected. On the other hand, the "as cured" glass transition temperature of the highly purified **1** is little different from the regular purity version (both are 275-280 °C). The onset temperature of residual cure is more difficult to discern for ESR-255, however, in this case the temperature of 245 °C indicated by TMA data (see Section S5) seems reasonable. Had the impurities that were removed been highly catalytic, a significant drop in the catalytic rate constant k_1 after further purification would have been expected. In a multi-step synthesis, there are many possible impurities that may have little catalytic activity. Conversely, it has been shown that some impurities at the level of tens of ppm can have significant effects on cyanate ester cure, and these may not have been removed by flash chromatography of the sample. Hence the van't Hoff purity is not always an indication of the degree of catalysis that can be expected.

Whatever the differences in cure kinetics that resulted from further purification of **1**, the glass transition temperatures of samples cured for 24 hours at 210 °C were not significantly affected. Figure S8-2 provides insight into why this is the case. The figure shows the estimated glass transition temperature (using the diBenedetto equation) as a function of cure time obtained from the DSC scans of the highly purified **1** and ESR-255. The vast majority of the cure for even the highly pure **1** takes place in the first hour or so, and the minor differences between the regular and high purity versions of **1** do not affect this time significantly (the times to 40% cure for instance, which can be compared using the standard 30-minute isothermal data for **1** at regular purity, show a difference of just 2 minutes, or about 8%). Both the regular and highly purified versions of **1** thus vitrify at about the same time, and have similar amounts of time available after vitrification for the T_g to slowly increase.

In contrast, the development of a high glass transition temperature is significantly slower in ESR-255 according to Figure S8-2. In the main manuscript, it was noted that "as cured" (in an oven, not the DSC) samples of ESR-255 had a lower glass transition temperature than **1** when cured for 24 hours at 210 °C, and the estimated glass transition temperature data appears to support the conclusion that the highly purified sample also exhibits an "as cured" glass transition temperature that is as high or higher compared to ESR-255, in accordance with the modulated DSC data seen in Figure S8-1. It should be noted that the data series in Figure S8-2 do not cover the entire range of cure times because, as cure proceeds, the reaction rate becomes so slow that it is indistinguishable from fluctuations in the DSC baseline. Note also that the data in Figure S8-2 does not depend on any particular kinetic model, simply the estimate of conversion from the DSC data and the diBenedetto parameters determined as described in Section S4.

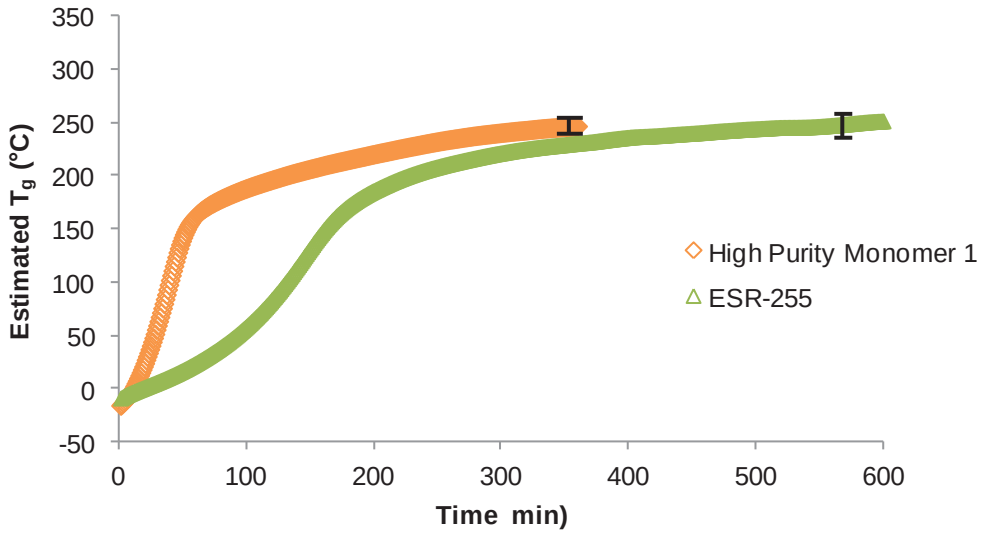

Figure S8-2. Estimated glass transition temperature as a function of cure time at 210 °C for highly purified monomer **1** compared to ESR-255.

References

S1. Hamerton, I., *Chemistry and Technology of Cyanate Ester Resins*. Chapman & Hall: London, 1994.

S2. Reams, J. T.; Guenthner, A. J.; Lamison, K. R.; Vij, V.; Lubin, L. M.; Mabry, J. M. *ACS Applied Materials & Interfaces* **2012,** *4*, 527-535.

S3. Sheng, X.; Akinc, M.; Kessler, M. R. *J. Therm. Anal. Calorim*. **2008,** *93*, 77-85.

S4. Simon, S. L.; Gillham, J. K. *J. Appl. Polym. Sci.* **1993,** *47*, 461-485.

S5. Marella, V. V. An Investigation on the Hydrolysis of Polyphenolic Cyanate Esters using Near-IR Spectroscopy. M. S. Thesis, Drexel University, Philadelphia, PA, 2008.

S6. Shimp, D. A.; Ising, S. J.; Christenson, J. R., Cyanate Esters -- A New Family of High Temperature Thermosetting Resins. In *High Temperature Polymers and Their Uses*, Society of Plastics Engineers: Cleveland, OH, 1989; pp 127-140.

S7. Guenthner, A. J.; Davis, M. C.; Lamison, K. R.; Yandek, G. R.; Cambrea, L. R.; Groshens, T. J.; Baldwin, L. C.; Mabry, J. M. *Polymer* **2011,** *52*, 3933-3942.

S8. Hamerton, I.; Emsley, A. M.; Howlin, B. J.; Klewpatinond, P.; Takeda, S. *Polymer* **2003,** *44*, 4839-4852 (also see references therein).

S9. Kamal, M. R.; Sourour, S. *Polym. Eng. Sci.* **1973,** *13*, 59-64.

S10. Kenny, J. M. *J. Appl. Polym. Sci.* **1994,** *51*, 761-764.

S11. Guenthner, A. J.; Lamison, K. R.; Davis, M. C.; Cambrea, L. R.; Yandek, G. R.; Mabry, J. M. In *Cure Characteristics of Tricyanate Ester High-Temperature Composite Resins*, 2011 SAMPE Spring Technical Conference and Exhibition - State of the Industry: Advanced Materials, Applications, and Processing Technology, Long Beach, CA, SAMPE International Business Office: Long Beach, CA, 2011; paper 56-1681.

S12. Kasehagen, L. J.; Haury, I.; Macosko, C. W.; Shimp, D. A. *J. Appl. Polym. Sci.* **1997,** *64*, 107-113.